OULU 2020
C 729

ACTA UNIVERSITATIS OULUENSIS

Ari Saastamoinen

PROCESSING AND MICROSTRUCTURE OF DIRECT-QUENCHED AND TEMPERED ULTRA-HIGH STRENGTH STEELS

UNIVERSITY OF OULU GRADUATE SCHOOL;
UNIVERSITY OF OULU,
FACULTY OF TECHNOLOGY

ACTA UNIVERSITATIS OULUENSIS
C Technica 729

ARI SAASTAMOINEN

PROCESSING AND MICROSTRUCTURE OF DIRECT-QUENCHED AND TEMPERED ULTRA-HIGH STRENGTH STEELS

Academic dissertation to be presented, with the assent of the Doctoral Training Committee of Technology and Natural Sciences of the University of Oulu, for public defence in the Wetteri auditorium (IT115), Linnanmaa, on 23 January 2020, at 12 noon

UNIVERSITY OF OULU, OULU 2020

Acta Univ. Oul. C 729, 2020

Supervised by
Professor Jukka Kömi
Professor David Porter

Reviewed by
Professor Esa Vuorinen
Doctor Per Hansson

Opponents
Professor Ronald Schnitzer
Doctor Per Hansson

ISBN 978-952-62-2453-4 (Paperback)
ISBN 978-952-62-2454-1 (PDF)

ISSN 0355-3213 (Printed)
ISSN 1796-2226 (Online)

Cover Design
Raimo Ahonen

JUVENES PRINT
TAMPERE 2020

Saastamoinen, Ari, Processing and microstructure of direct-quenched and tempered ultra-high strength steels.
University of Oulu Graduate School; University of Oulu, Faculty of Technology
Acta Univ. Oul. C 729, 2020
University of Oulu, P.O. Box 8000, FI-90014 University of Oulu, Finland

Abstract

The effect of thermomechanically controlled processing (TMCP) and various tempering conditions on the effect on microstructure and mechanical properties of low-carbon direct-quenched (DQ) high-strength steel has been studied.

All steels contained (in wt.%) 0.2Si-1Mn-1Cr-0.65Mo-0.03Al, while there were two levels of C (0.095 / 0.140), V (0 / 0.08), Ti (0 / 0.025) and B (0 / 0.0015). Thermomechanical treatment was studied by varying the finish hot rolling temperature (FRT) and the amount of reduction below recrystallization-stop-temperature (T_{nr}). Tempering treatments were conducted at 180–650 °C with an aim of simulating tempering conditions in an industrial batch annealing furnace.

The strength of final strip was shown to be dependent on an existing chemical composition and thermomechanical treatment, which both affected the transformed microstructures. Furthermore, the tempering temperature was greatly affecting the final strength. V-alloyed steels obtained superior resistance to softening in tempering. V-free steels, on the other hand, underwent significant improvement in toughness, but decrease in strength during high-temperature tempering. Toughness of the Ti- and V-alloyed strips was noticed mainly being dependent on the effective grain size in the final strip, which was mainly dependent on R_{tot}.

The bendability of DQ-T strip is affected by FRT and tempering temperature. FRT had an effect on the bendability by affecting transformed surface microstructures as well as intensity of shear texture component $\sim\{112\}\langle 111\rangle_{\alpha}$. Undesirable texture and microstructure was formed with FRT 865 °C, while FRT 775 °C lead to favourable microstructure of polygonal ferrite and granular bainite. High-temperature tempering softened the matrix and promoted bendability, but tempering at a temperature range of 400–500 °C leads to unfavourable formation of long carbide regions along lath and grain boundaries being detrimental for bendability.

Keywords: bainite, bendability, martensite, microstructure, tempering, texture, toughness

Saastamoinen, Ari, Ultralujien nuorrutusterästen prosessointi ja mikrorakenne.
Oulun yliopiston tutkijakoulu; Oulun yliopisto, Teknillinen tiedekunta
Acta Univ. Oul. C 729, 2020
Oulun yliopisto, PL 8000, 90014 Oulun yliopisto

Tiivistelmä

Termomekaanisen käsittelyn ja useiden päästökäsittelyjen vaikutusta mikrorakenteeseen sekä mekaanisiin ominaisuuksiin tutkittiin ultralujilla suorakarkaistuilla rakenneteräksillä.

Kaikki teräkset sisälsivät (paino-%) 0.2Si-1Mn-1Cr-0.65Mo-0.03Al, kun taas C (0.095 / 0.140), V (0 / 0.08), Ti (0 / 0.025) ja B (0 / 0.0015) tasoja varioitiin. Termomekaanisen käsittelyn vaikutusta tutkittiin varioimalla valssauksen lopetuslämpötilaa ja reduktion määrää rekristallisaation lopetuslämpötilan alapuolella. Koeterästen päästökokeet suoritettiin lämpötiloissa 180–650 °C simuloiden päästöolosuhteita teollisessa kellouunissa.

Teräksen lujuuden katsottiin olevan riippuvainen sekä kemiallisesta koostumuksesta että termomekaanisesta käsittelystä, jotka molemmat vaikuttivat syntyneisiin mikrorakenteisiin. Lisäksi päästölämpötilalla oli keskeinen vaikutus teräksen lopulliseen lujuuteen. V-seostetut koeteräkset omasivat erinomaisen päästönkestävyyden. V-vapaan teräksen iskusitkeys parani merkittävästi päästökäsittelyssä, johtaen kuitenkin merkittävään lujuuden laskuun. Ti- ja V-seostetun terästen lopullisen sitkeyden katsottiin riippuvan pääasiallisesti vallitsevasta raekoosta, johon termomekaaninen käsittely vaikutti keskeisesti.

Suorakarkaistun ja päästetyn teräksen särmättävyys riippui valssauksen lopetuslämpötilasta sekä päästökäsittelystä. Valssauksen lopetuslämpötilan vaikutus särmättävyyteen johtui syntyneistä mikrorakenteista sekä tekstuurikomponentin ~{112}<111>$_{\alpha}$ voimakkuudesta. Epäedullinen voimakas tekstuuri sekä yläbainiittinen mikrorakenne syntyi, kun valssauksen lopetuslämpötila oli 865 °C. Valssauksen lopetuslämpötila 775 °C taas johti edulliseen mikrorakenteeseen, joka koostui polygonaalisesta ferriitistä ja granulaarisesta bainiitista. Korkean lämpötilan päästö pehmensi matriisin lujuutta ja paransi särmättävyyttä. Kuitenkin, päästö 400–500 °C johti pitkien karbidien tai karbidijonojen epäedulliseen muodostumiseen heikentäen särmättävyyttä.

Asiasanat: bainiitti, iskusitkeys, martensiitti, mikrorakenne, päästö, särmättävyys, tekstuuri

Acknowledgements

The work carried out in this project is mainly contributed during 2014–2019 in the Materials and Production technology research unit at University of Oulu. The research has been mainly funded by Finnish Funding Agency for Technology and Innovation (Tekes) under the “Breakthrough Steels and Applications” programme of the Finnish Metals and Engineering Competence Cluster. The work has also received extra funding from SSAB Europe Oy, Jenny and Antti Wihuri foundation, Häme Foundation for Professional Higher Education and Research, Tauno Tönning Foundation and Walter Ahlström foundation. This extra support has been extremely important for finishing this work. SSAB Europe Oy has also been providing the researched materials. I feel extreme gratitude for this support.

I have been lucky to complete my degrees at the University of Oulu during the time spell when Professors Pentti Karjalainen, David Porter and Jukka Kömi have been leading the group. I thank them for their support in my studies. Special acknowledgment I give for David Porter and Jukka Kömi for their gratuitous work in supervising my thesis. Furthermore, despite not being formal supervisor, Dr. Antti Kaijalainen has provided invaluable support during my doctoral training. I would like to thank Antti for sharing his knowledge and supporting me during my writing periods. I also want to say my special thanks for my industrial partners Dr. Pasi Suikkanen, Dr. Saara Mehtonen, M.Sc Visa Lang and M.Sc Vili Kesti for supporting me in my research projects.

I also want to thank my doctoral committee, Professor Jari Larkiola and Dr. Olli Nousiainen. Furthermore, Dr. Mahesh Somani, Mr. Ilpo Alasaarela, Mr. Tun Tun Nyo, Mr. Jouko Heikkala and Mr. Seppo Järvenpää is thanked for their theoretical and practical help. Mr. Jussi Paavola is thanked for conducting laboratory hot rolling trials with me. In addition to them, the whole research group of advanced high-strength steels is thanked for their support. Special thanks to Mr. Ilkka Miettunen for sharing delightful conversations also outside metallurgy.

Thank you for my friends outside the lab. My mountain biking friends: You provided possibility to balance my life.

Finally, the most important part of the equation, Katariina, Ilari and Viena – thank you. Writing the thesis for me has been mostly just project that I have really enjoyed. For my family though, it has demanded much more patience. I can only express my gratitude for you.

Hattula, June 2019 Ari Saastamoinen

Abbreviations

α	ferrite
α’	martensite
γ	austenite
ρ	dislocation density
σ	tensile stress
σ_{ppt}	precipitation strengthening
σ_{SS}	solid solution strengthening
σ_C	carbon solid solution strengthening
A_5	total elongation
A_g	uniform elongation
ATM	auto-tempered martensite
BCC	body-centric cubic
CCT	continuous cooling transformation diagram
$d_{90\%}$	grain size at 90% cumulative grain size distribution
DQ	direct-quenched
DQT	direct-quenched and tempered
EBSD	electron back scatter diffraction
ECD	equivalent circle diameter
etc.	et cetera
FCC	face-centric cubic
FESEM	field emission scanning microscopy
FRT	finish rolling temperature
GB	granular bainite
HTT	high-temperature tempering
HV	Vickers hardness
i.e.	id est
e.g.	exempli gratia
IPF	inverse pole figure
LTT	low-temperature tempering
M	martensite
M_s	martensite start temperature
M_f	martensite finish temperature
M-A	martensite-austenite constituents

ODF	orientation distribution function
OM	optical microscope
$\bar{\bar{L}}$	mean grain size
LSCM	laser scanning confocal microscope
UB	upper bainite
r	aspect ratio
R	punch radius
RAQ	re-austenitized and quenched
RAQT	re-austenitized, quenched and tempered
RD	rolling direction
R_{tot}	total reduction below the recrystallization temperature
S_v	surface area per unit volume (mm^2/mm^3)
t	sheet thickness
T28J	28J transition temperature
TD	transverse direction
TMCP	thermomechanical controlled processing
T_{nr}	recrystallization stop temperature
UTS	ultimate tensile strength
wt.%	weight percentage
XRD	x-ray diffraction
YS	yield strength

Original publications

This thesis is based on the following publications, which are referred throughout the text by their Roman numerals I–IV:

I Saastamoinen A., Kaijalainen A., Nyo T. T., Suikkanen P., Porter D. & Kömi J. (2019) Direct-quenched and tempered low-C high-strength structural steel: The role of chemical composition on microstructure and mechanical properties, *Materials Science & Engineering: A*, 760, 346–358

II Saastamoinen A., Kaijalainen A., Porter D., Suikkanen P., Yang J-R. & Tsai Y-T. (2018) The effect of finish rolling temperature and tempering on the microstructure, mechanical properties and dislocation density of direct-quenched steel, *Materials Characterization*, 139, 1–10.

III Saastamoinen A., Kaijalainen A., Porter D. & Suikkanen P. (2017) The effect of thermomechanical treatment and tempering on the subsurface microstructure and bendability of direct-quenched low-carbon strip steel, *Materials Characterization*, 134, 172–181.

IV Saastamoinen A., Kaijalainen A., Heikkala J., Porter D. & Suikkanen P. (2018) The effect of tempering temperature on microstructure, mechanical properties and bendability of direct-quenched low-alloy strip steel, *Materials Science & Engineering: A*, 730, 284–294 .

In all publications, Ari Saastamoinen has done the main contribution. Except where the role of others is acknowledged below, the author has been responsible for doing the experimental work as well as the analysis and processing of the results.

Publication I describes the effect of chemical composition on the mechanical properties and microstructure of direct-quenched and tempered (DQ-T) high-strength steel. The results show the importance of vanadium, carbon and boron in controlling the mechanical properties. The results in this Publication were used to develop the compositions studied in later stages of the thesis.

Publication II presents the combined effect of thermomechanical treatment and tempering on microstructure, crystallography, dislocation density, strength and toughness of pilot-scale direct-quenched strip. The results show the significant effect of thermomechanical processing temperature on both microstructure and toughness by refining the effective grain size. The TEM investigations in this study were performed by Prof. Yang and Dr. Tsai in the University of Taiwan.

Publication III focuses on the bendability of DQ-T steels by studying the effect of thermomechanical treatment and tempering on surface microstructure and surface texture, which affect the bendability-strength combination of 960 MPa grade structural steel.

Finally, Publication IV deals with the effect of tempering temperature in the range of 250–650 °C on strength, toughness and bendability and their relation to the microstructure at different through-thickness positions. The publication also presents the fundamental differences between direct-quenched and conventional re-austenitized and quenched martensite.

Contents

1 Introduction

1.1 Background

During the past decades, the global steel industry has been under constant transformation. Growing competition, expanding demands of both customers and the environment and the need to minimize fabrication costs have led to a continuous pursuit for better levels of strength, toughness, formability and price – preferably all in one package.

One, originally impossible-looking task was to develop steel with improved properties and life-cycle environmental impact with lower alloying and processing costs. An example of such a development has been the establishment of direct-quench processing technology on an industrial scale. Direct-quenched high-strength steels have set new standards combining both the productivity but also novel steel properties and have shown the possibility to obtain excellent strength and toughness together with moderate manufacturing costs. (Kaijalainen, 2016; Kömi, Karjalainen & Porter, 2016; Pallaspuro, 2018). The importance of high strength and reduced manufacturing costs and carbon footprint cannot be overemphasized: in 2016, global steel production reached 1600 million tonnes – a remarkable figure that is estimated to grow 1.5 times higher by 2050 ("World steel association," n.d.). This combined with the facts that over 6 million people work in steel industry worldwide and that steel exists everywhere in our society, means that the steel industry can make remarkable global impacts in terms of emissions to the environment.

This thesis focuses on the tempering metallurgy of direct-quenched low-carbon steels including a comparison with re-austenitized, quenched and tempered martensite to understand the differences between the two. Conventional re-austenitizing, quenching and tempering is well understood, but the tempering of the relatively new direct-quenched steels has been little studied.

It has been shown that direct-quenched martensite possesses great combinations of strength and toughness without the need of the tempering that has been traditionally used to ensure the toughness of martensitic structural steels. However, in some circumstances, the tempering of direct-quenched martensite can still be desirable. Such reasons are related to improved weldability or a desire to further improve toughness.

1.2 Scope and aims of the thesis

As presented earlier, the microstructure and properties of direct-quenched martensitic-bainitic microstructures has been shown to be excellent already in the direct-quenched condition. However, solid knowledge on the effect of tempering on the microstructure and properties of direct-quenched high-strength steel has not yet been fully studied.

The scope of this thesis is to describe the effect of chemical composition, thermomechanical treatment and tempering on the microstructure and final properties of low-C high-strength steel. Furthermore, the difference between traditionally quenched and tempered martensite and direct-quenched and tempered martensite will be described. It is possible to further improve the already excellent properties of the direct-quenched condition by tailoring the heat treatment procedure and optimizing the composition. This means not only finding the optimal tempering temperature and thermomechanical treatment conditions for obtaining the best combination of strength and ductility, but also exploring new tempering procedures for improving productivity. The effect of chemical composition has been included in the experimental work with the aim of creating a tempering robust composition that, during high-temperature tempering, as far as possible, retains its yield strength while still providing improved ductility.

The research aims are the following:

1. Investigating the role of chemical composition on the softening and microstructural changes during tempering of direct-quenched, high-strength steel.
2. The combined effect of thermomechanical treatment and tempering on the microstructure of direct-quenched high-strength strip.
3. Establishing the relationship between microstructure and mechanical properties both prior to and after tempering.
4. Developing guidelines for optimizing the tempering of direct-quenched strip with respect to strength–ductility combinations.

Research aim number 1 is studied in Publication I. This work focuses on the effect steel composition on the tempering resistance and final microstructure of laboratory hot-rolled experimental strips. The study shows the effects of carbon, vanadium, titanium and boron on the microstructure, strength and toughness and direct-quenched laboratory strip. This part of the thesis also includes additional results to those published in the four journal articles to show the importance of certain

alloying elements in developing a composition with adequate hardenability for DQ process.

Research aims 2 and 3 are answered in Publications II, III and IV in combination. Publication II studies the effect of thermomechanical treatment and tempering on the microstructure, strength and toughness of direct-quenched martensite while Publication III focuses on studying the effect of tempering on the surface microstructure and therefore improving the combination of strength and bendability of high-strength steels. Finally, Publication IV summarises the work by investigating the effect of a wide range of tempering temperatures on the strength, toughness and bendability of direct-quenched and tempered martensite. The Publication also compared the mechanical properties with those obtained using re-austenitization and quenching to martensite instead of direct.

Research aim 4 is achieved through an overall summary of all the research Publications, which results in guidelines regarding compositional design, thermomechanical treatment, tempering parameters and processing route when aiming for certain desired property combinations.

A long-term objective of these research aims is the development of a new steel concept with excellent strength–ductility combinations and ultimately a step forward in the development of more refined and usable materials that promote environmental friendliness in all steps of the steel life cycle.

2 Theoretical framework

2.1 Thermomechanical treatment and direct quenching

The conventional process route used for quenched and tempered steels is hot rolling and slow cooling followed by re-austenitizing, quenching (RAQ) and furnace tempering (RAQT). However, direct quenching (DQ), where the steel plate is directly quenched after hot rolling stage, is a more efficient alternative to the conventional RAQ process due to eliminating the reheating stage from the steelmaking process (Fig. 1). Conventional RAQ and RAQT process routes are rather well understood based on the large volume of research that has been published (Caron & Krauss, 1972; Bhadeshia & Honeycombe, 2006; Krauss, 2017).

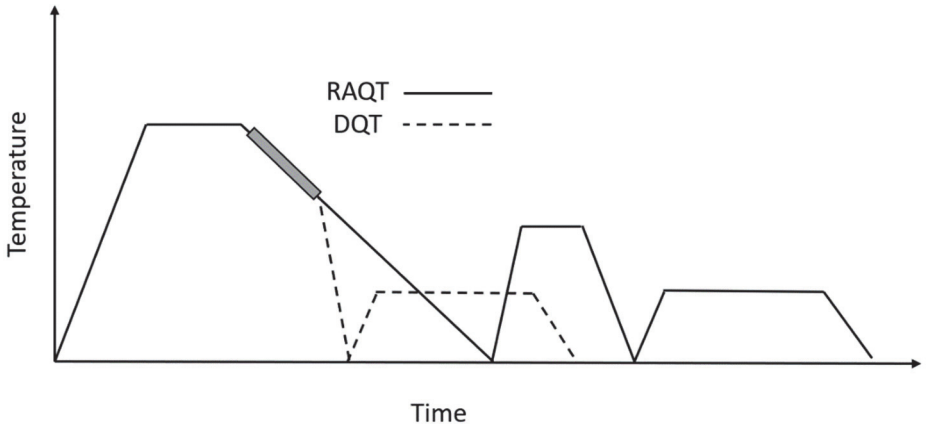

Fig. 1. Schematic presentation of difference between RAQT and DQT.

Thermomechanical treatment combined with direct-quenching, on the other hand, leads to different as-quenched microstructures compared to re-austenitized and quenched structures due to their differences in austenite grain morphology (Kaijalainen et al., 2010, 2013, 2014). For example, thermomechanical treatment prior to direct quenching, improves the toughness of martensite in the as-quenched condition due to austenite pancaking even without tempering, which is not typical for RAQ martensitic steels (Kaijalainen et al., 2014; Kaijalainen, 2016; Kömi et al., 2016; Pallaspuro, 2018). These differences have led to the necessity for further research on the tempering metallurgy of thermomechanically processed and direct-quenched steels.

Thermomechanical treatment, in fact, plays a significant role in the direct quenching process. A schematic presentation of thermomechanical treatment as a function of time and temperature is presented in Fig. 2. Thermomechanical treatment in the non-recrystallization region will lead to martensite formation from strained, unrecrystallized austenite (Nishioka & Ichikawa, 2012). An earlier study (Kaijalainen, 2016) showed the temperature dependence of grain size and shape in the combined TMCP and DQ process. Lower finish rolling temperature (FRT) leads to hotter working below recrystallization stop temperature and therefore more pancaking of the austenite. In conventional re-austenitization and quenching, recrystallization leads to the loss of the worked austenite microstructure. However, austenite pancaking is retained with direct quenching without re-austenitizing.

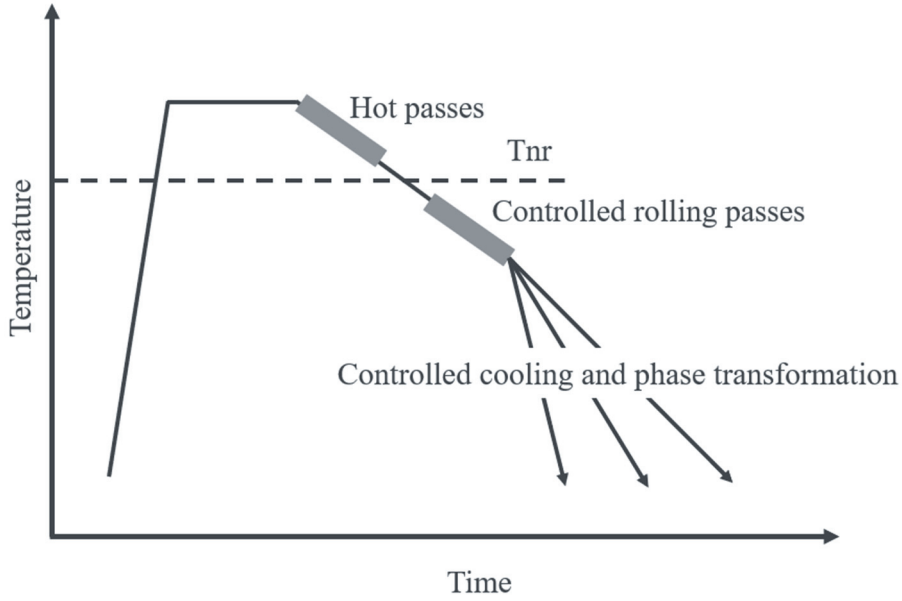

Fig. 2. Schematic presentation of TMCP processing.

A fine pancaked grain structure has been shown to be extremely beneficial for toughness (A. Kaijalainen, 2016). However, Kaijalainen also showed that FRT affects the transformation texture and therefore affects the mechanical properties such as bendability. FRT can also affect microstructure in general as lower FRT promotes the formation of softer non-martensitic microstructural components. Many authors have shown that hardenability is reduced when austenite is deformed below the recrystallization start temperature (Cizek, Wynne, Davies, Muddle &

Hodgson, 2002; Somani, Pyykkönen, Porter, Karjalainen & Kömi, 2015). If this is the case in the TMCP process, a decrease in hardenability is inevitable, which means higher cooling capacity is required to achieve martensite.

2.2 High-strength as-quenched microstructures

This thesis is mainly concerned with the austenite to martensite diffusionless transformation, but also the austenite to bainite and austenite to ferrite transformations are concerned to some extent. As we are dealing with low-carbon high-strength steels, even more specifically, we are working with lath martensite rather than plate martensite.

When the carbon content of the steel is low, martensite transformation from the face-centred cubic (FCC) lattice (austenite) to the body-centred cubic (BCC) lattice generally results in a lath shaped structure, i.e. lath martensite (Krauss & Marder, 1971). Typically, as the martensite transformation is shear-type diffusionless transformation no compositional changes occur and carbon is trapped inside BCC structure causing formation of strained BCC, i.e. tetragonal system, and thanks to diffusionless transformation, martensite transformation can occur at very low temperatures in a very short time period. For low-C martensite, though, traditional tetragonal lattice structure usually do not exist due to diffusion of C to dislocations and autotempering that usually occurs during quenching.

The Kurdjumov-Sachs (K-S) orientation relationship is usually close to the orientation relationship found experimentally between the parent austenite and martensite or ferrite or bainite in steels (Ray, Jonas, Butrón-Guillén & Savoie, 1994). It can be expressed as $\{111\}_\gamma//(011)_{\alpha'}; \langle\bar{1}01\rangle_\gamma//\langle\bar{1}\bar{1}1\rangle_{\alpha'}$, where γ refers to austenite and α' martensite.

There are 24 possible variants the K-S relationship. Austenite has four $\{111\}$ planes parallel or near parallel to $\{110\}_\alpha$ and in each case there are six ways of aligning $\langle\bar{1}01\rangle_\gamma//\langle\bar{1}\bar{1}1\rangle_{\alpha'}$.

In the case of low-carbon martensite (Fig. 3), current theory is that prior austenite grains are divided into packets and further into blocks, all of which are separated by high-angle boundaries. Packets are groups of laths with the same habit plan and blocks laths with the same orientation. Blocks are further divided into sub-blocks, one of which is dominant and having different K-S variants between each other. (Morito, Huang, Furuhara, Maki & Hansen, 2006; Morito, Adachi & Ohba, 2009).

Despite the diffusionless nature of the martensite transformation, diffusional phase transformations are not excluded from occurring in the laths during quenching after they have formed. One example of this is auto-tempering. During quenching of steels with high martensite start temperature (M_s), tempering can occur already immediately after martensite transformation, which might mean carbon segregation and/or fine cementite precipitation. M_s is highly dependent on carbon content and decreased carbon content leads to an increased M_s. Therefore, during the quenching of low-carbon steel auto-tempering is favoured by the high driving force for carbon to precipitate out of the strained BCC structure and the high mobility of carbon in the BCC lattice. In fact, according to Bhadeshia and Honeycombe (2006), no martensite tetragonality is apparent after quenching when carbon content is below 0.2 wt.%.

Understanding the microstructural hierarchy of lath martensite is considered essential due to their influence on strength and toughness. Due to the fact that blocks and packets are both surrounded by high-angle boundaries, they are often considered as defining an "effective grain size" (Morito, Huang, et al., 2006). Also, regardless of the low level of misorientation between sub-blocks, those units still hinder dislocation movement thereby promoting the strength of martensite (Morooka, Tomota, Adachi, Morito & Kamiyama, 2008).

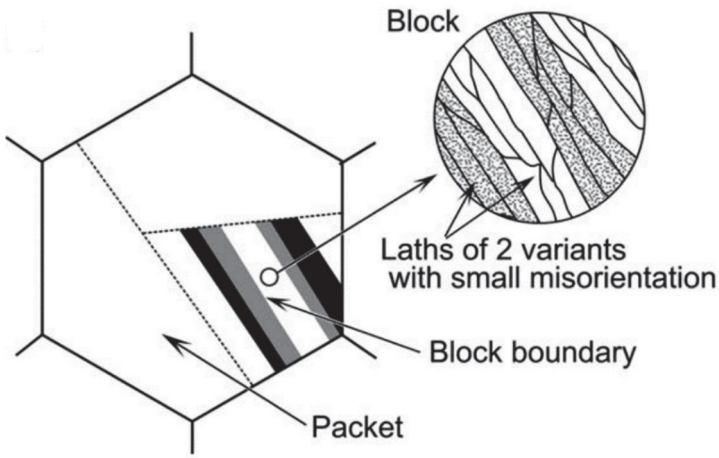

Fig. 3. Lath martensite presented by Morito et al. (Reprinted by permission from Morito, Huang, et al. 2006 © Elsevier B.V.).

When aiming to achieve a martensitic microstructure, the hardenability of the composition must be sufficient for the available cooling conditions. Carbon is a major source of strength and a major hardenability promoting factor in these concentrations, but high carbon contents are often associated with embrittlement (Krauss, 1999).

Another major hardenability-promoting element, used widely in low-carbon steels, is boron. Boron effectively retards phase transformations by segregating to austenite grain boundaries and controlling the bainite and ferrite formation during cooling. Boron tends to react with nitrogen forming boron nitrides, which leads to a loss of its hardenability effect. Therefore, titanium is widely used for formation of titanium nitrides to protect the boron (Ueno & Inoue, 1973; Taylor & Hansen, 1990). Shen and Hansen also showed that titanium in solution in excess of the stoichiometric Ti/N ratio of 3.42 promotes hardenability even further in its own right (Shen & Hansen, 1997).

An economical way of increasing hardenability is to include manganese in the composition (Calcagnotto, Ponge & Raabe, 2012). Typically, in commercial steels, manganese contents vary from 0.60 to 1.40 wt.%. Other elements that are effective in promoting hardenability are molybdenum and chromium (F. Han et al., 2008). These elements are typically alloyed up to 0.60 wt.% in case of molybdenum and even up to 4 wt.% chromium contents in commercial low-alloyed high-strength steels.

Copper also increases hardenability. It has little effect on solution strengthening, which in the martensitic steels is considered minor. (Llewellyn, 2005) Cu has been successfully used as a boron replacement in high-strength steels making it a good alternative due to its precipitation hardening potential in tempering (Ouchi, 2001).

Other elements affecting hardenability include vanadium, which has been shown to retard the formation of protectoid ferrite. (Fukui, Uehara & Isokawa, 1971) The effect of vanadium depends on the nitrogen content and the contents of other microalloying elements as free nitrogen will lead to formation of vanadium nitrides that decreases the effectiveness of vanadium with respect to hardenability by removing it from solid solution (Adrian, 2013). Adrian showed that microalloying with titanium, aluminium or zirconium promoted the hardenability effect of vanadium. Titanium is especially efficient because of its combining with nitrogen. Nickel has also been shown to improve hardenability (Yamada et al., 2014). However, the use of nickel is often restricted by its high price. Aluminium has also showed a hardenability improving effect in boron steels, due to aluminium nitride

formation (Habu, Miyata, Tamukai & Sekino, 2011). On the other hand, aluminium's tendency to form nitrides has been shown to reduce the secondary hardening effect of V-alloyed steels by hindering the formation of V(C,N) (Rothleutner & Tyne, 2014).

If the cooling rate is insufficient for transformation to martensite with the local hardenability of the austenite, transformation to different bainite and ferrite morphologies occur at various temperatures. The categorization of different bainite morphologies differs between researchers. One popular categorizing of bainite morphologies was performed by Zajac (Zajac, Schwinn & Tacke, 2005), see Table 1 and Fig. 4. Classification includes granular bainite, upper bainite, degenerated upper bainite, lower bainite and degenerated lower bainite. Zajac's classification is based on the morphology of the ferritic component, which can be irregular or lath-like, and the nature of the minor constituents. Lower bainite is similar to auto-tempered or tempered martensite due to its low transformation temperature. According to Zajac, in lower bainite, the cementite particles in the ferrite laths are parallel and inclined at 60° to the ferrite growth direction.

Table 1. Classification of bainite according to Zajac et al. (2005).

Classification	Ferrite morphology	Second phase type
Granular bainite	Irregular	Transformation product from carbon rich austenite: pearlite, cementite, bainite, MA, martensite.
Upper bainite	Lath-like	Coarse cementite precipitated into lath boundaries + finely dispersed intralath carbides.
Degenerated upper bainite	Lath-like	M-A microconstituents along lath boundaries.
Lower bainite	Lath-like	Cementite precipitated inside laths at 60° incline to lath direction
Degenerated lower bainite	Lath-like	Intralath M-A constituents

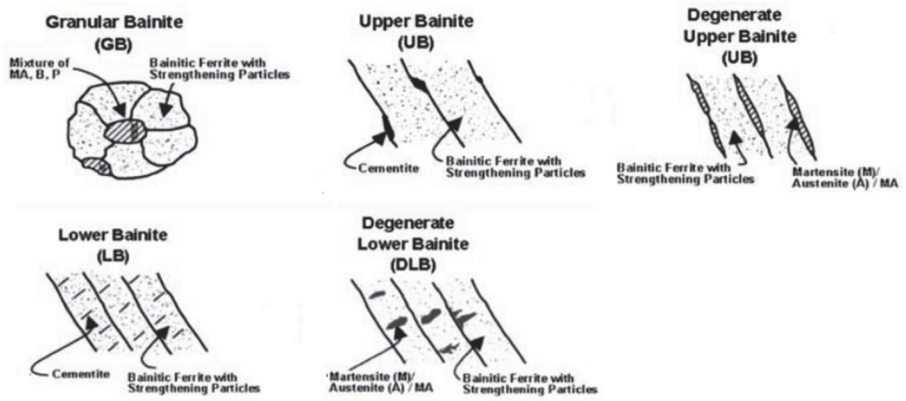

Fig. 4. Bainite morphologies classification according to Zajac et al. (Reprinted by permission from Zajac, et al. 2005 © Trans Tech Publications Ltd.).

The bainite committee of ISIJ categorizes the main microstructural components of bainite as given in Table 2. This is widely discussed in the review Publication by Krauss and Thompson (Krauss & Thompson, 1995).

Table 2. Classification of bainite according to Bainite committee of ISIJ. (Krauss & Thompson, 1995)

Classification	Morphology
Polygonal ferrite	Equiaxed grains and smooth boundaries.
Widmanstätten ferrite	Elongated ferrite crystals with dislocation substructure.
Quasi-polygonal ferrite	Ferrite grains with undulating boundaries, possible M-A constituents
Granular bainite	Granular shaped crystals with equiaxed M-A constituents.
Bainitic ferrite	Parallel ferrite laths, acicular M-A constituents between ferrite crystals
Dislocated cubic martensite	Highly dislocated lath-like morphology

In addition to microstructure, crystallographic texture is very important when considering properties such as strength and ductility. Texture leads to anisotropy in mechanical properties in the rolled material, e.g. different properties parallel to and transverse to the rolling direction.

For steels, when the texture formed in austenite during hot rolling affects the texture of the transformed martensite, bainite or ferrite. The transformed texture is

related to the texture of the parent material through the operation of the orientation relationship.

For body-centric cubic ferritic steels, the main texture fibres are alpha <110> parallel to the RD, gamma <111> parallel to the ND and epsilon <011> parallel to the TD. (Raabe, 2003). Using the orientation distribution function (ODF), these fibres and the main texture components can be efficiently presented using a φ_2 = 45° section (Fig. 5).

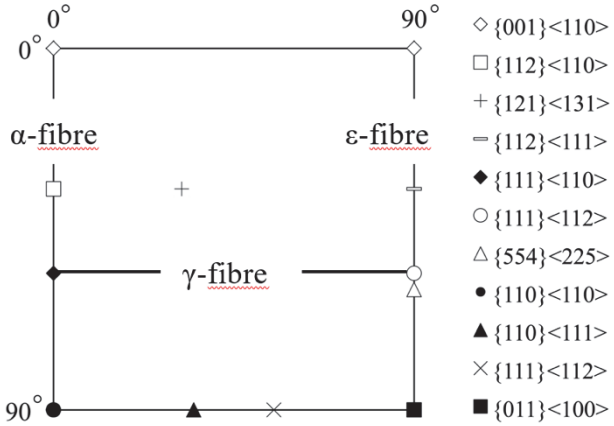

Fig. 5. The main texture components of the BCC structure in the φ2 = 45° ODF section (Reprinted by permission from Publication III © 2017 Elsevier Inc.).

According to Ray et al. (1994), if austenite is hot rolled above T_{nr}, the cubic texture {100}<001> of the recrystallized austenite is mainly transformed into the rotated cube {001}<110> component of the ferrite. If austenite, on the other hand, cannot recrystallize during hot rolling, which is the case for thermomechanically processed steels, the sharp austenite texture components Bs {110}<112>, Cu {112}<111> and S {123}<634>, and a weaker Goss {110}<001> are developed, and these lead to the major transformation textures {332}<113>, originating from Bs, and {113}<101>, originating from the austenite Cu component.

The hot rolling of austenite below T_{nr} will also lead to the formation of shear texture components near the rolled surfaces. These {111}<221> and {110}<112> components lead to the formation of the transformed shear components {112}<111>, {110}<112> and {110}<111>. High intensities of these components can be an indication of ferrite formation during rolling. This is well explained by Kaijalainen (A. Kaijalainen, 2016).

2.3 Strengthening mechanisms in high-strength steels

The strength of martensite is highly dependent on carbon content. As carbon content increases, the tetragonality, ultimate tensile strength and hardness of martensite increases nearly linearly (Krauss, 1995, 1999) as can be seen in Fig. 6. Even yield strength has a very strong correlation with carbon content even though there are other factors that affect the stress at which plastic yielding starts to take place. Factors such as grain size, residual stresses, dislocation structure as well as precipitates also affect the yield strength of martensitic or tempered martensitic microstructures (Young & Bhadeshia, 1994; Hutchinson, Lindell & Barnett, 2015). Often, as-quenched martensite has high hardness and strength but low toughness and tempering is then used to obtain adequate toughness (Caron & Krauss, 1972). However, recent studies have shown that low-carbon martensitic steels can have good toughness even in the as-quenched condition due to a refined austenite grain size and the low carbon content (A. Kaijalainen, 2016; Pallaspuro, 2018).

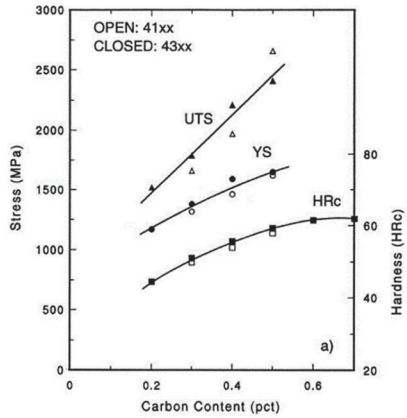

Fig. 6. Correlation between carbon content and both strength and hardness of as-quenched 41xx and 43xx steels (Reprinted by permission from Krauss 1999 © Elsevier Science S.A.).

Typically, strengthening mechanisms of steels are grouped into grain size strengthening, precipitation strengthening, dislocation strengthening and solid solution strengthening. However, the summation of these factors might not be straightforward especially when microstructures consists of multiple phases.

Young and Bhadeshia (1994) developed a model predicting the strength of bainitic-martensitic microstructures. They found that the highest level of yield

strength is obtained when the volume fraction of bainite is 20–30 %. This is due to bainite formation, which enriches the remaining austenite and subsequent martensite with carbon, thereby leading to increased strength. They factorized the strength of martensite + bainite mixtures as follows:

$$\sigma = \sigma_{Fe} + \sum_i \sigma_{SS}^i + \sigma_C + k_\epsilon(\bar{L}_3)^{-1} + \sigma_{ppt} + K_D\rho_d^{0.5} \quad (1)$$

The components in equation 1 are the strengthening contribution of pure iron (σ_{Fe}), the solid solution strengthening due to substitutional solute i (σ^i_{SS}), the solid solution strengthening contributed by carbon (σ_C), lath size strengthening $(k_\epsilon(\bar{L}_3)^{-1}$, precipitation strengthening (σ_{ppt}) and dislocation strengthening ($K_D\rho_d^{0.5}$).

According to Suikkanen (P. Suikkanen, 2009) the main strengthening mechanisms of low-carbon bainitic steels are grain size and dislocation strengthening. For low-C bainitic steels in Suikkanen's study, grain size and dislocation strengthening mechanisms accounted for 60–75% of the total yield strength. Suikkanen concluded that a notable part of the strengthening comes from low-angle boundaries, i.e. subgrain boundary strengthening. For as-quenched materials, solid solution strengthening played some role, but the precipitation strengthening contribution was rather small. However, for heat-treated materials, precipitation strengthening was important and provided 20–30% of the overall yield strength. In Suikkanen's microstructures, which included polygonal ferrite, quasi-polygonal ferrite, granular bainite and bainitic ferrite, the mechanical properties before and after heat treatments varied greatly. For example, the yield strength of microstructures including granular bainite and quasi-polygonal ferrite was increased and toughness was decreased by heat treatment, which was proposed to be due to precipitation increasing strength but reducing impact toughness. In the unheat-treated condition, bainitic ferrite obtained high strength and low toughness due to the presence of coarse M-A constituents. However, according to Suikkanen these constituents transform into spheroidized cementite and ferrite that improve the strength–-toughness combination after heat treatment.

Morito, Yoshida, Maki and Huang (2006) showed that the packet size of lath martensite scales with the prior austenite grain size and that decreased packet size leads to increased strength following a Hall-Petch type of behaviour. Takaki, Ngo-Huynh, Nakada and Tsuchiyama (2012) showed that there is a clear correlation between dislocation density and yield strength in lath martensite. Furthermore, Morito, Nishikawa and Maki (2003) showed a carbon content dependence of dislocation density in their XRD studies. Dislocation density increased with the carbon content up to 0.61 wt.% and decreased above that. Takaki et al. also noticed

that despite the fact that martensite has a very high ultimate tensile strength, the elastic limit of ultralow-carbon martensite is low. They proposed that the low elastic limit is due to the high level of mobile dislocations. Hutchinson, et al. (2015) also noticed that the initial yielding of martensite occurs at very low stresses leading to rounded stress - strain curves. They showed that this could be explained by the intragranular stresses resulting from the martensitic transformation leading to micro-yielding at very low externally applied stress. These internal stresses though can be reduced by tempering or plastic deformation.

Kennett (2014) proposed that yielding of martensite is primarily controlled by dislocation density and dislocation structure. According to his results, the primary stage of the yielding, i.e. micro-yielding, can occur at low stresses in as-quenched martensite, where the dislocation network is random and unpinned dislocations are mobile. However, as yielding continues, or during the high-temperature tempering, a dislocation cell structure forms leading closely spaced pinning obstacles for the dislocations. According to Kennett, this phenomenon during yielding leads to a high work hardening rate.

2.4 Tempering of as-quenched microstructures

According to Bhadeshia and Honeycombe (2006), the heating of as-quenched martensite leads to the following overlapping tempering stages.

- Stage 1: < 250 °C. Carbon segregation, ε-carbide formation, partial loss of tetragonality.
- Stage 2: 200–300 °C Decomposition of retained austenite.
- Stage 3: 200–350 °C. ε-carbide transforms into cementite and martensite loses its tetragonality.
- Stage 4: > 350 °C. Cementite spheroidizes and starts to coarsen. Ferrite recrystallizes.

Such descriptions of tempering stages in the literature are usually for medium and high carbon steels. For the steels in the scope of this thesis, i.e. low-C martensitic steels, ε-carbide formation is unlikely as is the presence of retained austenite. In fact, the main expected phenomenon in tempering at low-temperatures is the clustering of carbon leading to the pinning of dislocations, also known as the static aging phenomenon (Krauss, 1999, 2017). Furthermore, for low-C steels, as already presented, the formation temperature of martensite increases as carbon content decreases so that the level of autotempering, i.e. tempering occurring during

quenching, increases due to an increased mobility of carbon. (Bhadeshia & Honeycombe, 2006). This leads to carbon diffusion to dislocations and lath boundaries even during quenching when carbon content is low (< 0.20 wt.%) even for relatively fast quenching. According to Bhadeshia, cementite may be in the Widmanstätten form already after quenching, being typically 15 nm thick and 200 nm long. For higher carbon steel, these precipitates form at the sites of ε-carbides and boundaries before spheroidizing and coarsening at higher temperatures. For the materials in the present study (low-C high strength steels), autotempering is inevitable. Therefore, in addition to quenching and autotempering, the tempering phenomenon occurring in tempering stage 4 is the most important one. During this stage cementite first coarsens and later loses its needle-like morphology and becomes spheroidized (Bhadeshia & Honeycombe, 2006). The driving force for spheroidization is a decrease in total interfacial energy. Thermodynamically it is also more favourable that cementite precipitation and coarsening occurs at grain and lath boundaries. Baltazar Hernandez, Nayak and Zhou (2011) studied the tempering of dual phase steel in martensitic-ferritic microstructures. They tempered martensitic regions at 650 °C in isothermal and non-isothermal conditions and saw that isothermal holding provided spheroidized cementite structure compared to the quasi-spherical intralath and platelike interlath cementite of non-isothermal holding (Fig. 7). This is expected, though, as the peak temperature of the two tempering experiments was the same and the time at the peak temperature was shorter in the non-isothermal case. When comparing the tempering kinetics of isothermal and non-isothermal cases, the heating, holding and cooling stages must be considered. In such cases, the Hollomon-Jaffe tempering parameter can be used to help compare the isothermal and non-isothermal conditions. The Hollomon-Jaffe equation is:

$$P = T \times (log\, t + C) \tag{2}$$

where T is tempering temperature (K), t is the tempering time (h) and C is a material constant (Bhadeshia & Honeycombe, 2006). Furthermore, an integrated Hollomon-Jaffe parameter can be calculated using the method developed by Ulff. (Ulff, 1970) to take account the effects of the heating and cooling stages.

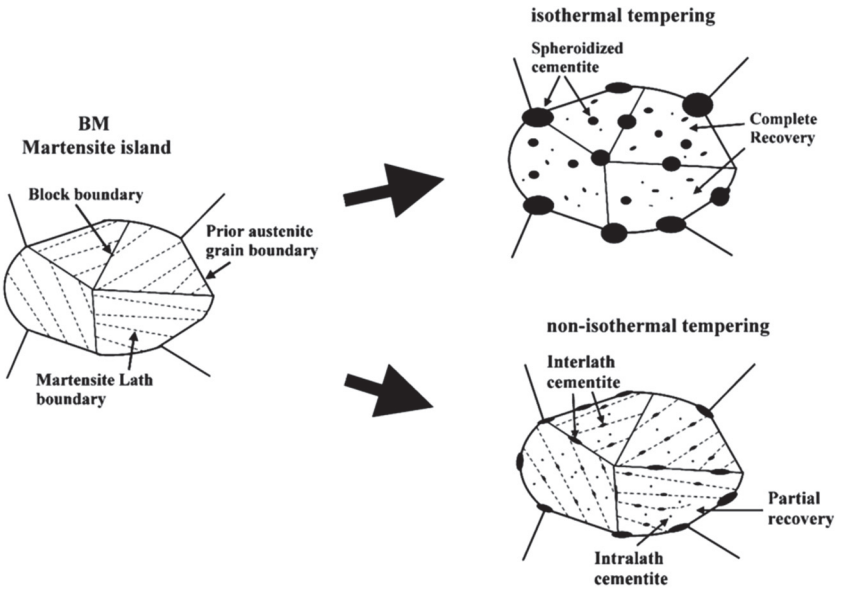

Fig. 7. Schematic presentation of cementite growth during high-temperature tempering according to Baltazar Hernandez et al. (Reprinted with permission Baltazar Hernandez, et al. 2011 © The Minerals, Metals & Materials Society and ASM International).

Similar findings have been made by the present author (Saastamoinen, Porter & Suikkanen, 2013) showing that non-isothermal holding seems to result in a slightly finer cementite structure despite higher tempering temperature and similar integrated Hollomon-Jaffe parameters. Biro, McDermid, Vignier and Norman (2014) also studied the cementite growth kinetics in isothermal and non-isothermal conditions and saw that hardness follows the Hollomon-Jaffe equation in both cases when the heating stage is considered in the equation. They also showed in their modelling that cementite growth and softening process could be divided into two stages: 1) carbide nucleation and 2) carbide coarsening. The first stage of this process occurred already at very short tempering times below 420 °C, which meant that cementite coarsening is the process controlling softening in high-temperature tempering (650 °C). However, with low-temperature tempering and non-isothermal holding, nucleation kinetics were considered important.

In addition to carbon content, many other alloying elements affect the properties of martensite by affecting the development of microstructure during slab reheating, thermomechanical processing and later heat-treating. The classical publication of Bain (Bain, 1939) describes the effects of the most important

alloying elements concerning heat treating. Vanadium (V) has been shown to be an effective carbide former during tempering even with low concentrations (Pacyna & Dabrowski, 2006). Excess titanium can also affect tempering behaviour. Excess titanium over stoichiometric ratio has shown to increase hardenability but also provide a secondary hardening effect and therefore increase hardness during high temperature tempering. (Shen & Hansen, 1997; Öhlund, Weidow, Thuvander & Offerman, 2014; Saastamoinen, Kaijalainen, Porter & Suikkanen, 2016). Furthermore, steels containing high concentrations of molybdenum, tungsten and chromium show good tempering resistance, i.e. retardation of softening. (Bain, 1939; Bhadeshia & Honeycombe, 2006) Molybdenum has also been shown to be beneficial for tempering resistance even in low concentrations (0.40 wt.%) (Bain, 1939; Saastamoinen et al., 2013). Alloying elements can affect strength after tempering through either carbide precipitation or solid solution strengthening of ferrite, as martensite transforms into ferritic during tempering. The most important alloying elements affecting tempering properties for low-alloyed high-strength steels are listed in Table 3.

Table 3. The effect of alloying elements on tempering resistance.

Element	Effect in LTT	Effect in HTT	Hardening mechanism	Reference
Si	Moderate hardening	Moderate hardening	Strengthening ferrite	(Bain, 1939)
Ni	No	Minor hardening	Strengthening ferrite	(Bain, 1939)
Mn	No	Very minor	Strengthening ferrite.	(Bain, 1939)
Cr	No	Strong	Precipitation hardening in high concentrations.	(Bain, 1939)
Cu	Minor	Strong	Precipitation hardening, solid solution strengthening.	(Dlouhy, Podany & Dzugan, 2019)
Mo	Mild	Very strong	Precipitation hardening in high concentrations	(Bain, 1939; Saastamoinen et al., 2013)
V	No	Moderate	Precipitation hardening	(Pacyna & Dabrowski, 2006)
Ti	No	Moderate	Precipitation hardening, recovery control	(Öhlund et al., 2014)

Element	Effect in LTT	Effect in HTT	Hardening mechanism	Reference
Nb	No	Moderate	Precipiation hardening	(Hulka, Kern & Schriever, 2005)

While cementite precipitation and growth from supersaturated ferrite might be the most obvious microstructural change during high-temperature tempering of martensite, it is not the only one. According to Kennett, Krauss & Findley (2015) the martensite laths remain stable up to 600 °C, but dislocation rearrangements occur at lower temperatures (200 °C). In addition to dislocation rearrangement, dislocation density decreases at the higher tempering temperatures (600 °C) due to recovery. (Kennett, Krauss & Findley, 2015; Shi et al., 2015). However, despite dislocation rearrangement, an actual decrease in the dislocation density did not happen at low tempering temperatures. Furthermore, Takebayashi, Kunieda, Yoshinaga, Ushioda and Ogata (2010) studied the dislocation structure at tempering temperatures in the range 180–650 °C for martensitic steel. They did not observe any dislocation rearrangement until the tempering temperature reached 350 °C. Furthermore, dislocation density did not decrease until higher tempering temperatures were used, i.e. 450–650 °C. This threshold level for a decrease in the dislocation density was also reported as 400 °C by Caron and Krauss (1972). Furthermore, another study focusing on dislocation structure of tempered martensite was done by Shi et al. (2015). Unlike the observations mentioned above, they did not find any changes in dislocation structure until the tempering temperature was raised to 400 °C. In tempering at 200 °C, no dislocation rearrangement occurred, but overall dislocation density was decreased according to them. They also proposed sub-grain coarsening due to the movement of dislocations when tempering above 400 °C. These mentioned studies are the main results presented in terms of dislocation density evolution in the tempering of martensitic steels. There are numerous reported attempts to use XRD to evaluate the dislocation density of martensite (Takebayashi, et al., 2010; Kennett, et al., 2015; Shi, et al., 2015). These methods are powerful, but the TEM method presented by Ham (1961) is the most accurate method tool for the determination of local dislocation densities. However, XRD can be a useful tool for comparing mean dislocation densities for different conditions.

Results above are mainly based on experiments using re-austenitized and quenched martensite. For direct-quenched martensite, similar studies have not been made and the effect of the finer grain size obtained via TMCP-DQ processing on the dislocation recovery kinetics is unknown. It is not clear how grain size and other

microstructural parameters affect tempering behaviour – especially as past tempering research has mainly focused on re-austenitized martensite.

While martensitic steels are the main group while considering tempering, other microstructures should also be considered. In such cases, the tempering temperature relative to the temperature at which the microstructure originally formed is important. Suikkanen (P. Suikkanen, 2009) studied the effect of heat treatment on low-carbon bainitic steels. He found that the M-A constituents in granular bainite transformed into cementite particles that were spheroidized in the heat treatment at 550–700 °C. However, precipitation hardening by the precipitation of Nb and Mo that occurred during the heat treatment was main factor that in fact lead to strengthening and eventually decrease in impact toughness. Garcia-Mateo, Peet, Caballero and Bhadeshia (2004) showed that the tempering of bainitic ferrite with a very fine lath structure for short times (< 1 h) at 400–550 °C only led to the precipitation of very fine precipitates. Tempering at 600 °C and above, however, with tempering periods of 1 h and above, led to a coarse precipitate structure that formed from carbon-rich thin austenite films.

As we can see, numerous factors affect microstructural transformation during quenching and tempering. Thermomechanical history prior to quenching and tempering, chemical composition, heat treatment parameters and microstructural features prior to tempering all affect the as-quenched microstructural details and therefore the tempering behaviour. As presented above, carbon content plays a significant role in auto-tempering and probably also affects the magnitude and distribution of residual stresses and dislocation density prior to tempering (Morito, et al., 2003; Hutchinson & Hagström, 2011; Suikkanen et al., 2013). Hutchinson et al. (2015) have also shown very well that the tempering of martensite possibly leads to increase in yield strength due to relaxation of residual stresses.

3 Experimental

3.1 Experimental materials

Experimental materials consisted of laboratory scale (Publication I) and pilot scale (Publications II–IV) thermomechanically processed and direct-quenched (TMCP-DQ) materials. In Publication IV, also re-austenitized, quenched and tempered equiaxed martensitic steel was manufactured in the laboratory.

Experimentally the thesis comprises two parts. In the first stage (Publication I) the effect of chemical composition on the properties of direct-quenched mainly martensitic steel was studied. This was to ensure a suitable tempering resistance of the steel and to develop a composition with a good strength–ductility combination for the later stages of the thesis. Based on the results from Stage 1, the composition was tailored for later wider studies focusing on thermomechanical treatment and tempering behaviour. A schematic illustration of the investigation strategy is presented in Fig. 8.

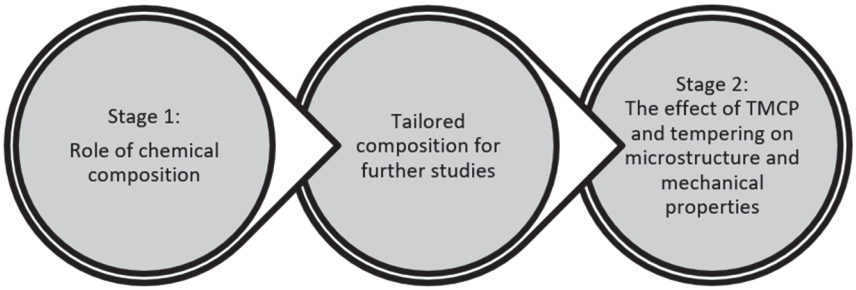

Fig. 8. Thesis flow chart.

Tempering trials in the thesis was simulations of tempering full-scale steel coils in batch annealing furnace, which has been seen as a potential application on promoting the productivity in the strip tempering process as a single tempering step. One part of the results that was not included in the original research Publications have also been included in the thesis. This includes a dilatometric hardenability investigation using a Gleeble 3800 and determination of CCT diagrams showing the combined effect of Ti, N and B on the hardenability of thermomechanically processed steel.

3.1.1 Experimental compositions

Chemical compositions were designed so that final yield strength of direct-quenched martensite would reach the level of 960 MPa. In Publication I, the effect of C, Ti, B and V was studied to see their effect on microstructure, mechanical properties and especially the tempering resistance of the direct-quenched state. Table 4 presents the experimental compositions used in Publication I.

Table 4. Experimental composition as in Stage 1 (Reprinted by permission from Publication I © 2019 Elsevier B.V.).

Composition	C	Si	Mn	Cr	Mo	V	Ti	B	Al	N	S	O
0.095C-0.08V-0Ti-15B	0.095	0.20	1.00	1.0	0.65	0.08	-	0.0015	0.030	0.004	0.006	0.004
0.095C-0.08V-0.025Ti-15B	0.095	0.20	1.00	1.0	0.65	0.08	0.025	0.0015	0.030	0.003	0.003	0.002
0.14C-0.08V-0Ti-15B	0.140	0.20	1.00	1.0	0.65	0.08	-	0.0015	0.030	0.003	0.003	0.002
0.14C-0V-0Ti-15B	0.140	0.20	1.00	1.0	0.65	-	-	0.0015	0.030	0.003	0.006	0.004
0.14C-0.08V-0Ti-0B	0.140	0.20	1.00	1.0	0.65	0.08	-	-	0.030	0.005	0.006	0.003

Based on the results of Stage 1 (Publication I), in Stage 2 (Publications II–IV) the experimental composition presented in Table 5 was designed with the aim of reaching the strength level of 960 MPa with high tensile ductility and adequate toughness after high-temperature tempering.

Table 5. Experimental composition used in Stage 2 (Publications II–IV) (Reprinted by permission from Publication II © 2018 Elsevier B.V.).

	C	Si	Mn	Al	V	Mo	Cr	Ti	B	N	S	T_{NR}
wt.%	0.095	0.2	1.0	0.03	0.08	0.63	0.98	0.012	0.0016	0.0053	0.0005	876 °C

Furthermore, to study the effect of Ti, N and B on hardenability, experimental compositions with varying contents of these elements were studied using a Gleeble 3800 thermomechanical simulator. The purpose of these experimental compositions was to systematically determine the combined effect of Ti/N-ratio

combined with B-alloying on hardenability of the direct-quenched steel. The compositions of these test materials are presented in Table 6.

Table 6. Composition design used for studying hardenability in direct quenching.

wt.%	C	Si	Mn	Al	Mo	Cr
Base composition	0.16	0.2	1.1	0.04	0.39	0.58
Studied elements	Ti	N	B	Excess N (ppm)	Excess Ti (ppm)	Ti/N-ratio
Ti-free B-free	-	0.0023	-	23	-	-
Ti-free	-	0.0029	0.0016	29	-	-
B+Ti – Low Ti/N	0.012	0.0046	0.0013	37		2.6
B+Ti - High Ti/N	0.029	0.0024	0.0017	-	208	12.1
B+Ti – Med Ti/N	0.011	0.0016	0.0016	-	21	4.2

3.1.2 Hot rolling trials

In Stage 1 (Publication I), the experimental steels were hot rolled using a 1 MN Carl Wezel laboratory hot rolling mill. Slab reheating of 55 mm thick ingots at 1225 °C was followed by hot rolling with a thermomechanical treatment giving a finish rolling temperature (FRT) of 800 °C and instant direct quenching (DQ) of 6mm strips. The target of the hot rolling schedule was to obtain a pancaked austenitic microstructure known to be beneficial for toughness (Kaijalainen, 2016; Pallaspuro, 2018).

In the experimental work done for the steels studied in Publications II and III, thermomechanical treatment was varied in pilot scale hot rolling trials to study the effect of FRT on microstructure and mechanical properties. Therefore, a total of three different types of thermomechanical treatments were used with varying FRTs in the range 775–915 °C prior to direct quenching (Table 7). In Stage 2, the slab reheating temperature was 1250 °C and slab thickness 210 mm. Based on the results from Publications II and III, a FRT of 915 °C was selected for the last stage (Publication IV) to study the effect of tempering variables on the microstructure and mechanical properties of thermomechanically hot rolled direct-quenched steel. Furthermore, in Publication IV, re-austenitized, quenched and tempered (RAQT) material was included in the test matrix to elucidate the microstructural and property differences between RAQT and DQT. The final strip thickness for all materials studied was 6 mm.

Table 7. Pilot scale hot rolling conditions.

Publication	Slab reheating temperature	Hot rolling conditions	FRT	Cooling rate
I	1225 °C	Laboratory hot rolling mill	800 °C	100 °C/s until M_s
II and III	1250 °C	Pilot scale direct-quenched	775, 865, 915 °C	70 °C/s
IV	1250 °C	Pilot scale direct-quenched and Re-austenitized martensite	915 °C + Re-austenitized (910 °C/30 min)	70 °C/s

3.1.3 Tempering trials

The tempering experiments in the thesis consisted of slow heating (30–35 °C/h) to some peak temperature and slow cooling (40 °C/h) to room temperature. In these slow tempering conditions, no soaking time at peak temperature was applied. The aim of the tempering strategy was to simulate the tempering procedure of full-scale steel coils tempered in a batch annealing furnace, which has been seen as a potentially efficient way of mass producing direct-quenched and tempered steels. In Publication I (see Table 8), the tempering conditions studied were low-temperature tempering (LTT) at 180 °C and high-temperature tempering (HTT) at 570 °C. For the experiments done in Publications II and III, a similar HTT procedure was performed with a peak temperature of 570 °C.

To evaluate the effectiveness of the slow tempering procedure, integrated Hollomon-Jaffe tempering parameters were calculated prior to the experimental work. The aim of this was to estimate the tempering parameter of slow process and the equivalent tempering conditions in faster tempering cycles. This can be integrated for non-isothermal conditions following the procedure of Ulff (1970). The integrated tempering parameter for the HTT experiments in Publication I, Publication II and Publication III (Table 8 and Table 9) is 17.37. This is equivalent to conventional tempering at 600–610 °C with a heating rate of 0.5–1.0 °C/s and a soaking time of 30 minutes.

Table 8. Tempering cycles as in Publication I (Reprinted by permission from Publication I © 2019 Elsevier B.V.).

Procedure	Condition prior to tempering	Peak temperature (°C)	Soaking time (min)
DQ+LTT	Direct-quenched	180	0
DQ+HTT	Direct-quenched	570	0

Table 9. Tempering cycle as in Publications II and III.

Procedure	Condition prior to tempering	Peak temperature (°C)	Soaking time (min)
DQ+HTT	Direct-quenched	570	0

Finally, to study the effect of tempering temperature over a wider range of temperatures, multiple tempering conditions were considered in Publication IV (Table 10). The aim of these experiments was to study the effect of tempering temperature in both LTT and various HTT conditions and to include the potential temper embrittlement temperature of 400 °C. Therefore, unfavorable tempering zones could be identified especially for toughness and bendability.

Table 10. Tempering trials in Publication IV.

Procedure	Condition prior to tempering	Peak temperature (°C)	Soaking time (min)
DQ+LTT	Direct-quenched	250	0
DQ+HTT	Direct-quenched	400, 500, 570, 600, 650	0
RAQ+HTT	Re-austenitized and quenched	570	0

3.1.4 Gleeble trials

To investigate the hardenability of compositions, continuous cooling transformation (CCT) diagrams were determined using dilatometric data obtained with Gleeble 3800 thermomechanical simulator. In the Gleeble, to simulate the conditions in thermomechanical treatment prior to direct quenching, the specimens were heated to 1100 °C at 20 °C/s, held for 4 minutes, cooled at 2 °C/s to 850 °C and held for 10 seconds, then given three compressions with a strain of 0.2 each and a strain rate of 1 s^{-1}. The compressions were performed with 25 second intervals. After the final compression, the samples were held at 850 °C for 25 seconds and cooled to room temperature with various cooling rates ranging from 1.5 to 96 °C/s.

The diameter of cylinder specimens was measured using a strain gauge during the compression tests and cooling. Specimens were later cut into half along the compression axis for hardness measurements and microstructural characterization. Using the dilatometric data obtained from the Gleeble and microstructural characterization, phase transformation temperatures and CCT diagrams were determined.

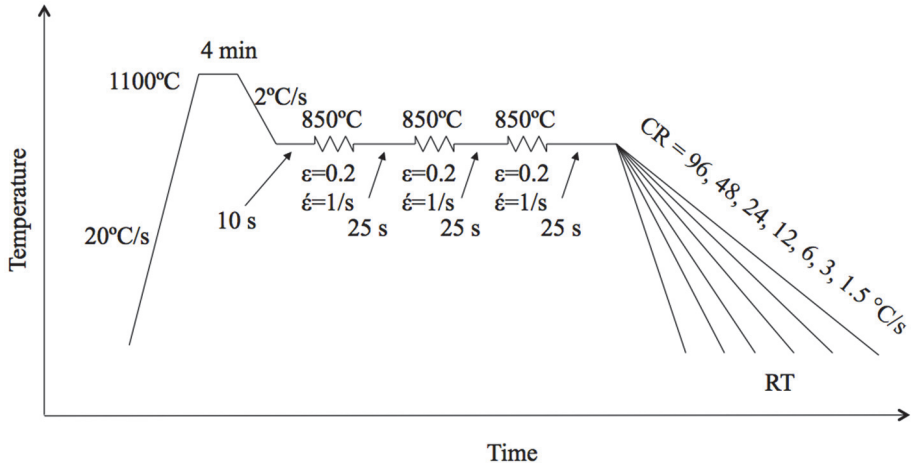

Fig. 9. Schematic presentation of the hardenability studies using a Gleeble 3800.

3.2 Research methods

3.2.1 Mechanical testing

Tensile tests for all test materials were conducted at room temperature with a gauge length of 50 mm in accordance with the European standard EN 10002 using flat 6 x 20 x 120 mm^3 specimens. In results presented in Publication I, the samples were cut along the rolling direction (RD). In later work, conducted in Publications II–IV, tensile specimens were cut both parallel to the RD and perpendicular to the RD.

Charpy-V experiments with sub-sized 6 mm specimens were conducted at various temperatures to determine the transition curves and 28J transition temperature (T28J). In Publication I, tests were conducted with specimens parallel to RD. In Publication II, impact tests were conducted transverse to RD and, to summarize the results in Publication IV, both parallel and perpendicular to RD. To

determine the T28J values and 95% confidence intervals, the tanh-fitting described by Oldfield (1975) using the procedure described by EricksonKirk, EicksonKirk, Rosinski and Spanner (2009) was used.

As Charpy-V specimens were sub-sized (6 mm), the impact energies are not equivalent to normal sized specimens (10 mm). To convert sub-sized T28J values to full sized equivalent, the method presented by Wallin (Wallin, 1986, 2011) was used.

In Publication III, microhardness indentation was used to study the potential existence and thickness of a soft ferritic surface layer below the top surface of the strip. Microhardness indentation profiles were performed using a CSM microhardness tester with a 1 N load from positions located between 50 and 400 μm below the strip top surface with an average of 10 indentations. Reference values were also measured from the centreline of the steels.

3.2.2 Minimum bending radius

In Publications III and IV, the effect of thermomechanical treatment and tempering on bendability was studied using 3-point bending tests on an Ursviken Optima 100 bending machine. For 6 x 300 x 300 mm^3 specimens 90° bending angle was used to determine the minimum usable bending radius relative to the sheet thickness (R/t). Tests were done both parallel and perpendicular to RD (Fig. 10) with a die opening width of 75 mm and varying punch radius. The quality of the bent surface was analysed after the test, as described by Heikkala & Väisänen (2012).

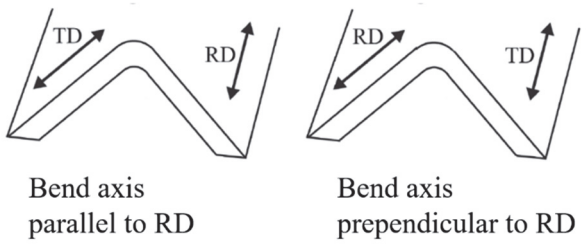

Fig. 10. Schematic illustration of bend axis according to Kaijalainen (2016) (Reprinted by permission from Kaijalainen © 2016 Acta Universitatis Ouluensis).

3.2.3 Microstructural characterization

During the course of the thesis work, numerous material characterization techniques were used to study the experimental materials.

Transformed microstructures and precipitation behaviour

Light optical microscopy (OM) and laser scanning confocal microscopy (LSCM) were used in Publications I-III to determine the effect of FRT and chemical composition on prior austenite grain structure from picric acid etched samples. Austenite grain sizes were then determined using the mean linear intercept method on the RD-ND plane, where ND refers to the plate normal direction. In addition to grain size, the grain morphology parameters presented in Table 11 were calculated. For some of the steels, it was very difficult to reveal the prior austenite grain size in this way, therefore the EBSD-based method of Nyyssönen, Isakov, Peura and Kuokkala (2016) was also used. The MTEX algorithm of Nyyssönen et al. (2016) reveals the grain boundaries of the parent austenite based on the orientation relationship between martensite and the prior austenite.

Table 11. Calculated austenite grain morphology parameters (Reprinted by permission from Publication I © 2019 Elsevier B.V.).

Parameter	Equation
Aspect ratio, r	$r = \bar{L}_{RD} / \bar{L}_{ND}$
Total reduction, R_{tot} (%)	$R = 1 - \sqrt{(1/r)}$
Surface area per unit volume (mm^2/mm^3)	$S_{V(g.b.)} = 0.429(N_L)_{RD} + 1.571(N_L)_{ND}$

L_{RD} is the mean linear intercept along RD, L_{ND} is the mean linear intercept along ND, r is the aspect ratio, R_{tot} is the total reduction below the recrystallization temperature and S_V is the grain boundary area per unit volume.

General material phase characterization was performed using OM, LSCM and field-emission scanning electron microscopy (FESEM) on a Zeiss Sigma and a Zeiss Ultra Plus. During the FESEM work, secondary electron imaging, back scattered electron imaging and In-lens imaging was used. Microstructural analysis

was performed in both the bulk of the material, at the quarter-thickness position, and just below surface of the strip with Nital etched specimens.

Electron backscattering diffraction studies

In all Publications, electron backscatter diffraction (EBSD) was performed. Lath size (dl) and grain size (d) were determined as equivalent circle diameter (ECD) values of subgrains surrounded by low-angle (2.5–15°) boundaries and grains surrounded by high-angle (>15°) boundaries, using AztecHKL acquisition and analysis software in Publications II, III and IV and EDAX acquisition and analysis software in Publication I. The FESEM for the EBSD measurements was made using an accelerating voltage of 15 kV and a step size of 0.2 μm for a total area of 80 x 360 μm to obtain a large area representative of the whole microstructure.

TEM

In Publication I, transmission electron microscopy (TEM) was used to study the precipitate sizes of direct-quenched and high-temperature tempered martensite using carbon extraction replicas.

In Publication II, TEM was also used to study the effect of thermomechanical treatment and tempering on the dislocation networks of direct-quenched martensite. In the TEM studies, dislocation networks in thin foil specimens were analysed both visually and by calculating the intra-lath dislocation density with the equation proposed by Ham (1961):

$$\rho = 2N / Lt \qquad (3)$$

where ρ is dislocation density, N is the number of intersections made by lines with a total length L and t is the foil thickness, which was calculated from

$$t = \lambda \ln (I_t / I_0) \qquad (4)$$

where λ is the mean free path for inelastic scattering, I_0 is the number of electron in the zero-loss peak and I_t is the number of electrons in the total electron energy loss spectrum. Dislocation densities were calculated using lines drawn parallel to the lath centrelines. Thin foils for TEM studies were prepared using twin-jet electropolishing at 25 V at 10 °C using 10 vol.% perchloric acid and 90 vol.% acetic acid. Throughout the research, TEM investigations were carried out using the g-vector type <110>. This gave the best contrast when studying the dislocations.

X-Ray diffraction line broadening analysis

X-Ray diffraction line broadening studies in Publications II–IV were carried out using Cu Kα radiation on a Rigaku SmartLab 9 kW X-ray diffractometer. The presence of dislocations affects the both crystallite size and strain broadening and therefore XRD peak analysis can be used for estimating dislocation density. However, simplifications are necessary and therefore quantification can contain systematic errors. The analyses in this study were done with the aim of seeing the relative effects of different tempering conditions on dislocation density, and here the XRD based technique was useful due to its power to average over relatively large volumes of material.

In present study, coupled 2theta-omega scans were executed and PDXL2 analysis software was used to estimate the lattice parameters, microstrains and crystallite sizes of the experimental steels with Rietveld refinement. Furthermore, dislocation densities were calculated using the method presented by Williamson and Hall (1953) and Williamson and Smallman (1956):

$$\rho = \sqrt{\rho_s \rho_p} \tag{5}$$

where ρ_s is dislocation density calculated from strain broadening and ρ_p is dislocation density calculated from particle i.e. crystallite size, see equations 6-7 according to Williamson and Smallman (1956):

$$\rho_s = (k\,\varepsilon^2)/(F\,b^2) \tag{6}$$

and

$$\rho_p = 3n/D^2 \tag{7}$$

where ε is microstrain, b is the Burgers vector, F is an interaction factor assumed to be 1, factor k is taken as 14.4 for body-centred cubic metals and D is crystallite size. In the equation n is dislocations per block face, assumed to be 1. This assumption is based on Williamson and Smallman (1956), as they state and assume that the metal is broken up into blocks and the dislocations are lying in the boundaries between the blocks. Therefore, the value 1 can be used as an assumption, which will lead to the minimum dislocation density.

XRD studies were performed on EBSD polished (colloidal silica) surfaces at either the quarter thickness of the strip (Publication II) or 150 µm below the top surface (Publications III and IV). The quarter-thickness measurements were conducted to obtain data to compare with data from TEM measurements and

provide correlations with general mechanical properties. Surface dislocation density was selected as a point of interest due to its influence on surface properties and therefore, potentially, the bendability of the strip.

The approach of Williamson and Smallman (1956) in XRD-based dislocation density experiments is based on models that are believed to give inexact values. It is also based on assumption that dislocation structure is random, therefore providing only approximate values. Therefore, Publication III compares the absolute dislocation density values calculated from TEM thin foil images with those obtained with the XRD method. Later due to its powerfulness, the XRD method is mainly used to compare the experimental steels with each other rather than to claim them to be absolute values.

Microstructural simulations

JMatPro® material simulator software was used to study the type, size and fraction of precipitates forming during high-temperature tempering of martensite were calculated.

4 Results

4.1 Role of chemical composition on direct-quenched and tempered steels

Publication I examined the role of chemical composition on the microstructure, mechanical properties and tempering resistance of direct-quenched and tempered steels. In addition to the results presented in Publication I, results obtained from Gleeble hardenability studies are included here.

4.1.1 Hardenability and microstructure

CCT-diagrams based on thermomechanical simulations for compositions presented above in Table 6 using a Gleeble are presented in Fig. 11. CCT-diagrams show the effect of low Ti/N (2.6), mid Ti/N (4.2), high Ti/N (12.1), Ti-free B-alloyed and Ti-Free B-free compositions. This way the effect of both excess nitrogen and excess titanium over stoichiometric ratio on hardenability can be studied as well as the difference between B-alloyed and B-free compositions when formation of BN is not protected with titanium. The diagrams show that Ti and N play an important role in retaining hardenability and achieving fully martensitic microstructures. Regardless of whether the material is B-alloyed or B-free, hardenability is poor when titanium is either missing or below the stoichiometric Ti/N-ratio for the formation of TiN (3.42). The results also show that when the Ti/N-ratio reaches the stoichiometric value, the B-alloyed steels improve their hardenability remarkably and the critical cooling rate for 100% martensite changes from 96 °C/s to 48 °C/s. However, excess titanium over the stoichiometric ratio provides no further improvement in hardenability.

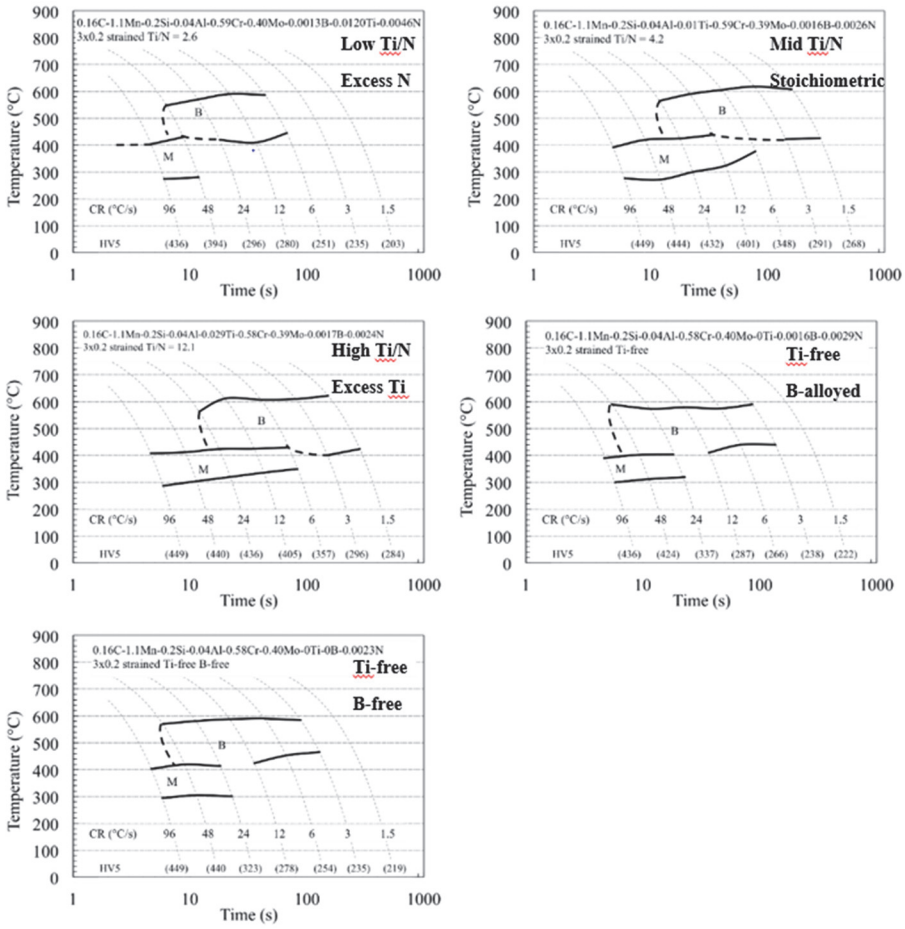

Fig. 11. The effect Ti, N and B on hardenability of TMCP processed steel. Excess Ti do not improve hardenability. Excess N deteriorates hardenability of B-alloyed steel.

In Publication I, the effect of chemical composition (Table 4) on austenite grain structure prior to and after thermomechanical treatment and direct quenching was investigated with varying C, B, Ti and V contents. Table 12 and Fig. 12 show that austenite grain size during slab annealing at 1225 °C is highly dependent on the titanium content. However, Ti-alloyed steel also showed signs of abnormal grain coarsening, i.e. the formation of some very coarse grains in a matrix of very fine grains. Table 13 shows austenite grain structural parameters after thermomechanical treatment and direct quenching. The importance of titanium in

overall grain size control is apparent as the Ti-alloyed variant has a significantly finer grain size also after thermomechanically controlled processing and direct quenching.

Table 12. The role of chemical composition on austenite grain size during slab annealing prior to hot rolling (Reprinted by permission from Publication I © 2019 Elsevier B.V.).

Composition	Matrix grain size (μm)
0.095C-0.08V-0Ti-15B	132 ± 19
0.095C-0.08V-0.025Ti-15B	44 * ± 3
0.14C-0.08V-0Ti-15B	189 ± 26
0.14C-0V-0Ti-15B	183 ± 26
0.14C-0.08V-0Ti-0B	157 ± 20

* Bimodal grain structure including coarse grains in fine matrix (size of the smaller, matrix grains given)

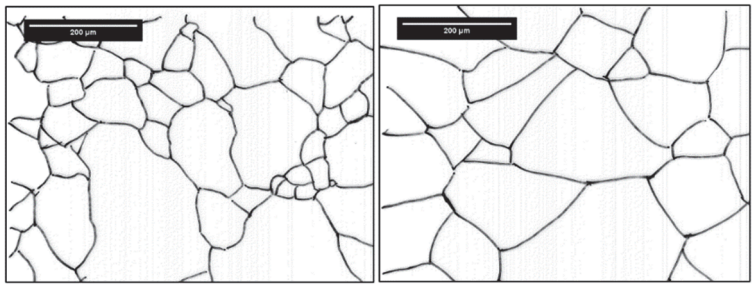

a b

Fig. 12. Austenite grain structure after slab annealing at 1225 °C for 2 h in (a) Ti-alloyed and (b) Ti-free composition. Reprocessed after optical microscope for image quality (Reprinted by permission from Publication I © 2019 Elsevier B.V.).

Table 13. Prior austenite grain size and morphology after thermomechanical treatment and direct quenching (Reprinted by permission from Publication I © 2019 Elsevier B.V.).

Composition	PAGS, ECD (μm)	R_{tot} (%)	S_V (mm^2/mm^3)
0.095C-0.08V-0Ti-15B	18.8	62	235
0.095C-0.08V-0.025Ti-15B	8.9	64	505
0.14C-0.08V-0Ti-15B	22.3	59	183
0.14C-0V-0Ti-15B	17.3	62	251
0.14C-0.08V-0Ti-0B	18.6	54	193

The microstructures of the thermomechanically processed and direct-quenched experimental steels with cooling rate approximately 100 °C/s are presented in Table 14. Microstructural characterization showed that the 0.14C steel with both B and V additions was the only fully martensitic steel. The V-free 0.14C steel contained a very small fraction of ferrite as did the Ti-alloyed 0.095C steel. The Ti-free 0.095C steel as well as the Ti- and B-free 0.14C steel on the other hand had a considerable amount of ferrite in the microstructure. The martensitic regions in all the steels are mainly autotempered (Fig. 13).

High-temperature tempering of these as-quenched compositions revealed only minor differences in the microstructural changes occurring in the different compositions. The main microstructural change detectable in FESEM images was the formation of coarse cementite in the martensitic regions (Fig. 14). Publication I also reported the properties of LTT steels in similar as-quenched materials but microstructurally, only carbon segregation is expected at the LTT temperature, i.e. 180 °C, as carbon content is too low for potential transition carbide formation.

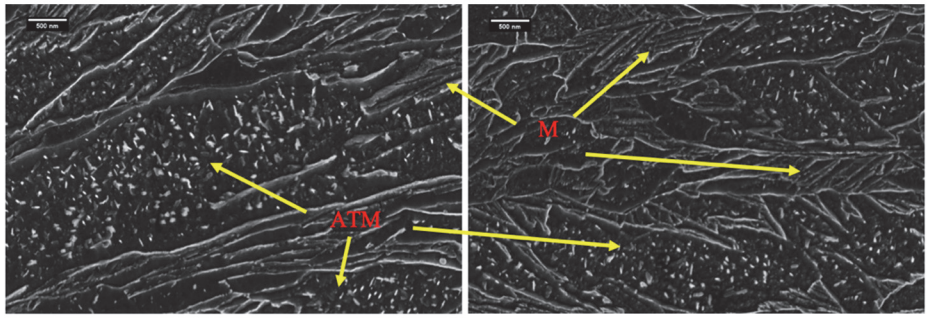

Fig. 13. FESEM In-lens images of (a) 0.095C-0.08V-0Ti-15B and (b) 0.14C-0.08V-0Ti-15B experimental steels in the direct-quenched and severily autotempered condition (Reprinted by permission from Publication I © 2019 Elsevier B.V.).

Table 14. Microstructures of the experimental steels in Publication I (Reprinted by permission from Publication I © 2019 Elsevier B.V.).

Material	As-quenched microstructure	frac α_m	frac α_f
0.095C-0.08V-0Ti-15B	M/ATM+F	0.89	0.11
0.095C-0.08V-0.025Ti-15B	M/ATM+F	0.94	0.06
0.14C-0.08V-0Ti-15B	M/ATM	1.00	0.00
0.14C-0V-0Ti-15B	M/ATM+F	0.96	0.04
0.14C-0.08V-0Ti-0B	M/ATM+F	0.88	0.12

TEM extraction replica studies were performed for selected specimens to obtain a general view of the existing carbide network. Analysis showed that high-temperature tempered materials have carbide networks mainly consisting of coarse Fe_3C particles as seen in the TEM extraction replica image of 0.095C-0.08V-0.025Ti-15B HTT condition (Fig. 14). Typically, carbides reach sizes up to 200 nm in length and approximately 50 nm in width and are semi-spheroidized. Replica studies in this Ti-alloyed composition also showed the presence of coarse titanium carbonitrides.

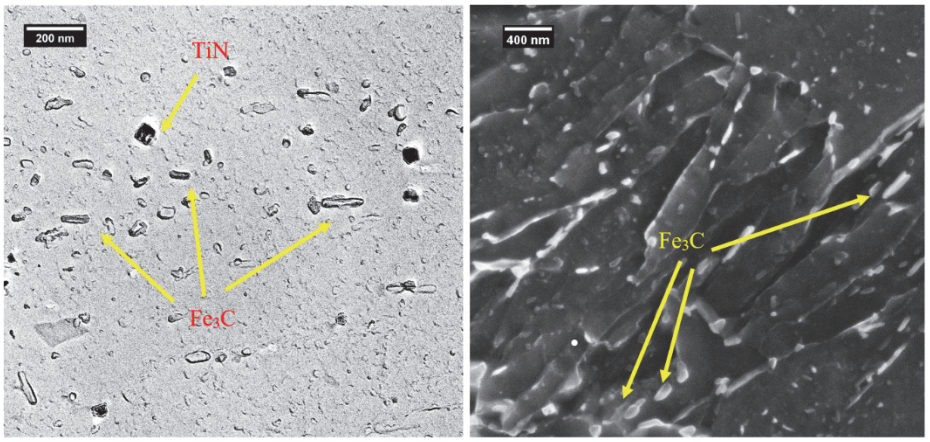

Fig. 14. (a) showing TEM extraction carbon replica image from 0.095C-0.08V-0.025Ti-15B HTT condition and (b) FESEM In-lens image from similar condition (Reprinted by permission from Publication I © 2019 Elsevier B.V.).

The above observations are generally in line with the results of calculations made using JMatPro® software (Fig. 15). They show that for the current tempering conditions and test compositions, two main types of precipitates are expected after tempering martensite at 570 °C: M_3C type with an equivalent circle radius of 100-120 nm and a volume fraction of 1.1%, and M_7C_3 type with an equivalent circle radius of 25 nm and a volume fraction of 0.5%. TEM and FESEM studies showed that the sizes of the coarser carbides, i.e. cementite, is generally very close to those predicted by JMatPro.

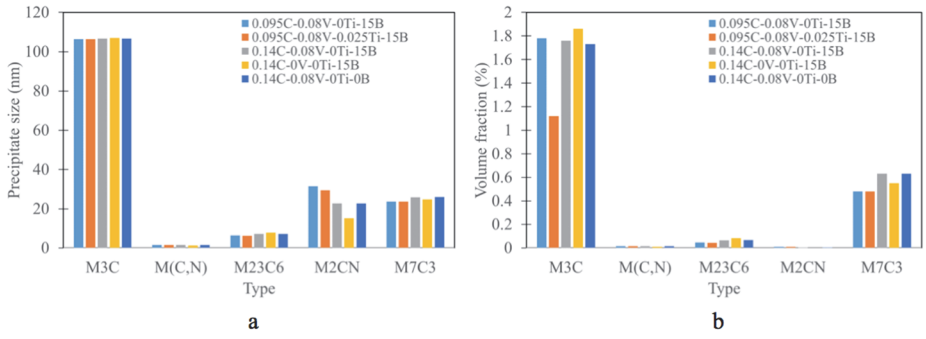

Fig. 15. Carbide size simulations calculated using JMatPro showing the size (a) and volume fraction (b) distributions (Reprinted by permission from Publication I © 2019 Elsevier B.V.).

Fig. 16 shows ECD sizes for grains surrounded by low-angle (> 2°) and high-angle (> 15°) boundaries, together with the ECD value of the 90th percentile in the cumulative grain area distribution ($d_{90\%}$) as determined from EBSD analyses. Chemical composition has a clear influence on $d_{90\%}$, i.e. the grain size of the coarsest grains. The additions of Ti and carbon and the removal of boron all refine $d_{90\%}$.

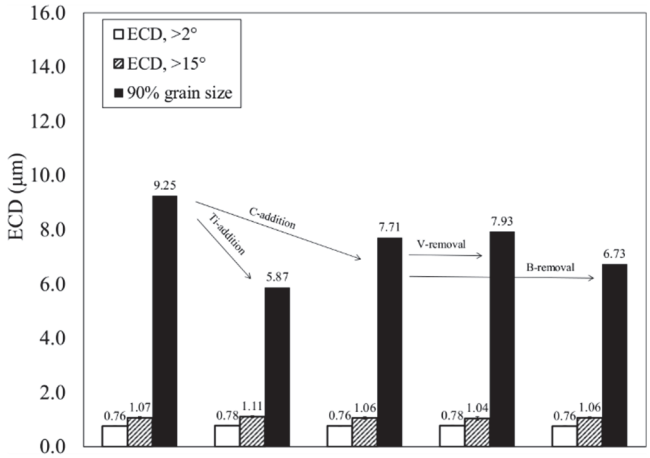

Fig. 16. Low-angle, high-angle and cumulative 90% high-angle ($d_{90\%}$) grain sizes for materials in Publication I (Reprinted by permission from Publication I © 2019 Elsevier B.V.).

4.1.2 Mechanical properties

Table 15 shows the effect of chemical composition on tensile properties and Charpy V 28 J transition temperatures both in the DQ condition and after tempering at low and high temperatures as studied in Publication I. Vanadium microalloying retards the softening of the direct-quenched conditions during high-temperature tempering at a significant rate: alloying of only 0.08% V leads to a 100 MPa UTS difference and 70 MPa YS difference after HTT compared to the V-free composition. However, softening also leads to increased toughness; the V-alloyed HTT composition with higher UTS has an almost 50 °C higher 28J transition temperature (T28J) than the V-free steel. Such differences are not seen in the low-temperature tempered condition. Excess titanium over the stoichiometric ratio, however, did not improve high-temperature tempering resistance as expected. The Ti-alloyed steel obtained higher strength, but this was most likely due to improved hardenability and a lower amount of ferrite in the structure.

High carbon content combined with vanadium and boron microalloying lead to the highest strengths but lowest toughness. High-temperature tempered 0.14C-0.08V-0Ti-15B steel obtains very poor toughness compared to the other compositions. Removal of either boron, titanium or vanadium as well as the lowering of carbon content lowered T28J, i.e. improved the toughness.

The results also showed that low-temperature tempering leads to higher yield strengths than obtained in the direct-quenched state, although ultimate tensile strength remains nearly unchanged. However, as the yield strength increased, the toughness and tensile ductility decreased as a result of low-temperature tempering.

The results in Publication I showed no improvement in absolute toughness after either low-temperature or high-temperature tempering. However, when comparing toughness at a certain strength level, the situation is different. In fact, as can be seen in Fig. 17, tempering either at high or low temperature leads to better 28J transition temperature at a given strength level. What is surprising though, is the fact that both the HTT and LTT conditions show remarkably similar correlations between yield strength and toughness.

The data in Fig. 17 imply that T28J correlates with yield strength and whether or not the material is tempered. After experimenting with multiple possible regression analyses, the following simple equation was obtained for T28J:

$$T28J(°C) = -32.0 \times Tempering + 0.48 \times YS - 535.4 \quad (8)$$

where *Tempering* is 1 for the HTT and LTT conditions and 0 for the DQ condition and *YS* is yield strength in MPa. R^2 for the equation is 0.9348.

Table 15. Mean yield strength (YS), ultimate tensile strength (UTS), total elongation, uniform elongation and 28J transition temperatures including 95% confidence intervals. Yield strength (YS) refers to the stress for 0.2% plastic strain (Reprinted by permission from Publication I © 2019 Elsevier B.V.).

	YS (MPa)	UTS (MPa)	A (%)	A_{gt} (%)	T28J (°C)
			DQ		
0.095C-0.08V-0Ti-15B	908 ± 13	1226 ± 9	12.1 ± 0.4	5.0 ± 0.1	-103 (-130…-92)
0.095C-0.08V-0.025Ti-15B	953 ± 0	1264 ± 8	12.5 ± 1.5	4.7 ± 0.1	-74 (-106…-60)
0.14C-0.08V-0Ti-15B	1011 ± 0	1404 ± 8	11.4 ± 0.4	4.8 ± 0.4	-50 (-75…-26)
0.14C-0V-0Ti-15B	1000 ± 15	1384 ± 9	11.8 ± 1.7	4.8 ± 0.2	-56 (-68…-45)
0.14C-0.08V-0Ti-0B	968 ± 28	1351 ± 48	12.1 ± 1.5	4.7 ± 0.8	-98 (-132…-52)
			DQ-T 180 °C (LTT)		
0.095C-0.08V-0Ti-15B	1027 ± 9	1237 ± 11	11.1 ± 1.2	3.9 ± 0.1	-76 (-99…-53)
0.095C-0.08V-0.025Ti-15B	1051 ± 9	1247 ± 11	11.5 ± 0.1	3.7 ± 0.2	-65 (-84…-46)
0.14C-0.08V-0Ti-15B	1113 ± 8	1387 ± 4	11.2 ± 0.2	3.8 ± 0.2	-36 (-53…-20)
0.14C-0V-0Ti-15B	1093 ± 21	1377 ± 3	11.4 ± 1.7	4.2 ± 0.4	-39 (-58…-38)
0.14C-0.08V-0Ti-0B	1044 ± 8	1310 ± 22	11.7 ± 0.2	4.2 ± 0.3	-73 (-88…-58)
			DQ-T 570 °C (HTT)		
0.095C-0.08V-0Ti-15B	1027 ± 17	1081 ± 12	15.9 ± 0.9	5.4 ± 0.7	-79 (-105…-54)
0.095C-0.08V-0.025Ti-15B	1085 ± 1	1128 ± 6	16.3 ± 1.0	5.2 ± 0.7	-54 (-75…-33)
0.14C-0.08V-0Ti-15B	1093 ± 2	1163 ± 2	13.7 ± 1.1	4.7 ± 0	-33 (-59…-7)
0.14C-0V-0Ti-15B	1021 ± 24	1063 ± 25	15.3 ± 1.1	5.6 ± 0.1	-80 (-96…-65)
0.14C-0.08V-0Ti-0B	1036 ± 47	1112 ± 30	14.4 ± 0.3	5.4 ± 0.1	-60 (-84…-38)

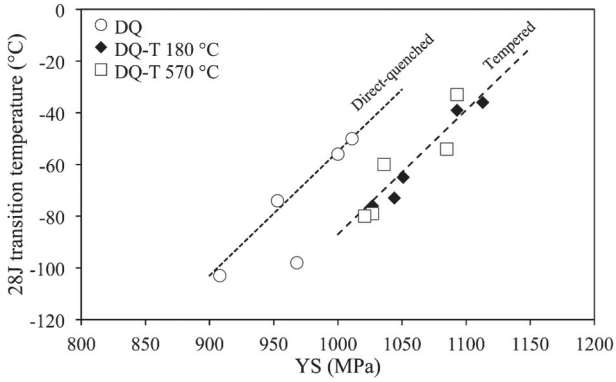

Fig. 17. Correlation between yield strength and Charpy V 28 J transition temperature. Dashed lines show T28J predicted with regression analysis (Reprinted by permission from Publication I © 2019 Elsevier B.V.).

Even though tempering shows improvement on toughness only at a given strength level, the tensile ductility shows great improvement after high-temperature tempering treatment. High-temperature tempering provides remarkable improvement in tensile ductility as can be seen in the YS-A_5 and YS-A_g plots in Fig. 18. HTT is especially beneficial for post-uniform-elongation at a given strength level.

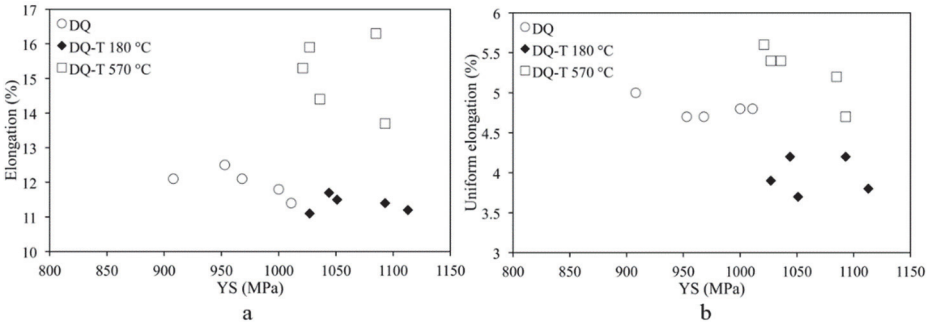

Fig. 18. Total elongation (a) and uniform elongation (b) as a function of yield strength in different tempering conditions (Reprinted by permission from Publication I © 2019 Elsevier B.V.).

4.2 Thermomechanical treatment and tempering

Publications II and III focus on the synergic effect of thermomechanical treatment on a pilot scale mill and tempering on the microstructure of direct-quenched high strength steel Ti-V microalloyed 0.095C steel. In Publication II, the effect of thermomechanical treatment on mechanical properties and microstructure at the quarter-thickness position. In Publication III, the effect of thermomechanical treatment and tempering on surface microstructure and bendability was studied.

4.2.1 Microstructure

Fig. 19 and Table 16 demonstrate the significant effect of thermomechanical treatment on the prior austenite grain structure. The material with the highest FRT (915 °C) had clearly less elongated austenite grains, i.e. there was more recrystallization during rolling, than in the other materials. The materials with lower FRT, i.e. Fig. 19a and Fig. 19b show that materials have clearly been thermomechanically processed below T_{NR}. Grain sizes determined with the mean linear intercept method (Table 16) show that grain boundary area increases as rolling procedure moves clearly below T_{NR}. However, in the case of FRT 775 °C the deformation temperature was sufficiently low to initiate ferrite formation either during deformation or subsequent quenching as can be seen from the white carbon-free areas. In fact, grain boundary area does not increase any more when lowering FRT from 865 ℃ to 775 ℃. Fig. 19c also shows that, even in the case of FRT 915 °C, the prior austenite grain structure is elongated, indicating that 915 °C is below the actual recrystallization temperature for the rolling conditions used.

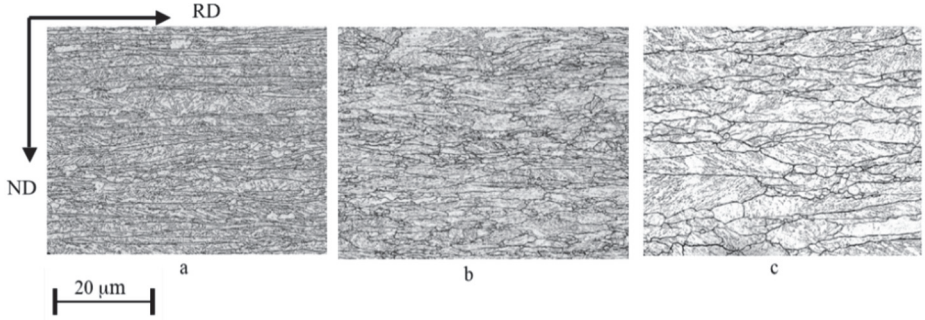

Fig. 19. Austenite grain morphology of FRT 775 °C steel (a), FRT 865 °C steel (b) and FRT 915 °C steel (c). Steel with a low FRT contains areas of ferrite. After picric acid etching (Reprinted by permission from Publication II © 2018 Elsevier Inc.).

Table 16. Austenite grain size parameters (Reprinted by permission from Publication II © 2018 Elsevier Inc.).

Material	LL_{RD} (μm)	LL_{ND} (μm)	R_{tot} (%)	S_V (mm^2/mm^3)
FRT 775 °C	27.5	2.5	70	475
FRT 865 °C	23.5	2.5	67	492
FRT 915 °C	18.5	3.6	56	377

The FESEM In-lens images in Fig. 20 show the effect of thermomechanical treatment on the microstructure of both the direct-quenched and direct-quenched and tempered (570 °C) conditions as studied in Publication II. While higher FRTs resulted mainly in martensitic microstructures, actually auto-tempered martensitic structures, the steel with the lowest FRT (775 °C) mainly consists of polygonal ferrite and granular bainite with some martensite. The two higher FRTs contained only minor fractions of other transformation products, which were mainly upper bainite. For mainly martensitic starting conditions, typical cementite coarsening occurred after HTT mainly on lath and grain boundaries. However, the FRT 775 °C steel also underwent clear cementite precipitation during tempering despite its microstructure consisting of ferrite and granular bainite. Naturally, ferritic regions stayed unchanged during tempering but strong precipitation occurred in granular bainitic regions. However, in contrast to the martensitic cases, all precipitation occurs on grain boundaries as martensite lath boundaries are rare in this condition.

Dislocation densities measured with TEM and estimated using the Williamson-Smallman method from XRD peak broadening are presented in Table 17 and Table 18. In general, TEM studies showed more moderate dislocation density compared to Williamson-Smallman method. Generally, dislocation density decreased during tempering. The only case that differed from this trend was the dislocation density in the FRT 775 °C steel measured with TEM. This is probably explained by the large uncertainty in the results due to mainly ferritic-bainitic microstructure and difficulty to measure martensite dislocation density.

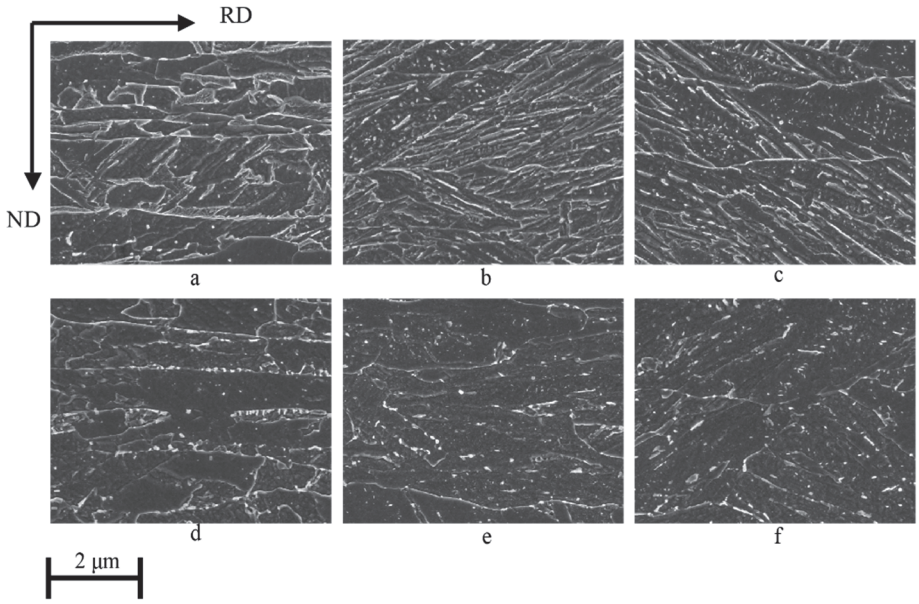

Fig. 20. DQ microstructures for FRT 775 °C (a), 865 °C (b) and 915 °C (c), and DQ-T (tempered at 570 °C) microstructures for FRT 775 °C (d), 865 °C (e) and 915 °C (f). Quarter-thickness position in all cases (Reprinted by permission from Publication II © 2018 Elsevier Inc.).

TEM studies also showed moderate dislocation cell network formation (Fig. 21). The direct-quenched conditions show very random dislocation structures while after tempering at 570 °C the dislocation structure has changed to a somewhat more cell-like formation. The TEM studies also showed that dislocation recovery is rather moderate compared to estimations made using XRD. Fig. 22 shows an overall view of tempered lath martensite in the FRT 915 °C HTT steel: it retains a high dislocation density despite the long tempering cycle with the peak temperature at 570 °C.

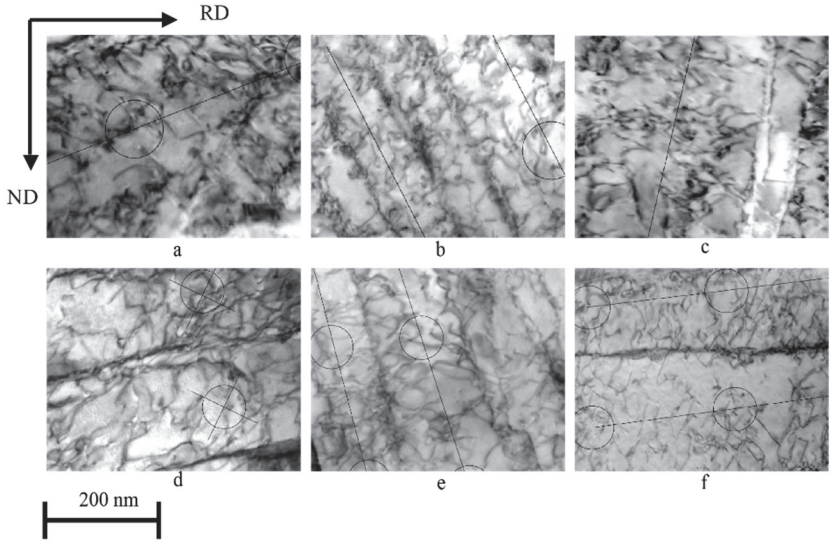

Fig. 21. Intra-lath dislocation structures for DQ steels with FRT 775 °C (a), 865 °C (b) and 915 °C (c) and DQ-T (tempered at 570 °C) steels with FRT 775 °C (d), 865 °C (e) and 915 °C (f), respectively. Lines and circles show linear intercept measurement positions (Reprinted by permission from Publication II © 2018 Elsevier Inc.).

Table 17. Mean martensite dislocation densities obtained with the TEM intercept method with 95% confidence interval (Reprinted by permission from Publication II © 2018 Elsevier Inc.).

FRT (°C)	Mean martensite lath dislocation density x 10^{15} (m^{-2})	
	DQ	DQ-T
775	2.60 ± 0.4	2.94 ± 1.9
865	2.60 ± 0.3	2.23 ± 0.3
915	2.84 ± 0.3	1.74 ± 0.2

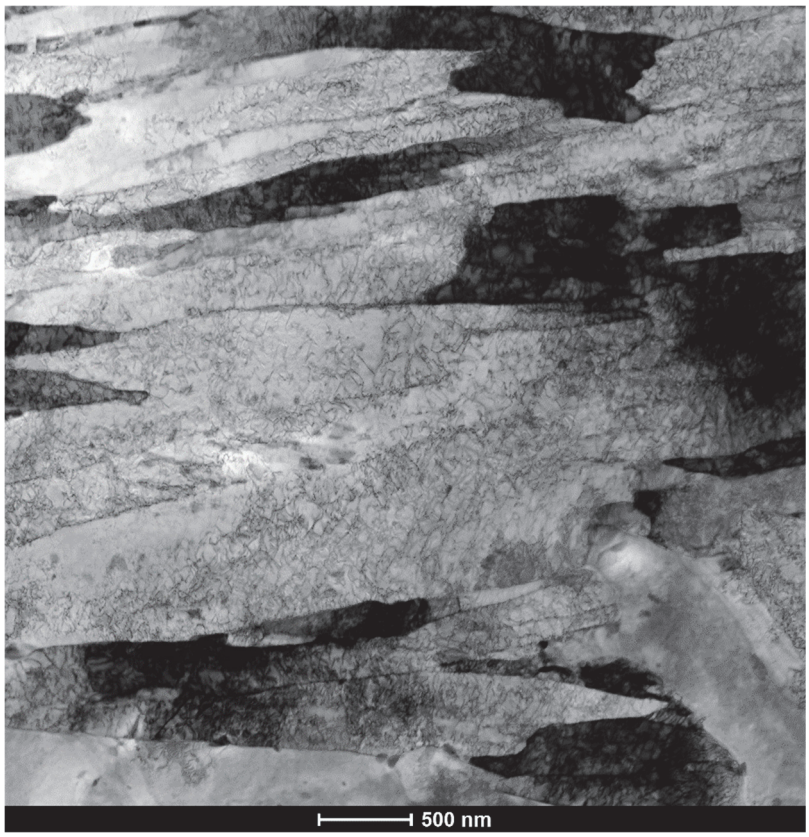

Fig. 22. High-temperature tempered FRT 915 °C steel. Lath martensite structure still has a high dislocation density, but cell-like structure has formed.

Table 18. The effect of thermomechanical treatment on microstrain and crystallite size obtained with the Rietveld refinement method and dislocation density calculated using the Williamson-Smallman method (Reprinted by permission from Publication II © 2018 Elsevier Inc.).

FRT (°C)	Microstructure	Microstrain (%)		Crystallite size (Å)		Dislocation density x 10^{15} (m^{-2})	
		DQ	DQ-T	DQ	DQ-T	DQ	DQ-T
775	PF+GB+M	0.276	0.146	290	296	3.08	1.60
865	M+UB	0.283	0.187	280	305	3.27	1.99
915	M+UB	0.295	0.195	256	318	3.73	1.88

Fig. 23 shows grain sizes obtained using EBSD in for different thermomechanical treatment conditions before and after tempering at 570 °C (Publication II). These finding are somewhat in line with the results above concerning prior austenite grain size. Effective coarse grain size, i.e. grain size at 90% in the cumulative grain size distribution, is decreased when lowering FRT from 915 °C to 865 °C. Further lowering, on the other hand, did not provide any further refinement. Tempering had no significant effect on the grain size.

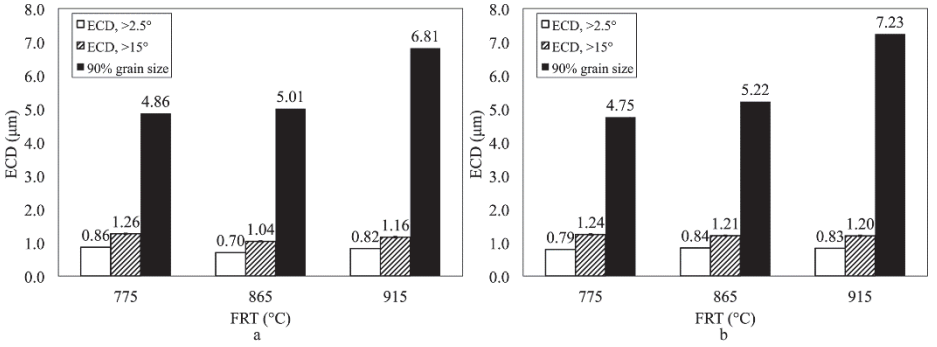

Fig. 23. Effect of thermomechanical treatment condition on ECD grain and subgrain sizes and grain sizes at 90% in the cumulative grain area distribution in (a) as-quenched and (b) quenched and tempered condition. Peak tempering temperature 570 °C (Reprinted by permission from Publication II © 2018 Elsevier Inc.).

Publication II did not include the transformation textures of the experimental steels. However, quarter thickness texture has later been studied and now included in the thesis manuscript to combine the data from Publication III and surface texture. Fig. 24 presents the quarter-thickness position texture components in φ_2 = 45° ODF sections. FRT 865 °C and FRT 915 °C steels show sharp intensities of {554}<225>, {112}<131> and{112}<110> while partly ferritic FRT 775 °C shows especially sharp {112}<110> but milder intensities of the other main components. These components are transformed from austenite textures {112}<111>, {110}<112> and {110}<001> also known as Cu, Br and Goss, respectively. The presence of these components is an indication of the heavy pancaking experienced by the austenite. This texture is also somewhat different from the surface texture, which is explained later.

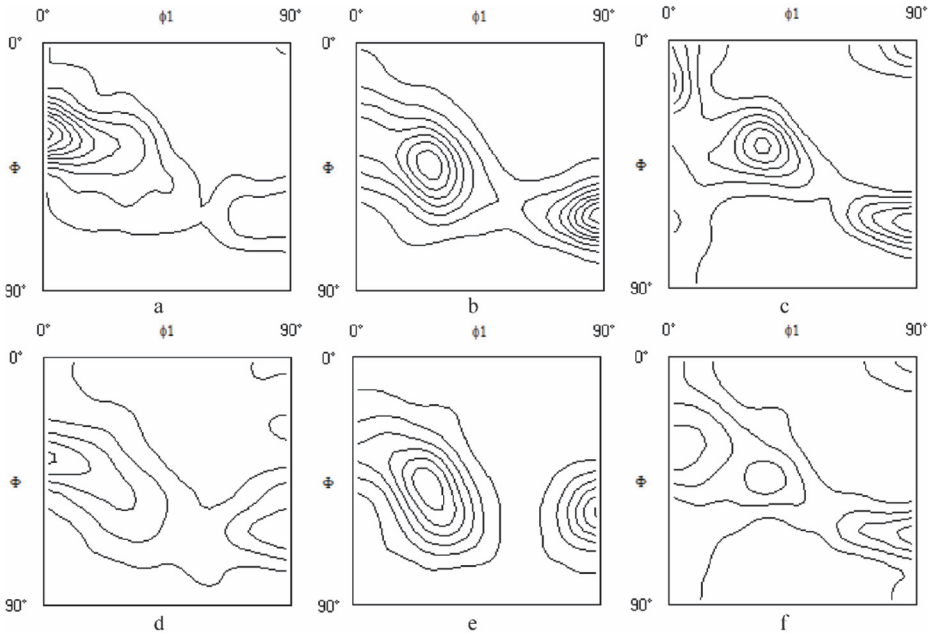

Fig. 24. φ_2 = 45° ODF sections presenting quarter thickness textures. (a) DQ FRT 775 °C, (b) DQ FRT 865 °C, (c) DQ FRT 915 °C, (d) DQ-T FRT 775 °C, (e) DQ-T FRT 865 °C and (f) DQ-T FRT 915 °C.

The surface microstructures with 865 °C and 915 °C finish rolling temperatures, as presented in Publication III, consisted of a thin layer of softer microstructural components than the bulk microstructure below the surface layer. The steel with FRT 775 °C did not have a softer surface layer as softer microstructural components extended deeper into the strip thickness, as we can see from the microstructure in Fig. 26 and the microhardness profiles in Fig. 25. As presented in Publication III, the microstructures 30 µm below surface are similar to those at the quarter-thickness position (Fig. 20). The microstructure of the steel with FRT 775 °C consists of highly elongated bainite and polygonal ferrite. The grain structure is extremely fine as the thickness of the ferritic and bainitic grains in the ND direction is about 1 µm. Tempering moves the carbon from the bainitic regions mainly into grain boundaries. The surface microstructures of the steels with FRT 865 °C and FRT 915 °C are more complex. For FRT 865 °C, the microstructure consists of auto-tempered martensite, ferrite, granular bainite, upper bainite and martensite-austenite constituents. The steel with the highest FRT show signs of auto-tempered martensite, lower bainite, granular bainite and some signs of martensite-austenite

constituents. The tempered microstructures of these steels are again straightforward: martensite and bainite (granular bainite at lower transformation temperature) undergoes cementite precipitation. Due to the fine grain size though, precipitation seems to occur at grain boundaries rather than inside the bainitic or martensitic laths.

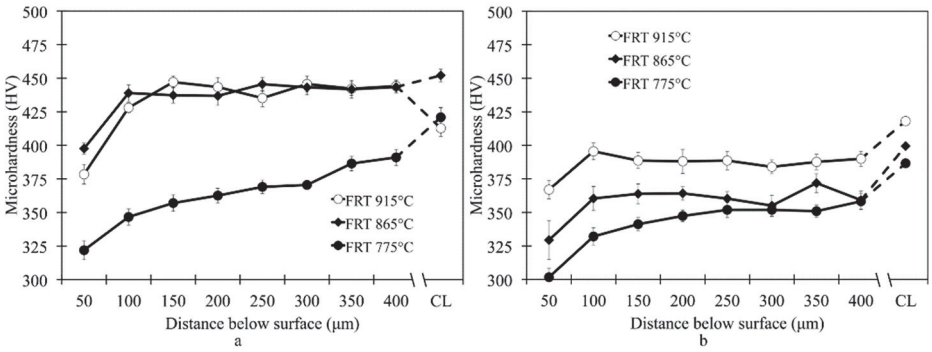

Fig. 25. Mean values of surface microhardness in (a) the direct-quenched and (b) the direct-quenched and tempered condition with centreline reference hardness (Reprinted by permission from Publication III © 2017 Elsevier Inc.).

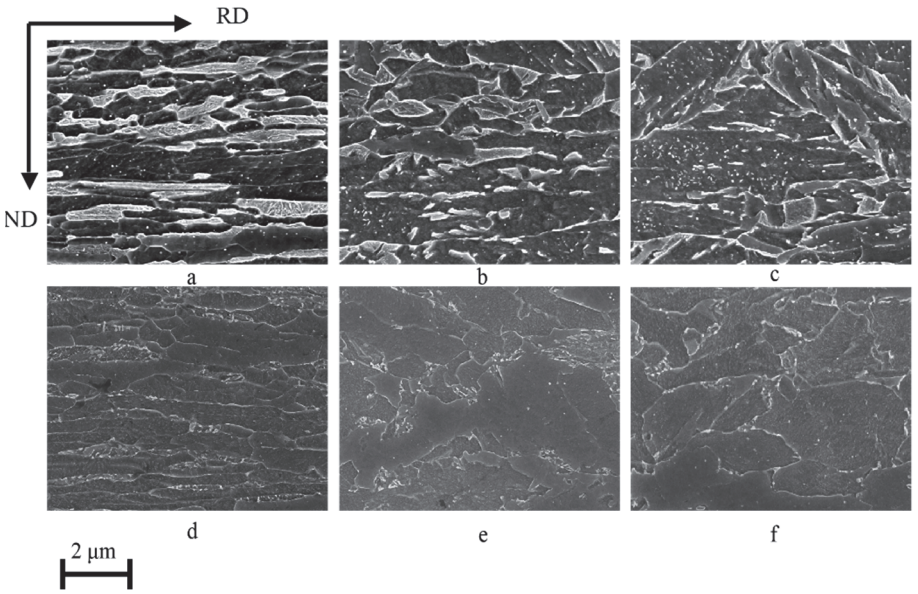

Fig. 26. Subsurface microstructures for (a) FRT 775 °C DQ, (b) FRT 865 °C DQ-T, (c) FRT 915 °C DQ, (d) FRT 775 °C DQ-T, (e) FRT 865 °C DQ and (f) FRT 915 °C DQ-T steel. (FESEM,

In-lens, approx. 30 µm below the surface) (Reprinted by permission from Publication III © 2017 Elsevier Inc.).

EBSD inverse pole figures from the sub-surface positions (Publication III) and from near the surface of the strips in the quenched conditions are presented in Fig. 28. The φ2 = 45° ODF section seen in Fig. 27 show the presence of an intense shear texture component {112}<111>α. This component is present in all TMCP conditions, but its intensity is highest in the intermediate FRT 865 °C. The shear texture components {111}<211>γ and {112}<110>γ are expected to be promoted when austenite close to the rolled surfaces is hot rolled below the recrystallization stop temperature and these are later transformed into the shear components {112}<111>α, {110}<112>α and {110}<111>α, after cooling and phase transformation. (Wittridge and Jonas, 2000) The measured Rtot values and the micrographs in Fig. 19 showed that all experimental materials were hot rolled with FRT below the recrystallization stop temperature. For the material with the highest FRT (915° C), which underwent the least reduction below the recrystallization stop temperature, these texture shear texture components are the weakest, as would be expected.

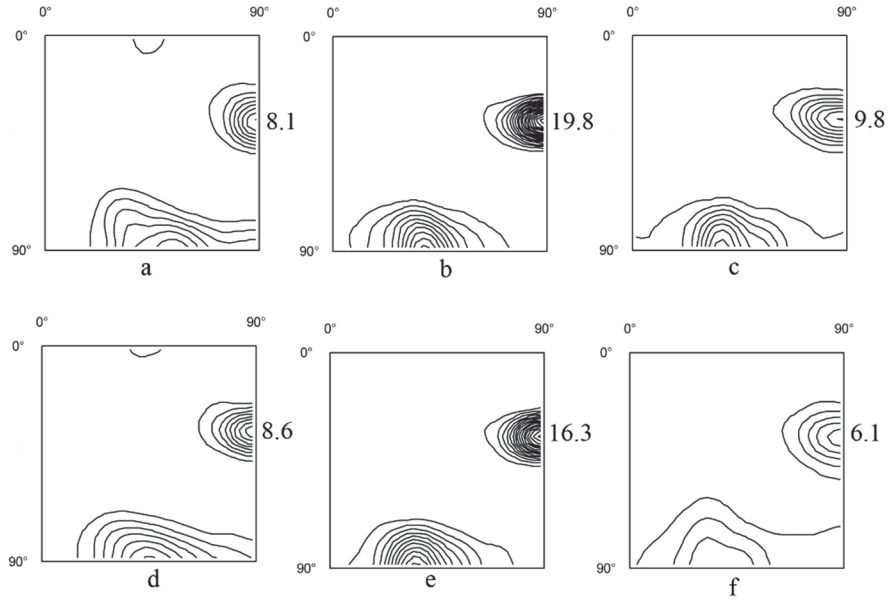

Fig. 27. φ_2 = 45° ODF sections presenting the subsurface textures from the depth of 0-0.45 mm below the surface. (a) DQ FRT 775 °C, (b) DQ FRT 865 °C, (c) DQ FRT 915 °C,

(d) DQ-T FRT 775 °C, (e) DQ-T FRT 865 °C and (f) DQ-T FRT 915 °C (Reprinted by permission from Publication III © 2017 Elsevier Inc.).

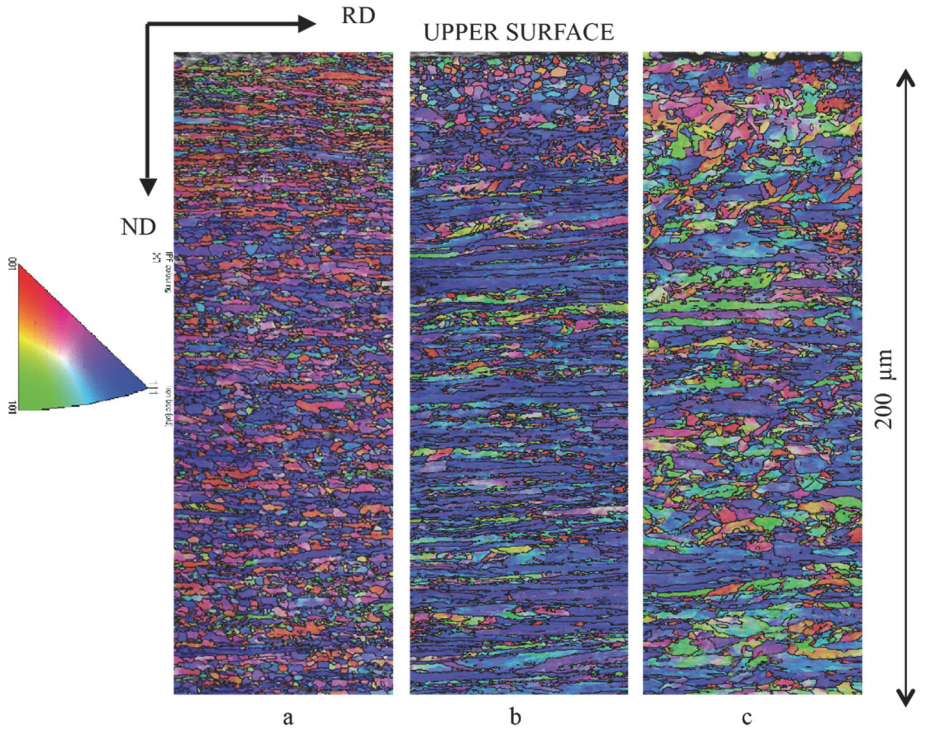

Fig. 28. Subsurface EBSD inverse pole figure maps in RD direction for the direct-quenched states with (a) FRT 775 °C, (b) FRT 865 °C and (c) FRT 915 °C (Reprinted by permission from Publication III © 2017 Elsevier Inc.).

As with the quarter-thickness position, surface dislocation densities were also estimated using the Williamson-Smallman method. Table 19 shows that compared to the quarter-thickness values (Table 18), dislocation densities and the values of microstrain in the surface are somewhat lower, due to the lower volume fraction of martensite. Tempering reduces the estimated dislocation density by 30–40% in all conditions. From the surface re-austenitized samples show a difference compared to martensitic regions. Re-austenitized and quenched condition showed possibly higher dislocation density compared to direct-quenched state – most likely due to fully martensitic state compared to direct-quenched state that included also bainite. However, for re-austenitized and quenched steel, decrease in dislocation density during tempering is more severe.

Table 19. Estimated dislocation density at the surface of the strip using Williamson-Smallman method. Tempering temperature 570 °C (Reprinted by permission from Publication III © 2017 Elsevier Inc.).

FRT (°C)	Surface microstructure	Microstrain (%)		Crystallite size (Å)		Dislocation density x 10^{15} (m^{-2})	
		DQ	DQ-T	DQ/	DQ-T	DQ	DQ-T
775 °C	PF+GB	0.156	0.110	314	322	1.61	1.11
865 °C	M+UB	0.226	0.157	303	331	2.42	1.54
915 °C	M+UB	0.171	0.103	287	295	1.93	1.13

4.2.2 Mechanical properties

Publication II shows the correlation between general microstructure and mechanical properties, i.e. strength and ductility. In Publication III, the research focuses on the relationship between surface microstructure and the bendability of the experimental steels and Publication IV studies strength, toughness and bendability in various tempering temperatures.

Strength and ductility

The work of Publication II, i.e. the effect of thermomechanical treatment on mechanical properties, is presented in Table 20. Low FRT (775 °C) leads to a bainitic-ferritic microstructure which leads to both lower strength and hardness. This low FRT steel shows the lowest strength values in both test directions but also shows the highest scatter in the strength values. FRT 865 °C leads to the highest strength values. As expected, tempering lowered tensile strength and increased tensile ductility, but surprisingly, it did not clearly lower T28J. In fact, no statistically significant effect on T28J was found to be due to tempering. However, what is considered important, was that lowering the FRT improved the 28J transition temperature regardless of the increased yield strength, when dropping from FRT 915 °C to 865 °C.

Table 20. Effect of FRT on mechanical properties of direct-quenched steel before and after tempering. Mean yield strength (YS), ultimate tensile strength (UTS), YS/UTS ratio, total elongation at fracture and 28J transition temperatures including 95% confidence intervals. Yield strength (YS) refers to the stress for 0.2% plastic strain (Reprinted by permission from Publication II © 2018 Elsevier Inc.).

FRT(°C) / Micro-structure	Condition	YS ($R_{p0.2}$, MPa)	UTS (R_m, MPa)	YS/UTS -ratio	Hardness (HV10)	A (%)	T28J (°C)
			Longitudinally to RD				
	DQ	900 ± 26	1118 ± 23	0.81	364	12.9 ± 1.0	n/a
775 / F+GB+M	DQ-T	946 ± 23	996 ± 18	0.95	312	16.0 ± 1.0	n/a
	DQ	1041 ± 3	1254 ± 6	0.83	401	11.0 ± 1.5	n/a
865 / Mainly M + minor UB	DQ-T	1096 ± 7	1100 ± 5	1.00	347	15.4 ± 0.5	n/a
	DQ	1078 ± 6	1212 ± 4	0.89	404	11.3 ± 0.5	n/a
915 / Mainly M	DQ-T	1058 ± 6	1079 ± 5	0.98	345	15.8 ± 0.6	n/a
			Transverse to RD				
775 / F+GB+M	DQ	931 ± 5	1133 ± 3	0.82	n/a	9.9 ± 0.4	-109 (-124…-94)
	DQ-T	960 ± 2	1017 ± 1	0.94	n/a	14.8 ± 1.0	-95 (-121…-69)
865 / Mainly M + minor UB	DQ	1078 ± 4	1249 ± 13	0.86	n/a	9.5 ± 0.6	-100 (-131…-71)
	DQ-T	1080 ± 2	1106 ± 1	0.98	n/a	12.7 ± 0.6	-96 (-109…-84)
915 / Mainly M	DQ	1051 ± 4	1212 ± 3	0.87	n/a	10.7 ± 1.5	-79 (-102…-57)
	DQ-T	1053 ± 5	1092 ± 3	0.96	n/a	12.5 ± 0.5	-55 (-89…-26)

Bendability

Minimum bending radii expressed as r/t ratios together with a summary of subsurface properties are presented in Table 21. Low FRT (775 °C), leads to excellent bendability even in the direct-quenched condition (r/t ratios 2.5 and 1.66). Bendability was further improved during tempering (r/t 1.66 and 1). On the other hand, steels with higher FRTs, which have poorer bendability in the direct-quenched condition show significant improvement in bendability after tempering.

The bendability can be associated with existing microstructural factors. The low-FRT steel has a soft ferritic microstructure near the surface of the strip which provides excellent bendability. Microstructures with higher hardnesses (FRT 865 °C and 915 °C) show poorer bendability in the direct-quenched state, but this is improved when tempering softens the microstructure. However, the FRT 865 °C steel showed clearly poorer bendability when the bend axis was in the transverse direction, and the bendability in this direction is not significantly improved by tempering. This is expected to be due to the strong shear texture component {112}<111>α promoting shear localization as well as to the presence of upper bainitic microstructural components that provide possible crack nucleation sites. In fact, these steels obtained better bendability with the bend axis parallel to the rolling direction in both the direct-quenched and direct-quenched and tempered states. The low-FRT steel differs from the high-FRT M+UB steels in that they have better bendability with the bend axis perpendicular to the RD in both the tempered and as-quenched conditions.

Anisotropy in bendability can be seen in Fig. 29 where Fig. 29b and Fig. 29c show the remarkable differences in bendability of the FRT 865 °C steel. With the bend axis perpendicular to RD (Fig. 29b) cracking occurs when r/t is less than 4.00, while when the bend axis is parallel to RD, bending is crack free even with r/t = 1.33. Respectively, Fig. 29a and Fig. 29b show the differences in bendability with the bend axis perpendicular to RD caused by a drop in FRT from 915 °C to 865 °C. FRT 865 °C steel show severe cracking with higher r/t-ratio.

In addition to microstructure and texture, surface hardness profiles are expected to be an important factor affecting bendability. As earlier was seen in Fig. 25, low FRT 775 °C leads to a substantially softer surface microstructure that extends deep into the steel. The hardness profiles of FRT 865 °C and 915 °C steels show that hardness is almost constant from just 100 µm below the surface until the centreline of the strip. In fact, the soft surface layer only is less than 100 µm thick and is only 50 HV lower in hardness than the bulk material. Fig. 25b also shows that harder microstructures soften clearly more during tempering, which potentially lead to higher benefits accruing from tempering. Nearly all the experimental steels showed hardness peaks on the centreline of the strips. This can be due to macrosegregation inducing either higher martensitic fractions, or higher carbon content of the martensite, there.

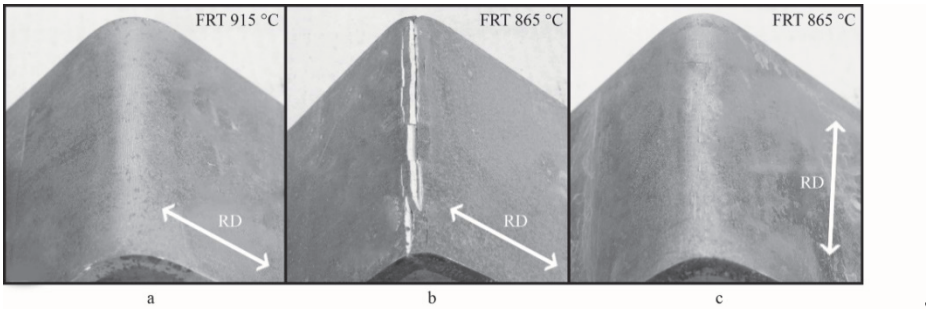

Fig. 29. Direct-quenched and tempered bend test samples. (a) FRT 915 °C, transverse bend, punch radius 12 mm (r/t 2.0), (b) FRT 865 °C, transverse bend, punch radius 16 mm (r/t 2.66) and (c) FRT 865 °C, longitudinal bend, punch radius 8 mm (r/t 1.33) (Reprinted by permission from Publication III © 2017 Elsevier Inc.).

Table 21. Minimum bending radii for longitudinal and transverse bend axes together with surface microstructures and hardnesses (Reprinted by permission from Publication III © 2017 Elsevier Inc.).

FRT (°C)	r/t longitudinal		r/t transverse		Subsurface microstructure	Subsurface hardness
	DQ	DQ-T	DQ	DQ-T		
775	2.50	1.66	1.66	1.00	PF+GB	Soft surface
865	3.66	1.33	5.00	4.00	UB+MA+ATM	No soft layer
915	4.00	2.00	4.00	2.33	LB+MA+ATM	No soft layer

4.3 The effect of tempering temperature and re-austenitization

Publications II and III showed the effect of tempering at 570 °C on the microstructure and properties of thermomechanically processed direct-quenched steel. In Publication IV, the wider effect of tempering temperature on tempered microstructure was studied. A re-austenitized, quenched and tempered condition was included as well to obtain a better understanding of the differences between the TMCP+DQ and classical HR+RAQ conditions.

4.3.1 Microstructure evolution

In Fig. 30, we see the effect of tempering temperature on the microstructure of the steel with a FRT of 915 °C. As already mentioned, the microstructure in the direct-quenched condition consists of martensite, auto-tempered martensite and some

areas of upper bainite. The FRT 915 °C steel was selected for further analyses due to its nearly fully martensitic microstructure, which provides a good basis for comparison with the fully martensitic re-austenitized condition.

When tempering is performed at low temperatures, i.e. 250 °C (Fig. 30b), precipitation of fine carbides might occur in addition to residual carbon segregation from martensite (after autotempering), but no significant cementite growth has occurred. These potential very small carbides are in size range of 2–4 nm and precipitate within the martensite crystals (Krauss, 1999) and their density increases as carbon content increases but are unlikely with current carbon content even though Okamoto, Matlock and Krauss (1991) characterized very minor fraction of transition carbides in C0.14 wt.% martensite. Furthermore, distinguishing such small precipitates is impossible with FESEM and their possible existence would need TEM studies, which was not done in the experimental of Publication IV. In fact, it is expected that the main microstructural change is simple carbon clustering that leads to static aging phenomena and the pinning of free dislocations.

Fig. 30c–d shows that the carbide morphology is different when the tempering temperature is in the range 400 – 500 °C. In this case, long carbides or long piles of carbides are formed at both the lath and prior austenite grain boundaries. This well-known phenomenon, called temper embrittlement has earlier been reported in the case of RAQ martensite (Horn & Ritchie, 1978). However, now the current results show that similar unfavourable carbide structures can be formed during the tempering of DQ martensite. Furthermore, Fig. 30e-g shows that tempering temperatures of 570 – 650 °C lead to more uniform and eventually coarsened and spheroidized, carbide morphologies. Cementite is expected to be the major carbide type for the current chemical compositions (Caron & Krauss, 1972; Horn & Ritchie, 1978; Krauss, 1999).

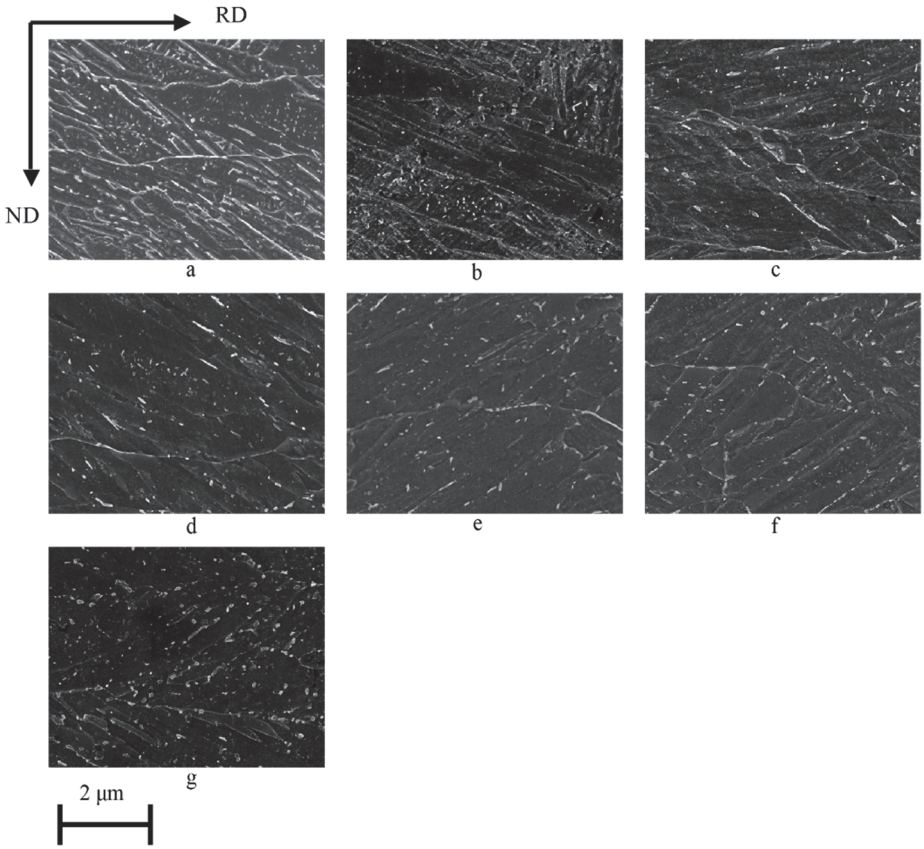

Fig. 30. Quarter-thickness microstructures of (a) DQ, (b) DQT (250 °C), (c) DQT (400 °C), (d) DQT (500 °C), (e) DQT (570 °C), (f) DQT (600 °C) and (g) DQT (650 °C). Nital etched samples with in-lens imaging (Reprinted by permission from Publication IV © 2018 Elsevier B.V.).

The study of the effect of tempering temperature on surface microstructure (Fig. 31) shows a similar trend to that seen in the quarter-thickness microstructures. Tempering temperature range 400–500 °C show the possibly unfavourable formation of rodlike cementite or possibly lines of smaller carbides on lath and grain boundaries. It is necessary to underline that some of these differences are due to more complex microstructure including also bainite. However, when the tempering temperature reaches 570 °C, the cementite distribution is homogenized and further at 600–650 °C spheroidized and coarsened.

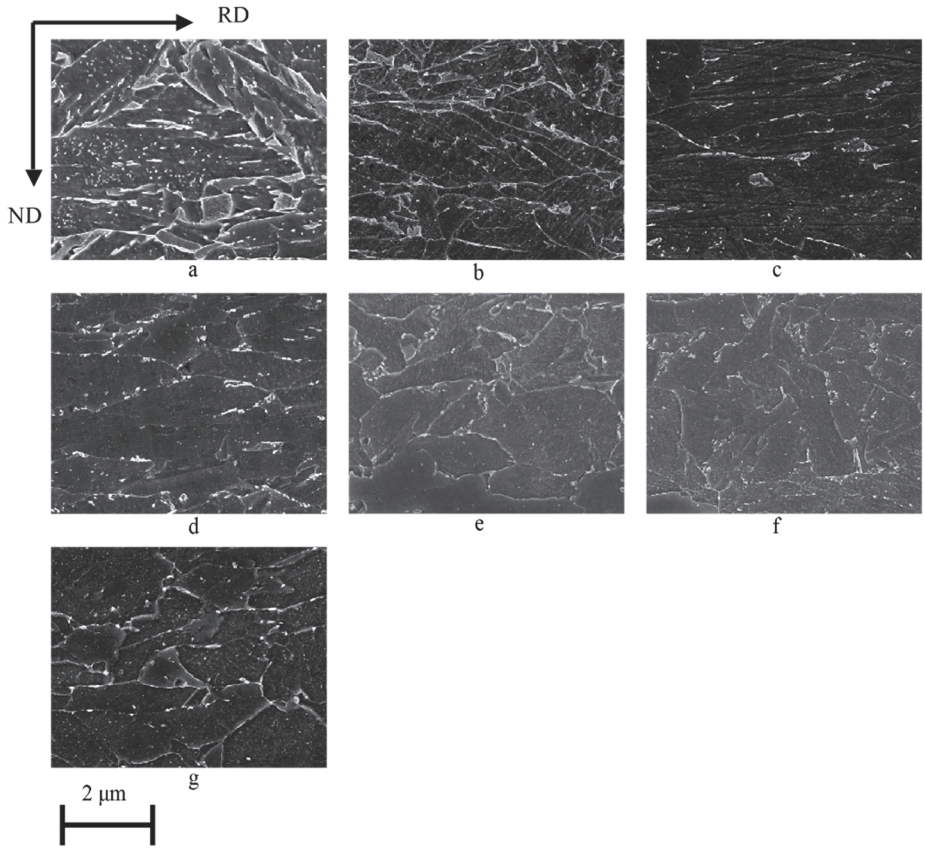

Fig. 31. Subsurface microstructure of (a) DQ, (b) DQT (250 °C), (c) DQT (400 °C), (d) DQT (500 °C), (e) DQT (570 °C), (f) DQT (600 °C) and (g) DQT (650 °C). Nital etched samples with in-lens imaging (Reprinted by permission from Publication IV © 2018 Elsevier B.V.).

The microstructure at the quarter-thickness position is representative of the bulk microstructure and it is mainly responsible for the overall strength and impact toughness of the experimental steels. The main microstructural difference between the re-austenitization and quenched (RAQ) and TMCP-DQ conditions is the crystallographic texture.

EBSD-IPF maps from the surface microstructure of the strip for the RD direction (Fig. 32) show a fundamental difference between the RAQ and DQ conditions. Thermomechanical treatment followed by direct quenching resulted in an elongated grain structure (Fig. 32c–d) whereas conventional re-austenitizing and quenching (Fig. 32a–b) led to an equiaxed prior austenite grain structure.

Furthermore, the direct-quenched conditions provided finer grain sizes as defined by the low-angle (> 2.5°) and high-angle (> 15°) ECD grain sizes obtained from the EBSD data (Fig. 35). This was also seen in the high-angle grain sizes at the 90th percentile in the cumulative grain area distributions, i.e. d90%. Tempering has no visibly clear effect on the grain structure (Fig. 34) even though the d90% values show minor differences especially in the case of the RAQ steels (Fig. 35).

Surface texture intensities in $\varphi 2 = 45°$ ODF sections were also studied for the RAQ and DQ conditions. As expected, the intense shear texture component {112}<111>α present in the DQ state, due to thermomechanical treatment below the recrystallization stop temperature, is absent in the RQ state.

Grain boundary misorientation data was analysed for the DQ and RAQ states both prior to and after tempering, and the data presented in Fig. 33 shows some differences between the RAQ and DQ conditions. The RAQ condition has a higher frequency of high-angle misorientation angles than the DQ conditions which have a higher frequency of angles in the range 7.5 – 50°. Even though tempering does not affect the misorientation profile of the DQ steels, for the RAQ condition a lower frequency of low-angle boundaries, below 7.5°, can be seen.

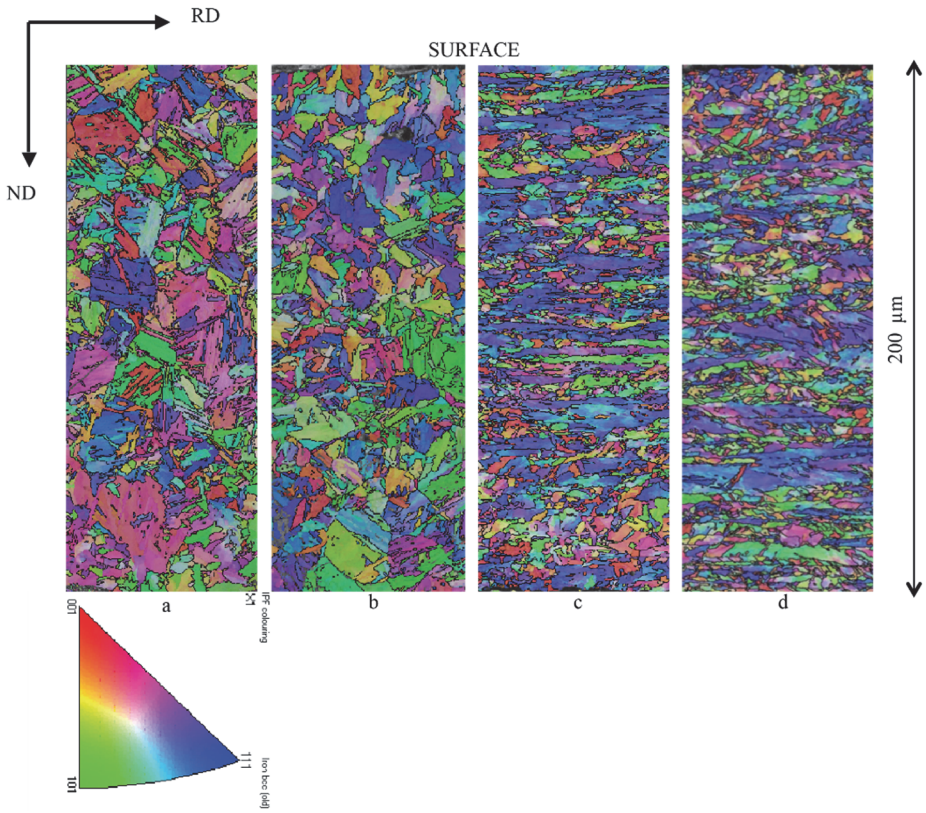

Fig. 32. Subsurface EBSD inverse pole figure maps for the RD direction for (a) RAQ, (b) RAQT (570 °C), (c) DQ and (d) DQT (570 °C) specimens. The sheet normal direction (ND) and the rolling direction (RD) in the cross-sections are shown (Reprinted by permission from Publication IV © 2018 Elsevier B.V.).

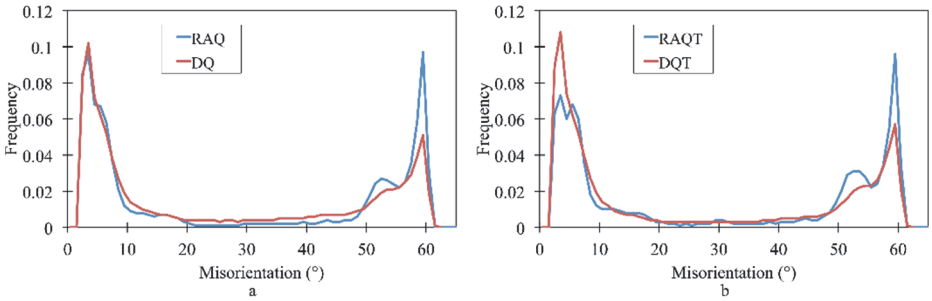

Fig. 33. Boundary misorientation distributions for the subsurface areas of (a) quenched and (b) quenched and tempered (570 °C) for martensitic RAQ and DQ conditions (Reprinted by permission from Publication IV © 2018 Elsevier B.V.).

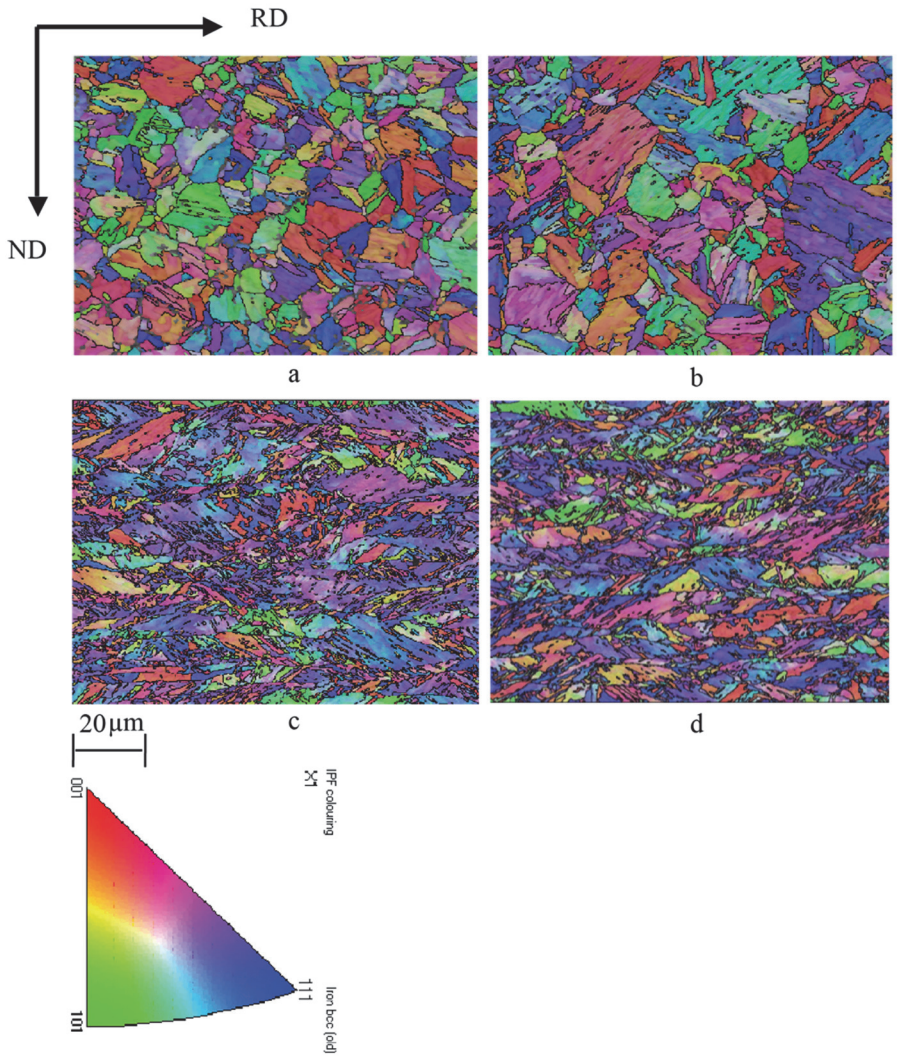

Fig. 34. Quarter-thickness EBSD inverse pole figure maps for the RD direction for (a) RAQ, (b) RAQT, (c) DQ and (d) DQT steels. The sheet normal direction (ND) and the rolling direction (RD) in the cross-sections are shown (Reprinted by permission from Publication IV © 2018 Elsevier B.V.).

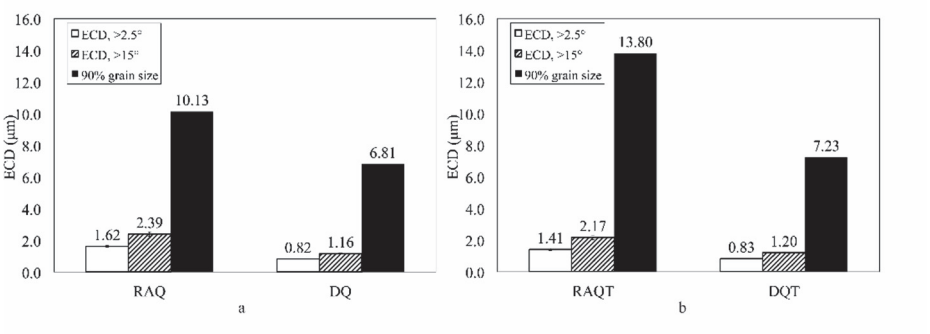

Fig. 35. Mean ECD grain and subgrain sizes and grain sizes at 90% in the cumulative grain area distribution for (a) RAQ and DQ steels and (b) RAQT and DQT steels. Tempering temperature 570 °C. Sub-grain sizes defined by misorientation angles > 2.5° and grain sizes by misorientation angles > 15° (Reprinted by permission from Publication IV © 2018 Elsevier B.V.).

To estimate differences between tempering conditions, XRD peak broadening analyses were done 150 µm below the surface. This depth was chosen due to its importance for bendability (A. Kaijalainen, 2016). Microstructural characterization and hardness measurements showed that material at this depth had already reached its full hardness and mainly martensitic microstructure, i.e. it also well represents the situation deeper below the surface of the strip. Table 22 shows the effect of tempering temperature and re-austenitization on estimated dislocation density. According to these results, dislocation density does not appear to decrease yet at the tempering temperature 250 °C. A drop can be seen after tempering at 400 °C and the decrease rate starts to increase as the tempering temperature reaches 600 °C.

Table 22. The effect of tempering temperature and re-austenitzation microstrain, crystallite size and estimated dislocation density. Data from Publication IV.

Condition	Microstrain (%)	Crystallite size (Å)	Dislocation density x 10^{15} (m^{-2})
DQ	0.295	256	3.73
DQ + 250 °C	0.265	246	3.49
DQ + 400 °C	0.266	321	2.68
DQ + 500 °C	0.115	269	1.38
DQ + 570 °C	0.185	318	1.88
DQ + 600 °C	0.079	273	0.94
DQ + 650 °C	0.044	303	0.47
RAQ	0.381	329	3.75
RAQ +570 °C	0.205	336	1.98

4.3.2 Mechanical properties and bendability

Strength and ductility

Table 23 shows the effect of tempering temperature on the mechanical properties of direct-quenched strip. The results for the re-austenitized, quenched and tempered condition are also provided. The yield strength is slightly increased from that of the DQ condition on tempering at 250 and 400 °C, but slightly decreased with the tempering temperatures 500 – 600 °C. Tempering at 650 °C provided the only condition showing a significant decrease in yield strength. Furthermore, when comparing the DQT and RAQT for the tempering temperature 570 °C, thermomechanical treatment seems to have had a significant effect on yield strength but not that great an effect on tensile strength and hardness.

Tensile ductility is also largely dependent on tempering temperature. Tempering at 500 °C and above improves the tensile ductility, i.e. total elongation and uniform elongation, of direct-quenched steel, which in this case is mainly martensitic. However, when tempered at 250–400 °C, both of these ductility parameters are reduced compared to the direct-quenched condition.

Like strength and ductility, impact toughness is affected by both tempering and thermomechanical treatment. Surprisingly, the results show that for current low-carbon TMCP-DQ steel, tempering at all temperatures up to 600 °C lead to embrittlement. Only the highest test temperature, 650 °C, leads to both significant softening and also to an improved T28J with respect to the as-quenched state. The longitudinal impact toughness of the 650 °C tempered steel is actually so high that T28J was lower than the lowest testing temperature (-140 °C), and therefore, could not be determined. Furthermore, for similar tempering conditions, i.e. 570 °C, the RAQT condition seems to lead to poorer toughness than the DQT condition.

Table 23. Effect of tempering temperature on mechanical properties of direct-quenched mainly martensitic steel before and after tempering (FRT 915 °C). Data from Publication IV. Mean yield strength (YS), ultimate tensile strength (UTS), YS/UTS ratio, total elongation at fracture and 28J transition temperatures including 95% confidence intervals. Yield strength (YS) refers to the stress for 0.2% plastic strain.

Condition	Direction to RD	YS ($R_{p0.2}$, MPa)	UTS (R_m, MPa)	YS/UTS-ratio	A (%)	T28J (°C)
DQ	Longitudinal	1078 ± 6	1212 ± 4	0.89	11.3 ± 0.5	-102 (-123…-81)
	Transverse	1051 ± 4	1212 ± 3	0.87	10.7 ± 1.5	-79 (-102…-57)
DQ + 250 °C	Longitudinal	1175 ± 5	1232 ± 8	0.95	10.8 ± 0.7	-56 (-82…-29)
	Transverse	1142 ± 6	1241 ± 3	0.92	10.3 ± 0.7	-45 (-59…-31)
DQ + 400 °C	Longitudinal	1117 ± 7	1152 ± 8	0.97	11.1 ± 1.4	-73 (-96…-52)
	Transverse	1098 ± 5	1156 ± 1	0.95	9.2 ± 0.7	-50 (-76…-24)
DQ + 500 °C	Longitudinal	1070 ± 9	1089 ± 9	0.98	13.6 ± 1.3	-83 (-100…-66)
	Transverse	1045 ± 4	1085 ± 4	0.96	13.4 ± 0.7	-39 (-71…-8)
DQ + 570 °C	Longitudinal	1058 ± 6	1079 ± 5	0.98	15.8 ± 0.6	-71 (-100…-41)
	Transverse	1053 ± 5	1092 ± 3	0.96	12.5 ± 0.5	-55 (-89…-26)
DQ + 600 °C	Longitudinal	989 ± 6	1019 ± 5	0.97	15.1 ± 0.6	-65 (-100…-30)
	Transverse	1027 ± 4	1061 ± 5	0.97	12.8 ± 0.8	-56 (-95…-23)
DQ + 650 °C	Longitudinal	848 ± 5	879 ± 3	0.96	16.8 ± 0.8	n/a
	Transverse	854 ± 3	880 ± 2	0.97	15.8 ± 0.9	-106 (-124…-61)
RAQ + 570 °C	Longitudinal	899 ± 16	1005 ± 4	0.89	16.8 ± 0.5	-35 (-60…-10)
	Transverse	927 ± 6	1015 ± 6	0.91	15.8 ± 0.5	-25 (-54…-5)

Bendability

The results from the bendability tests performed in Publication IV are summarized in Fig. 36. They show that bendability, i.e. minimum bending radius, is greatly affected by tempering. Bendability correlates with tempering temperature in a similar manner to tensile ductility as can be seen from Table 23. Tempering between 250 °C and 400 °C leads to decreased bendability compared to the initial DQ condition, but is improved significantly when the tempering temperature is 500 – 650 °C. Furthermore, tempering temperature seems to affect the anisotropy of the bendability as 400–570 °C tempered steels had better bendability when the bend axis was parallel to RD, whereas bendability is isotropic for the as-quenched state and for the lowest and highest tempering temperatures. Thermomechanical treatment can also be seen to affect the anisotropy of bendability as the RAQT steel was the only steel for which the bendability around an axis transverse to the RD was better than around an axis parallel to the RD.

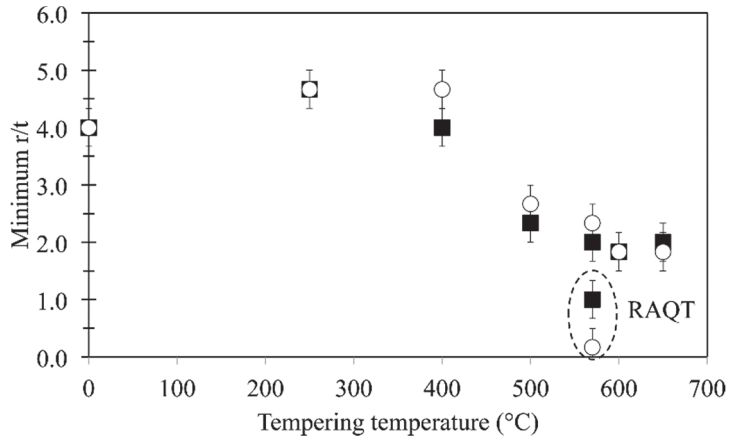

Fig. 36. The effect of tempering temperature on bendability of DQ and RAQ steels expressed as minimum bending radius (r) relative to the sheet thickness (t). Open symbols bending axis in the transverse direction and closed symbols longitudinal direction relative to RD. The uncertainty of the minimum r/t is based on bending radius step size in the test (Reprinted by permission from Publication IV © 2018 Elsevier B.V.).

5 Discussion

5.1 Role of chemical composition

The results presented in Publication I showed the importance microalloying levels in direct-quenched and tempered steels. Vanadium has earlier been shown to be a strong carbide former and even small additions of vanadium can form V_4C_3 or VC carbides at the tempering temperatures of 550–650 °C, leading to secondary hardening (Bhadeshia & Honeycombe, 2006). As seen in Publication I and in Fig. 37, vanadium plays an important role in retaining strength during the tempering of DQ steels. Despite fairly similar YS and UTS in the DQ condition, a 0.08% vanadium addition raises the UTS by 100 MPa and the YS by 70 MPa after high-temperature tempering. A strong secondary hardening effect of vanadium nitrides has been reported earlier by Lagneborg, Siwecki, Zajac and Hutchinson (1999), although in their study significantly higher level of nitrogen compared to our experimental was required to obtain this strengthening effect. Furthermore, coarse VN particles were not found in our microstructural characterization. In the Publication I, experimental consisted of tempering trials at 180 and 570 °C peak temperatures. However, in earlier Publication of present author (Saastamoinen, Porter & Suikkanen, 2015) it was noticed that higher peak temperature (600 °C) improves vanadium secondary hardening effect significantly.

Vanadium also promoted the occurrence of martensite in the steel as the V-free composition included a minor amount of ferrite in the direct-quenched condition compared to the fully martensitic V-alloyed steel. This could be very well be due to vanadium's tendency to form carbonitrides and possibly protect boron from forming BN particles. Adrian and Staœko (2008) did not find that V improved hardenability when in solution, i.e. when vanadium carbonitrides were not present. While V showed its importance in strength evolution also in tempering, carbon and boron mainly affected the phase transformation and initial structure and strength prior to tempering. As expected, carbon controls the strength of martensite in the DQ condition, but the strength difference between the low-C and high-C compositions vanished during high-temperature tempering (Publication I). The low-C 0.095C steel on the other hand, provides superior toughness compared to the hi-C 0.14C steel both before and after tempering, which makes it superior when aiming for a yield strength level of approximately 900–1000 MPa. A boron addition was essential in obtaining a fully martensitic microstructure in the low-C

composition but the absence of boron refined the microstructure and improved toughness significantly.

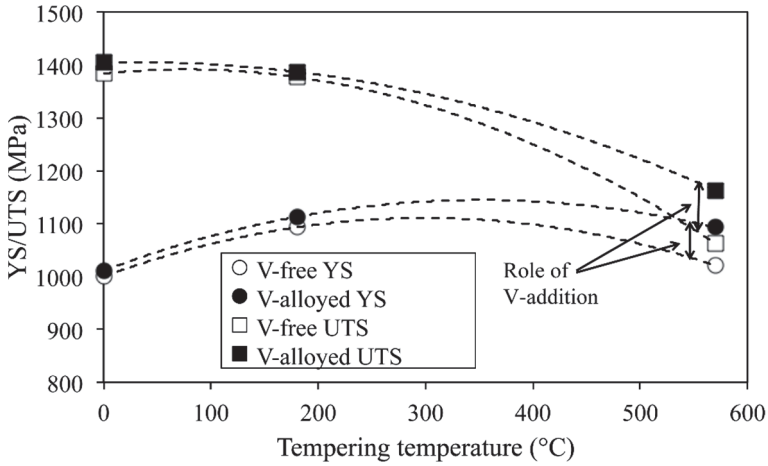

Fig. 37. The effect of vanadium on YS and UTS in DQ, LTT and HTT conditions (Reprinted by permission from Publication I © 2019 Elsevier B.V.).

The amount of nitrogen in the Ti-alloyed hot rolled composition was 27 ppm giving 150 ppm Ti in excess of that required to form TiN, which led to increased hardenability and a decrease in ferrite content, presumably due to the boron protection effect. Even though titanium was essential in obtaining a fully martensitic microstructure, excess Ti over the stoichiometric Ti/N-ratio, on the other hand, did not improve tempering resistance in the current study as much as was expected based on our earlier results (Saastamoinen et al., 2016), and it only provided a small increase in HTT strength levels compared to the DQ conditions. Shen and Hansen (1997) reported that Ti in excess of the stoichiometric ratio increases strength and hardness after HTT due to the precipitation of Ti(C,N). Despite its effective grain refinement effect, excess Ti was detrimental to impact toughness in all tempering conditions. The same conclusion was also reached earlier by Saastamoinen et al. (2016) and by Yan, Shan and Yang (2006), who observed a decrease in toughness with increasing Ti/N-ratio over stoichiometric ratio due to the coarsening of TiN particles.

Thermomechanical simulations using a Gleeble 3800 thermomechanical simulator confirmed the expected importance of optimizing the Ti/N-ratio in respect of boron to promote hardenability. The lower hardenability of boron alloyed steel in the presence of excess N is explained in the literature by Shen and Hansen

(1997) and is caused by the formation of boron nitrides, which leads to decreased hardenability due to lack of boron in solution. For Ti-free compositions and compositions containing Ti below stoichiometry with respect to N, the presence of boron was not found beneficial for the hardenability.

The vanadium microalloyed direct-quenched steel shows superior tempering resistance as it retained its high yield strength even after the demanding long tempering time at high temperatures. However, this comes with a cost as the V-alloyed DQ steel also shows embrittlement on tempering. The results in Publication I showed that only the V-free steel showed an improvement in toughness after HTT.

Lagneborg et al. (1999) have reported a similar negative effect of vanadium, but in that case it was due to coarse VN particles in steels containing significantly higher nitrogen levels than those in the steels studied here. It is more likely in the present case that fine VC and/or V_4C_3 act as a secondary strengthening components and simultaneously act counterproductively with regard to toughness. However, VC or V_4C_3 could not be distinguished using TEM, leaving possibility that vanadium effects cementite precipitation kinetics. For example, for high-carbon steels Han, Mottishaw, Smith and Edmonds (1994) proposed that vanadium increases the cementite nucleation rate leading to high density of small cementite particles. Furthermore, in high-carbon steels, vanadium has been found to exist as an alloying element in cementite (Ma & Wang, 2015) leading to possibility that it simply retards cementite coarsening and martensite softening process. The auto-tempering that occurs in the direct quenching of low-C steel seems to be adequate to provide both excellent toughness and strength already in the DQ condition (see also (Kaijalainen, 2016; Pallaspuro, 2018).

The regression analysis and the YS-T28J plot (Fig. 17) confirmed that at given strength level tempering is beneficial for toughness. This is an important observation as steels for commercial structural use are designed to meet minimum specified values for yield strength and toughness. For the DQ condition, no material reached the combination of YS 1000 MPa and T28J -75 °C. However, for the HTT condition, it was obtainable using either the low-C V-alloyed Ti-free concept or the high-C V-free concept. For LTT materials, on the other hand, the same level of strength and toughness was obtained with the high-C B-free concept and also the low-C V-alloyed composition.

Tensile ductility shows the opposite trend. A softened martensitic matrix leads to a significant improvement in tensile ductility at a given yield strength level after HTT. The most significant improvement can be seen in total elongation and post uniform elongation (Fig. 18). Due to this property relationship, when aiming to

achieve high strength combined with superior bendability together with the necessity of having a temper-resistant composition in coil batch annealing treatment, a low-C (adequate toughness) V-alloyed (superior tempering resistance) composition was selected for further studies in Publications II–IV. Coil batch annealing produces temperature gradients in the coil, which underlines the importance of tempering resistance so that homogeneous properties can be obtained in the final strip.

Not all the important elements in tempered steels were studied in this work. For example, molybdenum with a strong influence on tempering resistance was included in all the test compositions. The author of this thesis has shown the strong influence of molybdenum in retaining strength during high-temperature tempering in his earlier conference publication (Saastamoinen et al., 2013). An alloying concept including Mo, Cr, V and Ti seems suitable for direct-quenched and tempered steels. Final optimization of microalloying should be made depending on the application and manufacturing process: whether high toughness or high bendability is seen as the most desirable property. As bendability seems to be mainly be improved by high temperature tempering, highly bendable but still high-strength materials will require a robust alloying concept in order to retain high yield strength.

5.2 Thermomechanical treatment, direct quenching and tempering – factors affecting final properties

The effect of thermomechanical treatment, direct quenching and tempering was studied in the Publications II–IV focusing on the correlation between microstructure and mechanical properties. Tempering treatments simulated slow heating and cooling conditions if industrial steel coils would be tempered in the batch-annealing furnace.

5.2.1 Strengthening factors

Both as-quenched and tempered conditions have high yield strength. In fact, yield strength is often even increased during tempering: a clear decrease in yield strength is not seen until the tempering temperature reaches 650 °C (Fig. 38). The microstructural characterization showed high dislocation density and fine low- and high-angle grain sizes that both promote high strength. With 570 °C tempering temperature, the grain size is largely insensitive to the tempering and dislocation

density is only decreased moderately. An attempt was made to factorize yield strength in both the DQ and DQ-T conditions in Publication II. However, this remained unsatisfactory due to the complexity of the microstructures and the difficulty of evaluating the strengthening contributions from precipitation and solid solution strengthening.

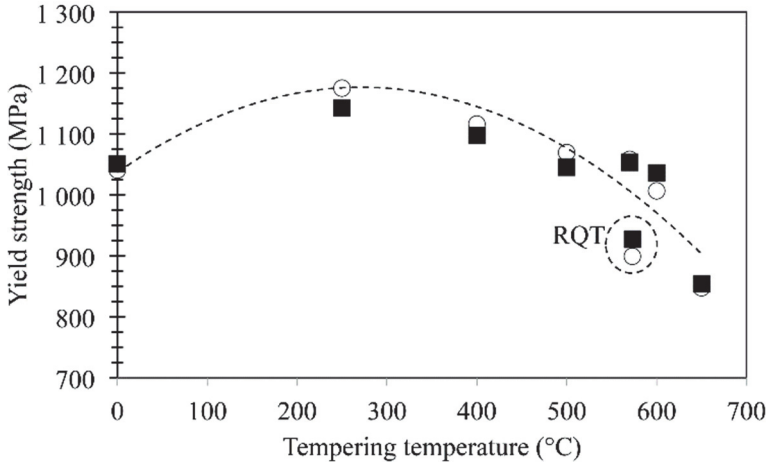

Fig. 38. Correlation between tempering temperature and yield strength. Open symbols represent strengths transverse to RD and closed symbols parallel to RD respectively (Reprinted by permission from Publication IV © 2018 Elsevier B.V.).

In our studies, tempering decreased the dislocation density estimated using the Williamson-Smallman equation in both the sub-surface and quarter-thickness positions of the strip. Furthermore, intra-lath dislocation densities measured with TEM also decreased as a result of tempering at 570 °C. However, the TEM method results in clearly lower values than the XRD method. This observation is in line with earlier similar findings that indicate an overestimation of dislocation density with the peak broadening analysis (Takebayashi et al., 2010). This view is supported by Hutchinson et al., (2018) who underline the fact that peak broadening is affected by factors other than dislocation density such as residual micro-stresses, which are unavoidably present after transformation to martensite. Therefore, the XRD results should not be taken as absolute values, but only as a powerful tool that allows the comparison of relative effects between different materials. For example, dislocation density measured with TEM only provides a microscopic average from a very limited area while the XRD measurements represent the macroscopic situation averaged throughout the structure. For example, a comparison between

microstructures resulting from the steels with FRT 775 °C and those with higher FRT was impossible using TEM due to the minor martensitic fraction in FRT 775 °C microstructure leading to high scatter in the results. Therefore, peak broadening analysis can be viable tool despite the probable overestimation. In the results of this thesis (Fig. 39), the dislocation density difference produced by using the XRD and TEM methods is smaller than that reported in an earlier study (Takebayashi et al., 2010). This is understandable due to the microstructural heterogeneity of the present steels: the TEM measurements were made by concentrating on the dislocation within martensitic laths, while the XRD measurements gave values averaged over volumes that included other microstructural components such as upper bainite, granular bainite and, in some cases, even ferrite. The hypothesis that lower FRT, i.e. a higher amount of austenite conditioning below T_{NR}, leads to higher dislocation density in the as-quenched martensite could not be verified. This has been earlier shown in Gleeble work done by Kennett et al., (2015), who also used the peak broadening analysis to estimate the dislocation density of martensite. Kennett also found that smaller PAGS obtained with thermomechanical processing would lead to higher hardness but also higher softening during high-temperature tempering (600 °C) which is understandable due to his results that also show higher relative dislocation density decrease when PAGS is finer and initial dislocation density is higher. In our studies, though, both XRD and TEM studies show that dislocation density remains high even after tempering and provides a high contribution to the yield strength both before and after tempering.

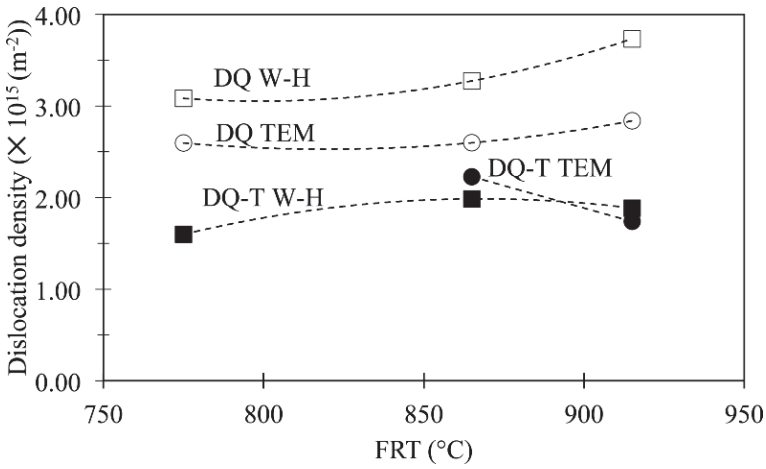

Fig. 39. Quarter-thickness dislocation densities for DQ and DQ-T materials studied with TEM (dislocation density of martensite) and the W-H method (XRD, i.e. average dislocation density of the whole microstructure) (Reprinted by permission from Publication II © 2018 Elsevier Inc.).

In general, grain size strengthening, precipitation strengthening, dislocation strengthening and carbon solid solution strengthening are known strengthening factors for lath martensite (S. Kennett, 2014). Due to the complexity of the final structure including martensite, autotempered martensite, severely tempered martensite and different bainite and even ferrite morphologies, the approach of Young and Bhadeshia (1994) was adopted; it is appropriate for mixtures of tempered bainite and tempered martensite (see equation 1).

The calculated strengthening factors for lath size and dislocation density in the present cases are given in Table 24. Precipitation strengthening contribution could not be estimated in this study due to the complex multiphase microstructure with locally varying carbide sizes and spacings. The dislocation strengthening factor is calculated based on the XRD measurements, which showed clear differences between the DQ and DQ-T conditions. However, as expressed earlier, no significant difference between different FRT conditions was found in dislocation density measurements. Furthermore, XRD based values show relatively high strengthening factors, which would represent 30–40% of total yield strength, which is possibly an overestimation. However, even when calculations are based on TEM dislocation densities, the dislocation strengthening factor remains high. For example, Morito et al., (2003) proposed that the dislocation density of as-quenched

martensite correlates with carbon content ($\rho \times 10^{-15} = 0.7 + 3.5$ wt.%C). Dislocation strengthening values calculated on the basis of this equation would be somewhat lower.

Table 24. Strengthening contribution of lath size (ECD from EBSD), dislocation density (XRD), and pure Fe to yield strength and the amount of residual, unexplained strength according to approach of Young and Bhadeshia (Reprinted by permission from Publication II © 2018 Elsevier Inc.).

FRT	Dislocation strengthening		Lath size strengthening		σ_{Fe}	YS actual Longitudinal		Residual	
(°C)	(MPa)		(MPa)		(MPa)	(MPa)		(MPa)	
	DQ	DQ-T	DQ	DQ-T	DQ and DQ-T	DQ	DQ-T	DQ	DQ-T
775	408	293	134	146	150	900	946	208	357
865	420	327	164	137	150	1041	1096	307	482
915	448	319	140	139	150	1078	1058	340	450

From Table 24 it can be seen that during tempering, dislocation strengthening is decreased while lath size strengthening based on EBSD analysis remains the same. Despite the high dislocation density and fine low-angle grain size of the low-FRT steel (PF + GB) the more martensitic steels resulting from higher FRTs still show higher strength. This difference could be explained by the solution strengthening of the supersaturated carbon in martensite as discussed by Young and Bhadeshia (1994). In fact, as we consider the amount of unexplained strength and compare FRT 915 °C (almost fully martensitic) and FRT 775 °C (only minor martensite fraction) steels, role of martensite solid solution strengthening compared to PF + GB microstructure is approximately 130 MPa. This factor is only expected in as-quenched martensite, while any residual supersaturation after tempering should, in theory, be almost non-existent with the martensite having transformed to a ferritic lattice containing cementite with its precipitation strengthening. In the current case, though, non-tempered martensite is minority even at as-quenched state. It should be underlined that the overall contribution of solid solution strengthening by carbon in martensite is made uncertain by the complexity of the microstructures in the various thermomechanical conditions, and the fact that autotempering reduces the carbon solid solution strengthening in that fraction of the martensite formed at relatively high temperatures close to Ms.

The unexplained strength contribution in the Table 24 is approximately 30% in the DQ states and 40% in the DQ-T states. In addition to obvious precipitation

strengthening in tempered martensite, another affecting factor can be the relief of internal micro-stresses during tempering as well as a reduced number of mobile dislocations. As-quenched martensite is known to possess high residual internal stresses that lead to the gradual yielding known as roundhouse yielding (Hutchinson et al., 2015) and tempering most likely relieves these stresses producing sharper yielding and a higher 0.2% proof stress. Takaki et al. (2012), on the other hand, suggested that the low elastic limit of the as-quenched martensite is due to a high density of mobile dislocations. Higher 0.2% proof stress was obtained with minor pre-straining (0.6%). Kennett (2014) also reported low initial yielding point in as-quenched martensitic microstructures explained as being due to a high density of mobile dislocations. 0.2% proof stress was again increased with either pre-straining or tempering, which both lead to dislocation cell network formation, which started to control the dislocation slipping. In the present work, Fig. 21 and Fig. 22 show the formation of a dislocation cell structure during high-temperature tempering (570 °C) despite the fact that the overall dislocation density remains high. A similar increase in yield strength after high-temperature tempering was reported by Hutchinson et al. (2015) and was mainly explained by the relaxation of residual stresses in the martensite leading to higher yield strength.

Nevertheless, high yield strength in the high-temperature tempered state is expected to be a combination of precipitation strengthening, relief of internal microstresses and the formation of a dislocation cell network effectively hindering dislocation movement. It should be noted that it is not sufficient to only consider dislocation density itself in relation to yield strength increments; the dislocation structure is also something that needs to be considered. Furthermore, another mechanism for increasing the lower elastic limit from DQ conditions could also be locking of mobile dislocations due to formation of Cottrell atmospheres. This is especially the case when considering low-temperature tempered materials where dislocation cell network and precipitation strengthening are unlikely due to low tempering temperature and low carbon contents, i.e. transition carbide formation seems unlikely. Therefore, formation of Cottrell atmospheres in addition to relaxation of internal stresses could possibly explain the increase in yield strength especially while the tensile curves showed slightly sharper yielding behaviour. Fig. 40 shows the engineering stress-strain curves of the FRT 915 °C materials tempered at 250–650 °C. Sharper yield point is obvious in tempered conditions compared to roundhouse yielding of DQ state. Low-temperature tempering also leads to lower uniform elongations, which has earlier discussed by Hutchinson et al. (2015). They explained that lower uniform elongation for low temperature tempered martensite

was due to internal compressive stresses in as-quenched states that defer plastic instability and therefore increased uniform elongations. However, these compressive internal stresses were decreased due to relaxation in low-temperature tempering leading to lower uniform elongations.

Due to the heteregeneity and complexity of the current materials, it was not possible to achieve a satisfactory analysis of the strengthening factors in Publication II. This would require a more focused analysis with certain well known microstructures. In general, though, V-alloyed experimental compositions in current study showed remarkable tempering resistance in terms of yield strength at high-tempering temperature without significant loss of strength until 650 °C. At 570 °C, which was the main focus in this thesis due to the aim of retaining high strength during tempering, retention of a fine lath structure and a high dislocation density in addition to propable relief of internal microstresses lead to the high yield strength.

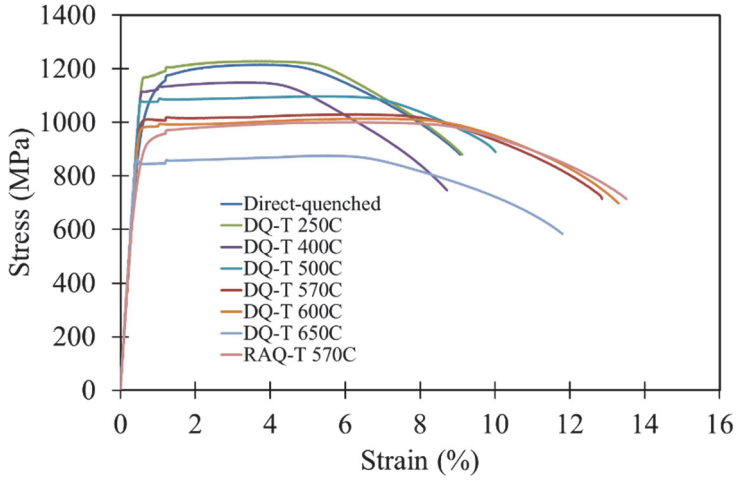

Fig. 40. Stress-strain curves for all the tempering conditions for FRT 915 °C steel. Increase in stress after 1% strain is due to increase in strain rate. Graph plotted from data published in Publication IV.

5.2.2 Toughness

Thermomechanical treatment showed its significant effect on the microstructure of the direct-quenched steel in Publication II. The lower the FRT, i.e. the higher the amount of deformation performed below the recrystallization stop temperature, the

finer the prior austenite grain size, which also led to a finer effective grain size ($d_{90\%}$). This is illustrated in Fig. 41. While the calculated value of T_{NR} for the present composition (in Publications II–IV) is 876 °C, it shows that T_{NR} only provides a rough estimate of the temperature region in which recrystallization ceases for specific deformation conditions. In general, T_{NR} is located in the partial recrystallization temperature region between the temperatures where there is full recrystallization and no recrystallization, which are known as the recrystallization limit and recrystallization stop temperatures. (Dutta & Sellars, 1987). The ultra-fine-grained FRT 775 °C differed from the higher FRT steels (865 and 915 °C) with its microstructural components, as the low FRT led to the formation of ferrite and granular bainite.

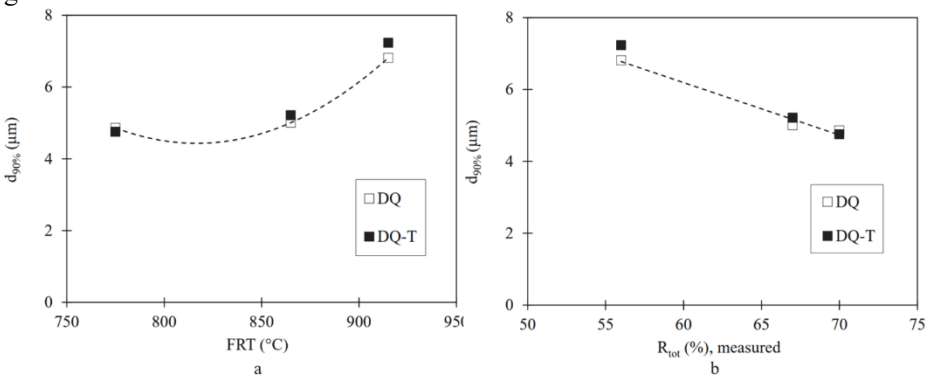

Fig. 41. Relationship between (a) finish rolling temperature and $d_{90\%}$ and (b) austenite reduction in the no-recrystallization temperature regime as measured from the microstructure and $d_{90\%}$. Graph plotted from data published in Publication II.

Regression analysis was used to evaluate the factors affecting the final impact toughness of the experimental steels. Multiple factors were included in the analyses done in Publication II, which ultimately showed that the transverse 28J transition temperature was mainly dependent on the size of the coarsest grains ($d_{90\%}$) irrespective of whether the steel was in the direct-quenched or tempered state:

$$T28J(TL) = -181.9 + 16.45 \cdot d_{90\%} \quad (10)$$

R^2 for this regression is 85.3 % and the standard error is 8.3 °C, which is consistent with the accuracy of the T28J values in Table 20 and what is generally observed (Wallin, 2011).

The result was somewhat surprising as tempering was found to have no significant effect on impact toughness of the strip as in Publication I. When

considering the results of the microstructural characterization it can be seen that $d_{90\%}$ is mainly dependent on the thermomechanical treatment, i.e. FRT (Fig. 41a) and, in fact, the reduction below the recrystallization stop temperature (Fig. 41b). This is well in line with earlier results for DQ steels that show that low FRT leads to refined grain size and improved toughness (Kaijalainen, 2016; Pallaspuro, 2018).

As Publication I showed, only the V-free concept would provide a clear improvement in Charpy V impact toughness and all V-alloyed compositions provide extremely robust behaviour in tempering leading to retained strength but also to embrittlement. In general, the laboratory treated steels (Publication I) and pilot-scale thermomechanically processed steels (Publications II–IV) are very well in line with each other in terms of mechanical properties for similar compositions and tempering conditions.

The effect of tempering temperature on the 28J transition temperature of the present low-carbon DQ steels is clearly different to that reported for higher carbon RAQ martensite, where embrittlement is seen after tempering in the range 300–500 °C and an improvement in toughness seen at higher temperatures (Horn & Ritchie, 1978). However, for low-C DQ martensite in Publication IV, tempering causes embrittlement, i.e. an increase in impact toughness transition temperature, for all temperatures up to 600 °C (Fig. 42). Low toughness in the tempering range of 250–500 °C can be understood on the basis of the observed microstructural changes in the martensite. As the microstructures showed, tempering in the 400–500 °C range results in the formation of long carbides in lath boundaries, which has been reported as being the cause of reduced toughness in the case of RAQ martensite (Horn & Ritchie, 1978). Tempering at 250 °C, on the other hand, did not show similar carbide formation, but led to a strong increase in yield strength which probably also affects the toughness. Tempering at 600 °C and above results in spheroidization of the carbides, which presumably reduces their embrittling potency.

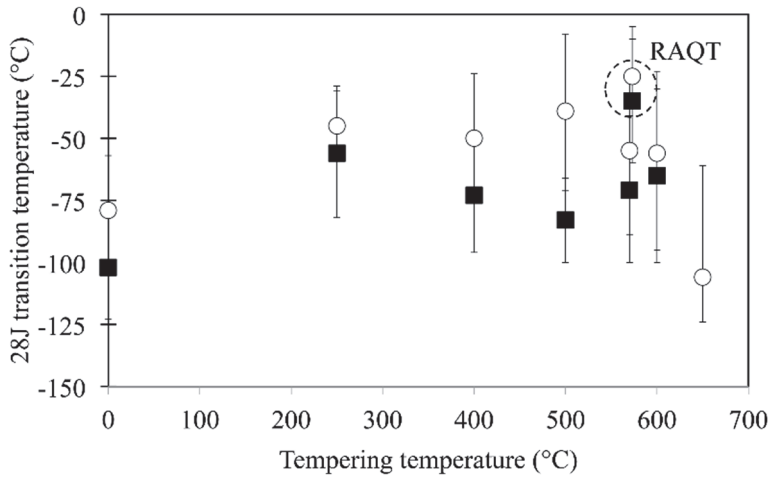

Fig. 42. Effect of tempering temperature on 28J transition temperature in martensitic direct-quenched steel (Publication IV). Open symbols transverse and closed symbols longitudinal with respect to RD. RAQT results included for comparison (Reprinted by permission from Publication IV © 2018 Elsevier B.V.).

For tempering with a peak temperature of 570 °C, the lower impact toughness, i.e. higher transition temperature, of the RAQT condition compared to the DQT condition seems to be due to the larger equiaxed grain structure of the RAQT microstructure. The fact that a fine elongated grain structure leads to improved toughness has been noted earlier (Kaijalainen et al., 2010; Kaijalainen et al., 2013). Furthermore, it is clear that the transition temperature of transverse specimens is always higher than it is for longitudinal specimens. All the experimental steels showed the presence of {112}<110> texture components at the quarter thickness positions. This has been shown by Yang, Xu, Tan and Wu (2015) to produce anisotropy in the steel resulting in excellent toughness for longitudinal specimens, slightly decreased toughness for transverse specimens and especially poor toughness for specimens at 45° to RD.

As presented above, several factors contribute to the changes in the impact toughness of DQ martensite on tempering. The formation of elongated carbides in grain boundaries and the increase in yield strength up to the tempering temperature of 600 °C both have a negative effect on toughness. Only when the tempering temperature is raised above 600 °C such that yield strength is clearly lowered and the carbides are spheroidized does impact toughness improve.

5.2.3 Bendability

The results in Publication III show the significant effect of thermomechanical treatment on surface texture and bendability. Kaijalainen (2016) showed that there is a strong dependence between thermomechanical treatment and texture. The results of this thesis are similar: FRT 865 °C promoted a strong surface texture, especially an intense shear texture component $\{112\}<111>_{\alpha}$. In fact, when considering bendability, surface hardness and texture were the main determining factors apart from the possible unfavourable presence of unfavourable features such as needle-like cementite, M-A constituents or upper bainite, which can act as sites for easy fracture initiation. In fact, both the formation of M-A and the upper-bainitic-like detrimental microstructure, in addition to the strong surface texture formed when FRT was 865 °C. This explains why the correlation of bendability to surface hardness presented by Kaijalainen (2016) did not exist when the bending axis was transverse to the rolling direction. This can be seen in Fig. 43. In fact, as can be seen, the tempered and the direct-quenched conditions follow a similar correlation between minimum bending radius and surface hardness with the only exception being the FRT 865 °C steel in transverse bending, which, as mentioned, has a very strong $\{112\}<111>_{\alpha}$ texture and a detrimental upper bainitic and M-A island structure in the surface of the strip. Tempering at 570 °C, on the other hand, did not have a clear effect on the crystallography of the direct-quenched strip and therefore, despite the improvement of bendability effected by HTT, a steel with a poor surface texture will have poor bendability even after HTT. In all thermomechanical treatment conditions (FRT 775–915 °C), low-angle grain size, high-angle grain size and the size of the coarsest grains remained roughly the same prior to and after tempering (570 °C). Furthermore, the intensities of the shear texture components $\{112\}<111>_{\alpha}$ and $\{110\}<111>_{\alpha}$ only showed a very slight decrease, which implies that tempering does not improve bendability due to any crystallographic effect.

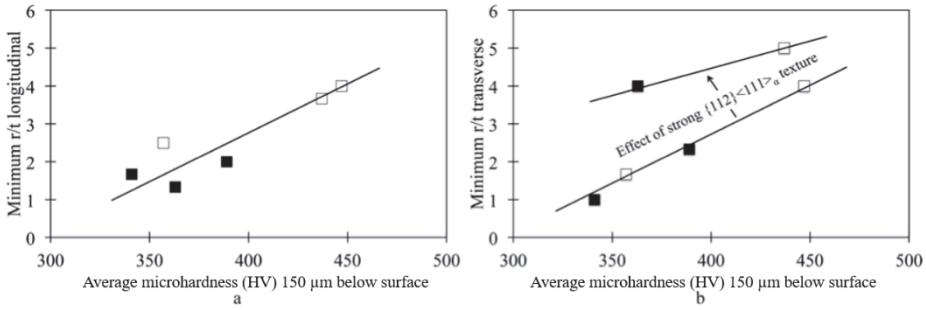

Fig. 43. Correlation between microhardness and minimum bending radius for (a) longitudinal bends and (b) transverse bends with with various FRTs and a single tempering temperature (570 °C). Open symbols are in the DQ condition and filled symbols the DQ-T condition (Reprinted by permission from Publication III © 2017 Elsevier Inc.).

A strong shear texture component leads to planar anisotropy due to geometric softening and shear band formation when the bend axis is transverse to the rolling direction (see Fig. 44) but not when the axis is parallel to rolling direction. As mentioned above, similar behaviour has also been reported earlier (Kaijalainen, 2016) which explains the anisotropy in bending. Similarly, geometric softening explains the different bendability behaviour of DQT martensite to RAQT martensite, as a strong shear texture component is absent from the latter.

However, combining the bendability results from Publications III and IV shows that in addition to strong texture, tempering temperature affects the correlation between bendability and surface hardness (Fig. 45). This is due to strong detrimental carbide precipitation on the lath and grain boundaries seen in Fig. 31b and Fig 31c.

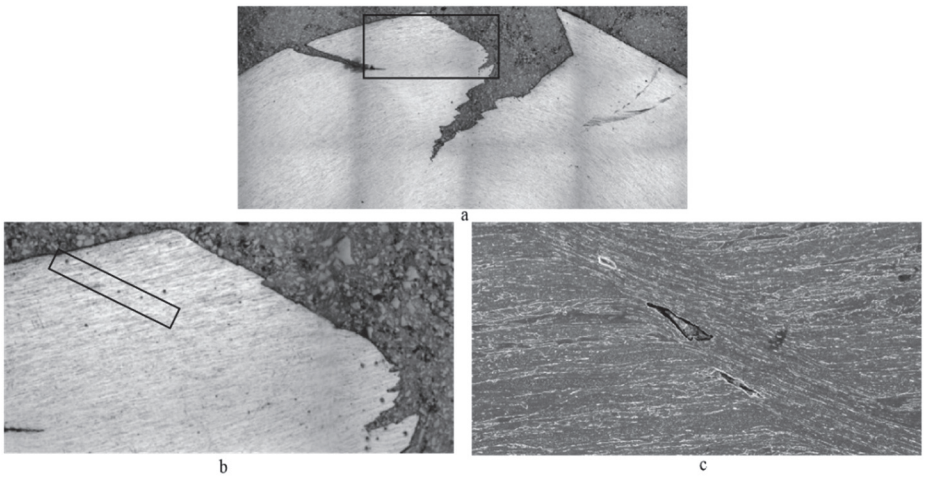

Fig. 44. (a) LSCM image of a cross section of a steel with a FRT of 865 °C after transverse bending with a punch radius of 16 mm (r/t 2.66), (b) LSCM image of a shear band formed near the surface and (c) FESEM image of a shear band containing voids in the same specimen (Reprinted by permission from Publication III © 2017 Elsevier Inc.).

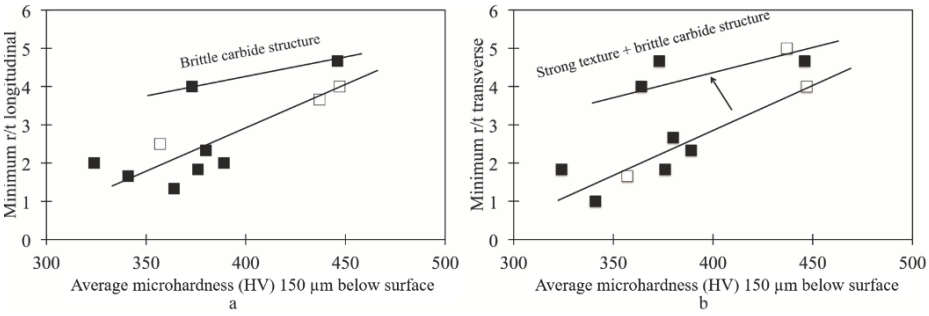

Fig. 45. Correlation between microhardness and minimum bending radius for (a) longitudinal bends and (b) transverse bends with with various FRTs and various tempering temperatures (250–650 °C). Open symbols are in the DQ condition and filled symbols the DQ-T condition. (Modified from Publication III)

Tempering had no significant effect on the grain size or the texture of the experimental steels, which led to the conclusion that the effect of tempering temperature on bendability depended on changes in dislocation density and structure, and carbide morphology. Kaijalainen (2016) already presented the effect of subsurface microstructure and texture on the bendability of DQ steel. In Kaijalainen's work, long M-A constituents had a detrimental effect on bendability,

and similar findings result in the case of the tempered microstructures in this work. The elongated carbides in the subsurface microstructures after tempering at 400–500 °C are expected to be unfavourable for bendability. Elongated microconstituents, either plate-like or needle-like M-A particles or long carbides, can act as intensifiers of plastic strain in the matrix leading to a detrimental effect on bendability. However, in the current work, when the tempering temperature was raised to 570 °C and above, the carbide structure was transformed into a more uniformly distributed state, which, together with decreased dislocation density, probably improved bendability.

These findings show that tempering provides significant improvement in bendability by lowering the hardness and the dislocation density (determined using the Williamson-Smallman method), which thereby lead improved tensile ductility and bendability. However, poor design of TMCP (FRT 865 °C) will lead to the formation of an unfavourable texture and microstructural components that cannot be removed by tempering. As well as poor TMCP design, poor choice of tempering temperature (400–500 °C) will lead to carbide formation on lath boundaries and grain boundaries and ultimately decreased bendability due to these crack-inducing features.

When re-austenitized, quenched and tempered (570 °C) steel was produced in the work published in Publication IV, it was found that re-austenitization led to a weak texture and eventually superior bendability compared to the original direct-quenched steel. The steel was especially ductile in the transverse bending test, which was the opposite of the behaviour seen with the direct-quenched steels, where a bending axis parallel to the rolling direction provides a tighter minimum bending radius than when the bending axis is perpendicular to the rolling direction. Despite the fact that the dislocation density and ultimate tensile strength of the RAQT and DQT steels was similar, the bendability of the RAQT steel was superior. The reason for the different behaviour is the more favourable texture of the RAQT condition possibly combined with the absence of other microstructural components than martensite.

While supporting the findings and conclusions of Kaijalainen (2016) regarding the importance of texture on the bendability of direct-quenched steel, this thesis shows that the conclusions can be extended to cover the direct-quenched and tempered state, which was not studied by Kaijalainen. The present study shows, for the first time, that tempering embrittlement due to the development of film-like carbides not only affects impact toughness (Horn & Ritchie, 1978; Zia-Ebrahimi & Krauss, 1984) but also bendability (Fig. 45).

5.3 High strength–high ductility concept

The results of this thesis show that careful consideration needs to be given concerning whether the tempering of direct-quenched steels is desirable or not. As Publications I and II showed, in terms of toughness, no straightforward improvement is obtained with either LTT or HTT treatments with V-alloyed DQ steels. In fact, direct-quenched high-strength strip with fine prior austenite grain size and fine effective transformed grain size results in good toughness even for the direct-quenched condition. This is especially the case with low FRT leading to ferritic-bainitic microstructures with a fine effective grain size (Fig. 46). Furthermore, direct-quenched low-carbon steels contain autotempered martensite that contains fine, uniformly dispersed carbides. This closely-spaced network of fine precipitates seems to be extremely beneficial for toughness.

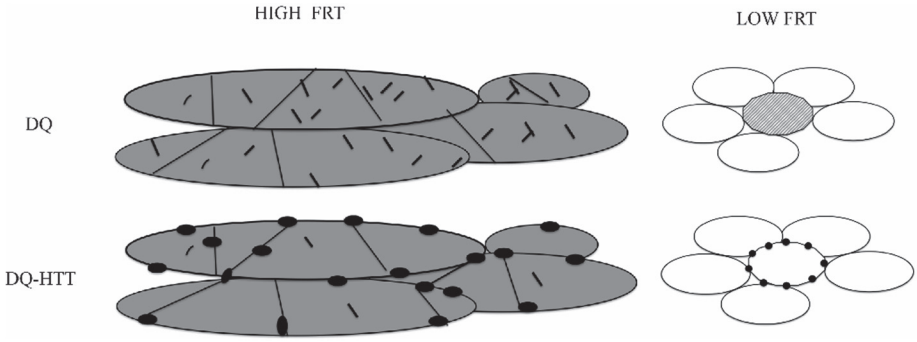

Fig. 46. Schematic illustration of high FRT direct-quenched martensitic and low FRT granular bainitic microstructures. High strength–high bendability obtained with two different morphologies.

However, when aiming at improved toughness at a certain strength level, which is usually the case when designing high-strength structural steels, either low-temperature or high-temperature tempering can provide some improvement as was shown by the results from the laboratory scale materials in Publication I. The results from the pilot scale hot-rolled and direct-quenched materials in Publication II, on the other hand, showed that tempering had no statistically significant effect on toughness; the only factors found to affect toughness in regression analyses were $d_{90\%}$ grain size and yield strength. The same conclusion was supported by all the experiments in this thesis: the tempering resistant composition in Publications II–IV including V, Mo, Cr and excess Ti provides remarkable tempering resistance regarding strength, but causes embrittlement as measured by the T28J toughness.

However, if the application demands high tensile yield strength together with high tensile elongation and/or bendability, i.e. tensile ductility, V-alloyed direct-quenched and high-temperature tempered low-C martensite will provide a viable option. Because the V-free direct-quenched steel undergoes significant softening during tempering, vanadium microalloying was selected for the composition used for Publications II–IV, where the aim was high strength combined with high bendability and adequate toughness. Furthermore, tempering resistance was seen as an essential property as tempering at batch annealing furnace would create temperature gradients in the coil. Indeed, Publications III and IV showed that the improvement in the properties of direct-quenched and tempered strip brought about by tempering is mainly obtained in terms of tensile ductility and especially bendability. Fig. 47 illustrates the remarkably improved yield strength–bendability combination after tempering at 570 °C and Fig. 48 summarizes the effect of both tempering temperature and texture on the yield strength – bendability combination.

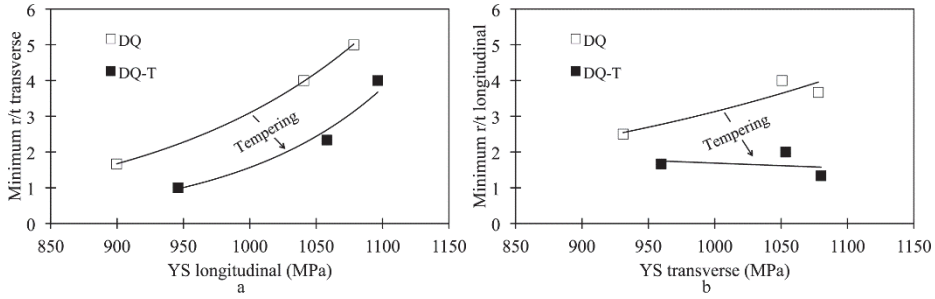

Fig. 47. Correlation between (a) transverse bendability and longitudinal YS and (b) longitudinal bendability and transverse YS in DQ and DQ-HTT (570 °C) conditions (Reprinted by permission from Publication III © 2017 Elsevier Inc.).

The current results show that the answer to the question as to whether or not to use tempering depends on the final application. Steel users may request tempering because of their earlier experiences regarding the benefits of tempering based on the use of re-austenitized and quenched martensite. Tempering may be beneficial for those steels, but as this study shows, low-C direct-quenched steels behave somewhat differently. Due to their fine grain size and autotempering, they have high toughness (low T28J) even in the as-direct-quenched state. Furthermore, a very tempering-resistant composition required for tempering at batch annealing furnace significantly affects the optimal processing route for a given application.

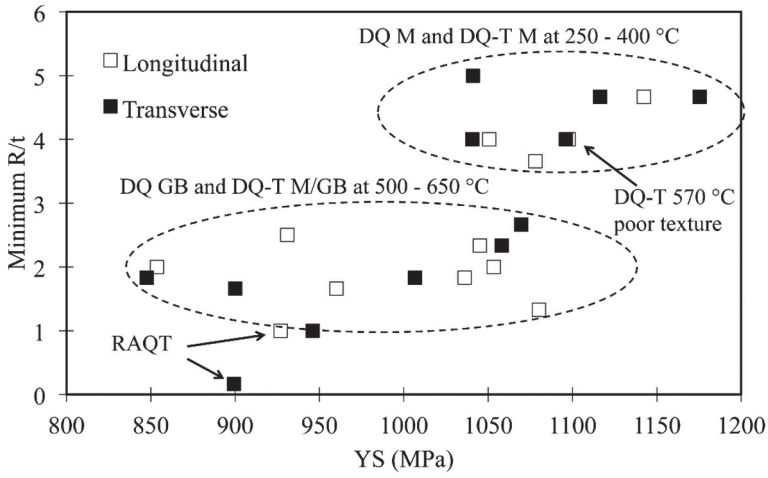

Fig. 48. Correlation between transverse bendability and longitudinal YS and longitudinal bendability and transverse YS in different tempering conditions (Publications III and IV).

It is obvious, though, that a tempering resistant composition with an optimal thermomechanical treatment that avoids the formation of a strong shear texture, combined with high-temperature tempering will lead to a remarkable combination of yield strength, tensile ductility and bendability. Therefore, when these properties are seen as essential, direct quenching and tempering provides superior process route. However, with properly designed thermomechanical treatment, as seen in Publication III, good bendability and relatively high strength can be obtained with a ferritic-bainitic surface microstructure combined with mixed ferritic-bainitic-martensitic bulk microstructure.

5.4 Future research

For future research in the case of direct-quenched and tempered steels a few remarks can be presented. As this work was mainly focussed on pilot scale direct-quenched steels and their processing by slow tempering in batch annealing furnaces, the final microstructures consisted of various components including ferrite, granular bainite, upper bainite and martensite. It would be important to study the microstructural effects with more controlled thermomechanical treatments and then present the behaviour of solely martensitic microstructures in tempering for better characterization of strengthening factors of direct-quenched martensite.

Extraction replica studies using TEM were started in the early work leading to Publication I. However, coarse cementite particles were difficult to extract onto the carbon films. Due to this, carbides were mainly characterized with FESEM. It would be useful to extend this with improved TEM characterization techniques. This topic would demand another project where the focus would be on TEM analysis. It would be useful to obtain a better understanding of the effect of tempering on carbide compositions and structure, thereby improving our understanding of the role of vanadium during HTT and its strong effect on mechanical properties.

Evaluation of the dislocation strengthening factor still remains rather difficult due to the probable overestimation of dislocation density in XRD analysis and the poor statistics typical of TEM analysis. This situation is exacerbated in the case of microstructures consisting of mixtures of lath martensite, different morphologies of bainite and even ferrite. In the future, studies should be aimed at single-component microstructures, e.g. lath martensite produced with various different levels of thermomechanical treatment.

6 Summary and conclusions

The work done during this thesis was aimed at studying direct quenching and tempering with industrially relevant laboratory experiments covering thermomechanical treatment, direct quenching and various tempering treatments simulating slow tempering conditions in batch annealing furnace. The pivotal aspects considered when planning the thesis were: 1) the role of chemical composition on the tempering resistance of direct-quenched steel, 2) the relationship between thermomechanical treatment, microstructure and properties of direct-quenched steel, and 3) the relationship between tempering parameters, microstructure and properties of direct-quenched strip.

A total of 27 different pilot-scale steels were produced with different combinations of chemical composition, thermomechanical treatment and subsequent heat treatment. All steels contained (in wt.%) 0.2Si-1Mn-1Cr-0.65Mo-0.03Al, while the levels of C (0.095 - 0.140), V (0 - 0.08), Ti (0 - 0.025) and B (0 - 0.0015) varied. Thermomechanical treatment was conducted with varying FRT between 775–915 °C to provide different rolling reductions below the recrystallization stop temperature. Quench rates ranged from 70 °C/s to 100 °C/s resulting in mixtures of microstructural components including martensite, auto-tempered martensite, granular bainite, upper bainite and polygonal ferrite. Furthermore, for these microstructures, tempering experiments were conducted with peak temperatures varying from 180 to 650 °C. The following is a summary of the main results and the conclusions that can be drawn:

- Vanadium microalloying leads to remarkable tempering resistance but a decrease in impact toughness as measured by the 28J transition temperature during high-temperature tempering. Titanium on the other hand is essential to obtain the desired hardenability increase from B-microalloying.
- From the toughness point of view, the need for tempering is composition dependent for TMCP-DQ processed steels. The direct-quenched experimental steels obtained good toughness (T28J) even in the as-quenched condition, but only the V-free composition showed a clear increase in toughness after high-temperature tempering (570 °C). However, this was accompanied by a radical decrease in strength. V-alloyed steels, on the other hand, retained high strength during tempering and did not improve their T28J until the tempering temperature was increased to 650 °C.

- The thermomechanical history, i.e. finish hot rolling temperature (FRT) and amount of austenite deformation below the recrystallization stop temperature had a remarkable effect on both prior austenite grain size and effective grain size of the transformed final microstructure, and therefore toughness, and on the general microstructural components and texture of the direct-quenched strip. A strong shear texture $\{112\}<111>_{\alpha}$ component is promoted in the near-surface regions with the intermediate FRT of 865 °C. This also promotes transformation to bainitic microstructures especially in the sub-surface layers of the strip. Higher FRT (915 °C) and lower FRT (775 °C) lead to slightly different microstructural conditions. The textures of both conditions were somewhat weaker than with the intermediate FRT. Low FRT also promoted the formation of softer phases including ferrite and granular bainite. High FRT, on the other hand, was the most martensitic of the FRT conditions studied.
- The toughness of the DQT strip is mainly affected by the chemical composition and the FRT: the lower the FRT, the finer both the austenite grain size and the grain size of the coarsest transformed grains ($d_{90\%}$), which leads to a lower T28J, i.e. improved toughness. For V-alloyed DQ strip, tempering is not beneficial until the tempering temperature reaches 650 °C, which also leads to severe softening. Regarding composition, toughness is reduced by additions of boron, vanadium and carbon, and, in the case of the tempered state, titanium in excess of stoichiometry with respect to N. Furthermore, tempering in the embrittlement temperature range (400–500 °C) leads to the formation of brittle carbide structures.
- The bendability of the strip is affected by several factors. Generally, the results showed that tempering at 500 °C and above improves the bendability of the direct-quenched strip. This is due to a reduction of the surface hardness of the strip. However, the correlation between surface hardness and bendability can be disrupted strong detrimental texture components or unfavourable carbide precipitation. If thermomechanical treatment is executed with intermediate FRT, a strong shear texture leads to a decrease in bendability that cannot be improved with tempering. Tempering at 400–500 °C leads to unfavourable carbide precipitation as rod-like particles and lines of smaller particles on lath and grain boundaries, which act as nucleation sites for cracks thereby decreasing the bendability of the strip, i.e. temper embrittlement occurs from the bendability point of view.
- Carbide formation during tempering depends on the initial microstructure and the tempering treatment. Microstructural characterization showed that

martensite and granular bainite will undergo strong carbide precipitation during high-temperature tempering. As-quenched martensite is almost always autotempered and section of untempered martensite are minority. The autotempering of low-C martensite is probably an important factor contributing to the good toughness of the direct-quenched condition.

- For a given chemical composition and high-temperature tempering treatment, the re-austenitized, quenched and tempered state obtained superior bendability compared to the direct-quenched state. This is due to a lack of strong texture in the RAQT condition and the absence of microstructural components other than martensite, which leads to extremely ductile behaviour in three-point-bending after tempering. On the other hand, the RAQT state obtained slightly lower yield strength and considerably poorer T28J mostly due to its coarser grain size.
- Despite the expected decrease in hardness and ultimate tensile strength, V-Ti-Mo-Cr alloyed robust composition retains its yield strength even after relatively high temperature tempering (up to 600 °C). This leads to a remarkable combination of ultrahigh yield strength and very good bendability. High yield strength is proposed to be due to a combination of precipitation strengthening, dislocation cell structure formation and relief of internal micro-stresses.
- This thesis has shown that numerous composition and processing options exist when designing different combinations of strength and toughness or strength and ductility / bendability. In general, a high level of strength and toughness is obtainable even in the direct-quenched condition. However, high-temperature tempering can provide a desirable process route when aiming to improved toughness at a given yield strength level especially above 1000 MPa. When aiming at a high level of yield strength and bendability or yield strength and tensile ductility, high-temperature tempering provides a very interesting process route alternative.

7 Novel features

The following results are believed to be original for this thesis:

- The concept of direct-quenching and tempering in a batch annealing furnace has been established.
- A chemical composition giving superior tempering resistance as required by the tempering of coils in batch annealing furnaces has been developed.
- This is the first time that a correlation between tempering temperature and the yield strength – bendability balance has been presented. The bendability of the direct-quenched strip is effectively improved by tempering without loss of yield strength. However, tempering at 400–500 °C will lead to decreased bendability due to unfavourable carbide formation. Similarly, the bendability of both direct-quenched and direct-quenched and tempered steel is decreased when rolling with an intermediate FRT (865 °C) that leads to a strong shear texture component $\{112\}\langle 111\rangle_{\alpha}$.
- It has been shown that tempering does not provide a straightforward improvement in the impact toughness of direct-quenched low-C martensitic-bainitic steel. Grain size and yield strength are the main controlling factors of T28J leading to the fact that direct-quenched strip obtains excellent toughness even in the as-quenched state when thermomechanical rolling parameters are optimised. However, tempering in the range 250–500 °C can be detrimental to toughness.
- Direct-quenched and tempered steels show a correlation between surface hardness and minimum bending radius in the same way as direct-quenched steels. However, this correlation is lost in the presence of a strong detrimental texture component or grain boundary carbide precipitation from tempering at 400–500 °C.
- Microalloying plays an important role for the tempering behaviour of direct-quenched strip. Both 160 ppm excess Ti and an addition of 0.08 wt.% V significantly increases the final yield strength of the direct-quenched and high-temperature tempered strip.

List of references

Adrian, H. (2013). A mechanism for effect of vanadium on hardenability of medium carbon manganese steel. *Materials Science and Technology*, 15, 366–378.

Adrian, H., & Staœko, R. (2008). The effect of nitrogen and vanadium on hardenability of medium carbon 0.4 %C and 1.8 %Cr steel, *Archives of Materials Science and Engineering*, 33, 69–74.

Bain, E. C. (1939). Functions of the Alloying Elements in Steel. *American Society for Metals*, 312 pages.

Baltazar Hernandez, V. H., Nayak, S. S., & Zhou, Y. (2011). Tempering of martensite in dual-phase steels and its effects on softening behavior. *Metallurgical and Materials Transactions A*, 42, 3115–3129.

Bhadeshia, H. K. D. H., & Honeycombe, R. (2006). Steels: Microstructure and Properies. *Butterworth-Heinemann*, 183–208.

Biro, E., McDermid, J. R., Vignier, S., & Norman Zhou, Y. (2014). Decoupling of the softening processes during rapid tempering of a martensitic steel. *Materials Science and Engineering A*, 615, 395–404.

Calcagnotto, M., Ponge, D., & Raabe, D. (2012). On the Effect of Manganese on Grain Size Stability and Hardenability in Ultrafine-Grained Ferrite/Martensite Dual-Phase Steels. *Metallurgical and Materials Transactions A*, 43, 37–46.

Caron, R. N., & Krauss, G. (1972). The tempering of Fe-C lath martensite. *Metallurgical Transactions*, 3, 2381–2389.

Cizek, P., Wynne, B. P., Davies, C. H. J., Muddle, B. C., & Hodgson, P. D. (2002). Effect of composition and austenite deformation on the transformation characteristics of low-carbon and ultralow-carbon microalloyed steels. *Metallurgical and Materials Transactions A*, 33, 1331–1349.

Dlouhy, J., Podany, P., & Dzugan, J. (2019). Strengthening from Cu Addition in 0.2C-(1-2)Mn Steels during Tempering. *Materials*, 247, 1-13.

Dutta, B. & Sellars, C. M. (1987). Effect of composition and process variables on Nb(C, N) precipitation in niobium microalloyed austenite. *Materials Science and Technology*, 3, 197–206.

EricksonKirk, M. A., EricksonKirk, M. T., Rosinski, S., & Spanner, J. (2009). A Comparison of the tanh and Exponential Fitting Methods for Charpy V-Notch Energy Data. *Journal of Pressure Vessel Technology*, 131, 31404–31413.

Fukui, S., Uehara, N., & Isokawa, K. (1971). The Effect of Vanadium on the Hardenability and Mechanical Properties of High Strength Steels. *DENKI-SEIKO*, 42, 272–287.

Garcia-Mateo, C., Peet, M., Caballero, F. G., & Bhadeshia, H. K. D. H. (2004). Tempering of hard mixture of bainitic ferrite and austenite. *Materials Science and Technology*, 20, 814–818.

Habu, R., Miyata, M., Tamukai, S., & Sekino, S. (2011). Improvement of Hardenability of Steel Containing Aluminum and Boron by Double Quenching. *Transactions of the Iron and Steel Institute of Japan*, 23, 176–183.

Ham, R. K. (1961). The determination of dislocation densities in thin films. *Philosophical Magazine*, 6, 1183–1184.

Han, F., Hwang, B., Suh, D.-W., Wang, Z., Lee, D., & Kim, S.-J. (2008). Effect of Molybdenum and Chromium on Hardenability of Low-Carbon Boron-Added Steels. *Metals and Materials International*, 14, 667–672.

Han, K., D. Mottishaw, T., Smith, G., & Edmonds, D. V. (1994). Effects of vanadium addition on nucleation and growth of pearlite in high carbon steel. *Materials Science and Technology*, 10, 955–963.

Heikkala, J., & Väisänen, A. (2012). Usability testing of ultra high-strength steels. *Proceedings of the 11th Biennial Conference on Engineering Systems Design and Analysis*, 1–13.

Horn, R. M., & Ritchie, R. O. (1978). Mechanisms of tempered martensite embrittlement in low alloy steels. *Metallurgical Transactions A*, 9, 1039–1053.

Hulka, K., Kern, A., & Schriever, U. (2005). Application of Niobium in Quenched and Tempered High-Strength Steels. *Materials Science Forum*. 501, 519–526.

Hutchinson, B., Bate, P., Lindell, D., Malik, A., Barnett, M., & Lynch, P. (2018). Plastic yielding in lath martensites – An alternative viewpoint. *Acta Materialia*, 152, 239–247.

Hutchinson, B., & Hagstro, J. (2011). Microstructures and hardness of as-quenched martensites (0.1–0.5%C). *Acta Materialia*, 59, 5845–5858.

Hutchinson, B., Lindell, D., & Barnett, M. (2015). Yielding Behaviour of Martensite in Steel. *ISIJ International*, 55, 1114–1122.

Kaijalainen, A. (2016). Effect of microstructure on the mechanical properties and bendability of direct-quenched ultrahigh-strength steels. *Acta Universitatis Ouluensis C* 582, 115 pages.

Kaijalainen, A., Suikkanen, P., Karjalainen, L. P., Komi, J., & DeArdo, A. J. (2010). Effect of austenite conditioning in the non-recrystallization regime on the microstructures and properties of ultra high strength bainitic/martensitic strip steel. *Proc. 2nd Int. Conf. Super-High Strength Steels. Associazone Italiana di Metallurgica – AIM, 1-18.*

Kaijalainen, A., Suikkanen, P., Limnell, T., Karjalainen, L. P., Kömi, J., & Porter, D. (2013). Effect of austenite grain structure on the strength and toughness of direct-quenched martensite. *Journal of Alloys and Compounds*, 577, 642–648.

Kaijalainen, A., Suikkanen, P., Karjalainen, L. P., & Jonas, J. J. (2014). Effect of Austenite Pancaking on the Microstructure, Texture, and Bendability of an Ultrahigh-Strength Strip Steel. *Metallurgical and Materials Transactions A*, 45, 1273–1283.

Kennett, S.C, Krauss, G., & Findley, K. O. (2015). Prior austenite grain size and tempering effects on the dislocation density of low-C Nb–Ti microalloyed lath martensite. *Scripta Materialia*, 107, 123–126.

Kennett, S. C. (2014). Strengthening and toughening mechanisms in low-c microalloyed martensitic steel as influenced by austenite conditioning. Doctor dissertation. Colorado School of Mines.

Kömi, J., Karjalainen, P., & Porter, D. (2016). Direct-Quenched Structural Steels. In R. Colás & G. E. Totten (Eds.), *Encyclopedia of Iron, Steel and Their Alloys,* 1109–1125.

Krauss, G. (1995). Heat Treated Martensitic Advanced Manufacture Steels : Microstructural Systems for Advanced Manufacture. *ISIJ International*, 35, 349–359.

Krauss, G. (1999). Martensite in steel: strength and structure. *Materials Science and Engineering: A*, 273–275, 40–57.

Krauss, G. (2017). Tempering of Lath Martensite in Low and Medium Carbon Steels: Assessment and Challenges. *Steel Research International*, 88.

Krauss, G. & Marder, A. R. (1971). The morphology of martensite in iron alloys. *Metallurgical Transactions*, 2, 2343–2357.

Krauss, G., & Thompson, S. W. (1995). Ferritic Microstructures in Continuously Cooled Low- and Ultralow-carbon Steels. *ISIJ International*, 35, 937-945.

Lagneborg, R., Siwecki, T., Zajac, S., & Hutchinson, B. (1999). The Role of Vanadium in Microalloyed Steels. *Scandinavian Journal of Metallurgy*, 28, 186–241.

Llewellyn, D. (1995). Copper in Steels. *Ironmaking and Steelmaking*, 22, 25–34.

Ma, H., & Wang, L. (2015). Application of vanadium and titanium in high carbon steel. *Journal of Iron and Steel Research*, 27, 69-74.

Morito, S., Adachi, Y., & Ohba, T. (2009). Morphology and Crystallography of Sub-Blocks in Ultra-Low Carbon Lath Martensite Steel. *Materials Transactions*, 50, 1919–1923.

Morito, S., Huang, X., Furuhara, T., Maki, T., & Hansen, N. (2006). The morphology and crystallography of lath martensite in alloy steels. *Acta Materialia*, 54, 5323–5331.

Morito, S., Nishikawa, J., & Maki, T. (2003). Dislocation Density within Lath Martensite in Fe–C and Fe–Ni Alloys. *ISIJ International*, 43, 1475–1477.

Morito, S., Yoshida, H., Maki, T., & Huang, X. (2006). Effect of block size on the strength of lath martensite in low carbon steels. *Materials Science and Engineering A*, 438–440, 237–240.

Morooka, S., Tomota, Y., Adachi, Y., Morito, S., & Kamiyama, T. (2008). Hierarchical Characterization by EBSD and Neutron Diffraction on Heterogeneous Deformation Behavior of a Martensitic Steel. *Tetsu-to-Hagane*, 94, 313–320.

Nishioka, K., & Ichikawa, K. (2012). Progress in thermomechanical control of steel plates and their commercialization. *Science and Technology of Advanced Materials*, 13.

Nyyssönen, T., Isakov, M., Peura, P., & Kuokkala, V. T. (2016). Iterative Determination of the Orientation Relationship Between Austenite and Martensite from a Large Amount of Grain Pair Misorientations. *Metallurgical and Materials Transactions A*, 47, 2587–2590.

Öhlund, C. E., Weidow, J., Thuvander, M., & Offerman, S. E. (2014). Effect of Ti on Evolution of Microstructure and Hardness of Martensitic Fe–C–Mn Steel during Tempering. *ISIJ International*, 54, 2890–2899.

Okamoto, S., Matlock, D. K., & Krauss, G. (1991). The transition from serrated to non-serrated flow in low-carbon martensite at 150 °C . *Scripta Metallurgica et Materialia*, 25, 39-44.

Oldfield, W. (1975). Curve fitting impact test data: a statistical procedure, *ASTM Stand. News*, 3, 24–29

Ouchi, C. (2001). Development of Steel Plates by Intensive Use of TMCP and Direct Quenching Processes. *ISIJ International*, 41, 542–553.

Pacyna, J., & Dabrowski, R. (2006). Vanadium influence upon changes at tempering steels of small content of other elements. *Journal of Materials Processing Technology*, 175, 330–333.

Pallaspuro, S. (2018). On the factors affecting the ductile-brittle transition in as- quenched fully and partially martensitic low-carbon steels, *Acta Universitatis Ouluensis C,* 655*,* 79 pages.

Raabe, D. (2003). Overview on Basic Types of Hot Rolling Textures of Steels. *Steel Research*, 74, 327–337.

Ray, R., Jonas, J., Butrón-Guillén, M., & Savoie, J. (1994). Transformation textures in steels. *International Materials Reviews*, 34, 927–942.

Rothleutner, L. M., & Van Tyne, C. J. (2014). Effect of Aluminum on Vanadium Microalloyed Forging Steels. Colorado School of Mines Advanced Steel Processing and Products center. Retrieved from http://www.forging.org, 1–9.

Saastamoinen, A., Porter, D., & Suikkanen, P. (2015). The microstructure and properties of direct quenched martensite subjected to both ultra slow tempering and conventional tempering cycles. *European Conference on Heat Treatment 2015 and 22nd IFHTSE Congress - Heat Treatment and Surface Engineering from Tradition to Innovation.* 1-11.

Saastamoinen, A., Porter, D., & Suikkanen, P. (2013). The microstructure and properties of direct quenched martensite subjected to both slow furnace tempering and rapid induction tempering cycles. *9th International ROLLING Conference & 6th European ROLLING Conference*, Venice, Italy. Associazione Italiana di Metallurgia. 1-13.

Saastamoinen, A., Kaijalainen, A., Porter, D. & Suikkanen, P. (2016). Effect of titanium and nitrogen content on the microstructure, hardenability and mechanical properties of direct quenched and tempered ultra-high strength structural steel. *5th International Conference on Thermomechanical Processing*. Milano, Italia, Associazione Italiana di Metallurgia, 5050, 1-9.

Shen, Y., & Hansen, S. S. (1997). Effect of the Ti/N ratio on the hardenability and mechanical properties of a quenched-and-tempered C-Mn-B steel. *Metallurgical and Materials Transactions A*, 28, 2027–2035.

Shi, Z. M., Gong, W., Tomota, Y., Harjo, S., Li, J., Chi, B., & Pu, J. (2015). Study of tempering behavior of lath martensite using in situ neutron diffraction. *Materials Characterization*, 107, 29–32.

Somani, M., Pyykkönen, J., Porter, D., Karjalainen, L. P., & Kömi, J. (2015). Influence of Composition and Prior Deformation on Phase Transformation Temperatures and Hardness in Direct Quenching Using Physical Simulation. *Materials Performance and Characterization*, 4, 341-364.

Suikkanen, P. (2009). Development and processing of low carbon bainitic steels. *Acta Universitatis Ouluensis C*, 340, 486 pages.

Suikkanen, P., Ristola, A.-J., Hirvi, A., Sahu, P., Somani, M., Porter, D., & Karjalainen, L. P. (2013). Effects of Carbon Content and Cooling Path on the Microstructure and Properties of TRIP-aided Ultra-High Strength Steels. *ISIJ International*, 53, 337–346.

Takaki, S., Ngo-Huynh, K., Nakada, N., & Tsuchiyama, T. (2012). Strengthening Mechanism in Ultra Low Carbon Martensitic Steel. *ISIJ International*, 52, 710-716.

Takebayashi, S., Kunieda, T., Yoshinaga, N., Ushioda, K., & Ogata, S. (2010). Comparison of the Dislocation Density in Martensitic Steels Evaluated by Some X-ray Diffraction Methods. *ISIJ International*, 50, 875–882.

Taylor, K. A., & Hansen, S. S. (1990). The boron hardenability effect in thermomechanically processed, direct-quenched 0.2 Pct C steels. *Metallurgical Transactions A*, 21, 1697–1708.

Ueno, M., & Inoue, T. (1973). Distribution of boron at austenite grain boundaries and bainitic transformation in low carbon steels. *Transactions of the Iron and Steel Institute of Japan*, 13, 210–217.

Ulff, C. (1970). Effect of stress-relief annealing on the mechanical properties of steel grades for pressure vessels. *Jernkontorets Annaler*, 154, 53–64.

Wallin, K. (1986). Mini- ja normaalikokoisten Charpy-V-koesauvojen tulosten välinen korrelaatio. *VTT Research Reports*, 428, 31.

Wallin, K. (2011). Fracture Toughness of Engineering Materials, *EMAS Publishing, 566 pages*.

Williamson, G. & Hall, W. (1953). X-ray Line Broadening from Filed Aluminium and Wolfram. *Acta Metallurgica*, 1, 22–31.

Williamson, G. & Smallman, R. E. (1956). Dislocation densities in some annealed and cold-worked metals from measurements on the X-ray debye-scherrer spectrum. *Philosophical Magazine*, 1, 34–46.

Wittridge, N. J., & Jonas, J. J. (2000). The austenite-to-martensite transformation in Fe–30%Ni after deformation by simple shear. *Acta Materialia*, 48, 2737–2749.

World steel association. (n.d.). Retrieved from https://www.worldsteel.org/

Yamada, M., Yan, L., Takaku, R., Ohsaki, S., Miki, K., Kajikawa, K., & Azuma, T. (2014). Effects of Alloying Elements on the Hardenability, Toughness and the Resistance of Stress Corrosion Cracking in 1 to 3 mass% Cr Low Alloy Steel. *ISIJ International*, 54, 503–510.

Yan, W., Shan, Y. Y., & Yang, K. (2006). Effect of TiN inclusions on the impact toughness of low-carbon microalloyed steels. *Metallurgical and Materials Transactions A*, 37, 2147–2158.

Yang, X. L., Xu, Y. B., Tan, X. D., & Wu, D. (2015). Relationships among crystallographic texture, fracture behavior and Charpy impact toughness in API X100 pipeline steel. *Materials Science and Engineering A*, 641, 96–106.

Young, C. H. & Bhadeshia, H. K. D. H. (1994). Strength of mixtures of bainite and martensite. *Materials Science and Technology*, 10, 209–214.

Zajac, S., Schwinn, V., & Tacke, K. H. (2005). Characterisation and Quantification of Complex Bainitic Microstructures in High and Ultra-High Strength Linepipe Steels. *Materials Science Forum*, 500–501, 387–394.

Zia-Ebrahimi, F., & Krauss, G. (1984). Mechanisms of tempered martensite embrittlement in medium-carbon steels. *Acta Metallurgica*, 32, 1767–1778.

Original publications

I Saastamoinen A., Kaijalainen A., Nyo T. T., Suikkanen P., Porter D. & Kömi J. (2019) Direct-quenched and tempered low-C high-strength structural steel: The role of chemical composition on microstructure and mechanical properties, *Materials Science & Engineering: A,* 760, 346–358

II Saastamoinen A., Kaijalainen A., Porter D., Suikkanen P., Yang J-R. & Tsai Y-T. (2018) The effect of finish rolling temperature and tempering on the microstructure, mechanical properties and dislocation density of direct-quenched steel, *Materials Characterization 139*, 1–10.

III Saastamoinen A., Kaijalainen A., Porter D. & Suikkanen P. (2017) The effect of thermomechanical treatment and tempering on the subsurface microstructure and bendability of direct-quenched low-carbon strip steel, *Materials Characterization*, 134, 172–181.

IV Saastamoinen A., Kaijalainen A., Heikkala J., Porter D. & Suikkanen P. (2018) The effect of tempering temperature on microstructure, mechanical properties and bendability of direct-quenched low-alloy strip steel, *Materials Science & Engineering: A*, 730, 284–294.

Original publications are not included in the electronic version of the dissertation.

713. Javaheri, Vahid (2019) Design, thermomechanical processing and induction hardening of a new medium-carbon steel microalloyed with niobium

714. Hautala, Ilkka (2019) From dataflow models to energy efficient application specific processors

715. Ruokamo, Simo (2019) Single shared model approach for building information modelling

716. Isohookana, Matti (2019) Taistelunkestävä hajaspektritietovuo kansalliseen sotilasilmailuun

717. Joseph, Nina (2019) $CuMoO_4$: a microwave dielectric and thermochromic ceramic with ultra-low fabrication temperature

718. Kühnlenz, Florian (2019) Analyzing flexible demand in smart grids

719. Sun, Jia (2019) Speeding up the settling of switched-capacitor amplifier blocks in analog-to-digital converters

720. Lähetkangas, Kalle (2019) Special applications and spectrum sharing with LSA

721. Kiventerä, Jenni (2019) Stabilization of sulphidic mine tailings by different treatment methods : heavy metals and sulphate immobilization

722. Fylakis, Angelos (2019) Data hiding algorithms for healthcare applications

723. Juuso, Ilkka (2019) A cellular automaton environment for the complex system of speech

724. Aho, Pekka (2019) Automated state model extraction, testing and change detection through graphical user interface

725. Bergna, Davide (2019) Activated carbon from renewable resources : carbonization, activation and use

726. Nuottila, Jouko (2019) Flexibility in agile projects : Contracting practices and organisational arrangements

727. Adesanya, Elijah D. (2019) A cementitious binder from high-alumina slag generated in the steelmaking process

728. Hannila, Hannu (2019) Towards data-driven decision-making in product portfolio management : From company-level to product-level analysis

Book orders:
Virtual book store
http://verkkokauppa.juvenesprint.fi

UNIVERSITY OF OULU P.O. Box 8000 FI-90014 UNIVERSITY OF OULU FINLAND

ACTA UNIVERSITATIS OULUENSIS

UNIVERSITY of OULU
OULUN YLIOPISTO

ISBN 978-952-62-2453-4 (Paperback)
ISBN 978-952-62-2454-1 (PDF)
ISSN 0355-3213 (Print)
ISSN 1796-2226 (Online)